Fuzzy Functions, Relations, and Fuzzy Transforms 2013

Guest Editors: Salvatore Sessa, Ferdinando Di Martino, and Irina G. Perfilieva

Fuzzy Functions, Relations, and Fuzzy Transforms 2013

Fuzzy Functions, Relations, and Fuzzy Transforms 2013

Guest Editors: Salvatore Sessa, Ferdinando Di Martino, and Irina G. Perfilieva

Editorial Board

Contents

Editorial

Fuzzy Functions, Relations, and Fuzzy Transforms 2013

Salvatore Sessa,[1,2] Ferdinando Di Martino,[1] and Irina G. Perfilieva[3]

[1] *Dipartimento di Costruzioni e Metodi Matematici in Architettura, Università degli Studi di Napoli Federico II, Via Monteoliveto 3, 80134 Napoli, Italy*

[2] *Centro Interdipartimentale di Ricerca per l'Analisi e la Progettazione Urbana Luigi Pisciotti, Via Toledo 402, 80134 Napoli, Italy*

[3] *Centre of Excellence IT4Innovations, Division of the University of Ostrava, Institute for Research and Applications of Fuzzy Modeling, 30. dubna 22, 701 00 Ostrava 1, Czech Republic*

Correspondence should be addressed to Salvatore Sessa; sessa@unina.it

In this issue which continues the series of these specials devoted to fuzzy functions, relations, and fuzzy transforms, these concepts must be here intended in the widest sense, as noted in the papers whose contents can be resumed in the following way.

In a paper by F. Di Martino and S. Sessa, two algorithms for constructing a GOP sequence of colour frames (differentiated in intra, predictive, and bidirectional in the space RGB) are proposed. A classification of these frames is made by means of a similarity measure defined by the Lukasiewicz t-norm. Furthermore, they are divided in subframes called blocks and are compressed via direct fuzzy transforms. These blocks are decompressed with the inverse fuzzy transforms; successively they are reassembled for giving the reconstructed frames whose PSNR (calculated as mean in the three bands R, G, and B) is fully comparable with the PSNR obtained by using the traditional fuzzy transforms and MPEG-4 methods.

In the paper by L.-C. Chang et al., the authors propose a fuzzy inference system for management of surface and subsurface resources water. A detailed discussion of all fuzzy rules and related parameters is presented as well.

In another paper by F. Di Martino and S. Sessa, the authors use the fuzzy transforms for matching problem with many grey images extracted from a well-known dataset. The authors prove that their results are analogous to those obtained with the GEFS and SEFS based methods contained in their previous work for images of square dimensions, but the presented method is extended to images of arbitrary dimensions. Experiments are performed also over colour images.

In the paper by B. D. Pant et al., the authors prove a common fixed point theorem for two pairs of compatible and subsequentially continuous (or, in alternative, subcompatible and reciprocally continuous) maps under a suitable contractive condition in a fuzzy metric space. Two numerical examples support their results.

In the paper by P. Vlašánek, the author shows that the choice of the basic functions in the reconstruction of images based on fuzzy transforms is crucial. Indeed, he analyzes how to improve this choice by finding the best basic functions also for damaged testing images and by proposing an algorithm for reconstruction.

We hope that these topics are stimulating for wide audience.

Salvatore Sessa
Ferdinando Di Martino
Irina G. Perfilieva

Research Article

A Coupled Fixed Point Theorem in Fuzzy Metric Space Satisfying ϕ-Contractive Condition

B. D. Pant,[1] Sunny Chauhan,[2] Jelena Vujaković,[3] Muhammad Alamgir Khan,[4] and Calogero Vetro[5]

[1] *Government Degree College, Champawat, Uttarakhand 262523, India*

[2] *R. H. Government Postgraduate College, Kashipur (Udham Singh Nagar), Uttarakhand 244713, India*

[3] *Faculty of Sciences and Mathematics, Lole Ribara 29, 38 200 Kosovska Mitrovica, Serbia*

[4] *Department of Natural Resources Engineering and Management, University of Kurdistan, Erbil 22570, Iraq*

[5] *Università degli Studi di Palermo, Dipartimento di Matematica e Informatica, Via Archirafi 34, 90123 Palermo, Italy*

Correspondence should be addressed to B. D. Pant; badridatt.pant@gmail.com

The intent of this paper is to prove a coupled fixed point theorem for two pairs of compatible and subsequentially continuous (alternately subcompatible and reciprocally continuous) mappings, satisfying ϕ-contractive conditions in a fuzzy metric space. We also furnish some illustrative examples to support our results.

1. Introduction

The evolution of fuzzy mathematics commenced with the introduction of the notion of fuzzy sets by Zadeh [1], where the concept of uncertainty was introduced in the theory of sets, in a nonprobabilistic manner. Fuzzy set theory has applications in applied sciences such as mathematical programming, model theory, engineering sciences, image processing, and control theory. In 1975, Kramosil and Michalek [2] introduced the concept of fuzzy metric space as a generalization of the statistical (probabilistic) metric space. Afterwards, Grabiec [3] defined the completeness of the fuzzy metric space and extended the Banach contraction principle to fuzzy metric spaces. Since then, many authors contributed to the development of this theory, also in relation to fixed point theory (e.g., [4–9]).

Mishra et al. [10] extended the notion of compatible mappings (introduced by Jungck [11] in metric spaces) to fuzzy metric spaces and proved common fixed point theorems in presence of continuity of at least one of the mappings, completeness of the underlying space, and containment of the ranges amongst involved mappings. Further, Singh and Jain [12] weakened the notion of compatibility by using the notion of weakly compatible, mappings in fuzzy metric spaces and showed that every pair of compatible mappings is weakly compatible but converse is not true. Inspired by Bouhadjera and Godet-Thobie [13, 14], Gopal and Imdad [15] extended the notions of subcompatibility and subsequential continuity to fuzzy metric spaces and proved fixed point theorems using these notions together due to Imdad et al. [16]. In recent past, several authors proved various fixed point theorems employing more general contractive conditions (e.g., [17–26]).

On the other hand, Bhaskar and Lakshmikantham [27] and Lakshmikantham and Ćirić [28] gave some coupled fixed point theorems in partially ordered metric spaces (see also [29–31]). In 2010, Sedghi et al. [32] proved common coupled fixed point theorems in fuzzy metric spaces for commuting mappings. Motivated by the results of [33], Hu [34] proved a coupled fixed point theorem for compatible mappings satisfying ϕ-contractive conditions in fuzzy metric spaces with continuous t-norm of H-type and generalized the result of Sedghi et al. [32]. In an interesting note, Zhu and Xiao [35] showed that the results contained in Sedghi et al. [32] are not true in their present form.

Inspired by the work of Zhu and Xiao [35], we prove coupled common fixed point theorems for two pairs of

mappings satisfying a general contractive condition in fuzzy metric spaces, by using the notions of compatibility and subsequential continuity (alternately subcompatibility and reciprocal continuity). Our results improve many known common coupled fixed point theorems available in the existing literature. We support our results with two illustrative examples.

2. Preliminaries

In this section, we collect some basic notions and results. In the sequel $\mathbb{R}^+$ will denote the set of all positive real numbers while $\mathbb{N}$ will denote the set of natural numbers.

Definition 1 (see [1]). Let X be any set. A fuzzy set A in X is a function with domain X and values in $[0, 1]$.

Definition 2 (see [36]). A binary operation $* : [0, 1] \times [0, 1] \to [0, 1]$ is a continuous t-norm if $*$ satisfies the following conditions:

(a) $*$ is commutative and associative;

(b) $*$ is continuous;

(c) $a * 1 = a$ for all $a \in [0, 1]$;

(d) $a * b \leq c * d$ whenever $a \leq c$ and $b \leq d$ for all $a, b, c, d \in [0, 1]$.

Definition 3 (see [37]). One says that a t-norm $*$ is of H-type if the family $\{*^n\}$ of its iterates is equicontinuous at $x = 1$; that is, for any $\lambda \in (0, 1)$, there exists $\delta(\lambda) \in (0, 1)$ such that $x > 1 - \delta$ implies $*^n(x) > 1 - \lambda$, for all $n \in \mathbb{N}$.

The t-norm $*_m = \min\{a, b\}$ for all $a, b \in [0, 1]$ is an example of t-norm of H-type, but there are some other t-norms $*$ of H-type (see [37]).

Definition 4 (see [2]). A 3-tuple $(X, M, *)$ is said to be a fuzzy metric space if X is an arbitrary nonempty set, $*$ is a continuous t-norm, and M is a fuzzy set in $X^2 \times (0, +\infty)$ satisfying the following conditions, for each $x, y, z \in X$ and $t, s > 0$:

(a) $M(x, y, t) > 0$;

(b) $M(x, y, t) = 1$ for all $t > 0$ if and only if $x = y$;

(c) $M(x, y, t) = M(y, x, t)$;

(d) $M(x, y, t) * M(y, z, s) \leq M(x, z, t + s)$;

(e) $M(x, y, \cdot) : (0, \infty) \to (0, 1]$ is continuous.

Example 5 (see [7]). Let (X, d) be a metric space. Define the t-norm $a * b = ab$ for all $a, b \in [0, 1]$, and, for all $x, y \in X$ and $t > 0$,

$$M(x, y, t) = \frac{t}{t + d(x, y)}. \tag{1}$$

Then $(X, M, *)$ is a fuzzy metric space, and the fuzzy metric M induced by the metric d is often referred, as the standard fuzzy metric.

Example 6 (see [32]). Let (X, d) be a metric space and ψ be an increasing and continuous function from $\mathbb{R}^+$ into $(0, 1)$ such that $\lim_{s \to \infty} \psi(s) = 1$. Four typical examples of these functions are $\psi(s) = s/(s + 1)$, $\psi(s) = \sin(\pi s/(2s + 1))$, $\psi(s) = 1 - e^{-s}$, and $\psi(s) = e^{-1/s}$. Let $a * b = ab$ for all $a, b \in [0, 1]$, and, for each $x, y \in X$ and $t > 0$, define

$$M(x, y, t) = [\psi(t)]^{d(x, y)}. \tag{2}$$

It is easy to see that $(X, M, *)$ is a fuzzy metric space.

Definition 7 (see [34]). Define $\Phi = \{\phi : \mathbb{R}^+ \to \mathbb{R}^+\}$ such that $\phi \in \Phi$ satisfies the following conditions:

(ϕ-1) ϕ is nondecreasing;

(ϕ-2) ϕ is upper semicontinuous from the right;

(ϕ-3) $\sum_{n=0}^{\infty} \phi^n(s) < +\infty$ for all $s > 0$, where $\phi^{n+1}(s) = \phi(\phi^n(s))$, $n \in \mathbb{N}$.

Clearly if $\phi \in \Phi$, then $\phi(s) < s$ for all $s > 0$.

Definition 8 (see [27]). An element $(x, y) \in X \times X$ is called

(a) a coupled fixed point of the mapping $f : X \times X \to X$ if

$$f(x, y) = x, \qquad f(y, x) = y; \tag{3}$$

(b) a coupled coincidence point of the mappings $f : X \times X \to X$ and $g : X \to X$ if

$$f(x, y) = g(x), \qquad f(y, x) = g(y); \tag{4}$$

(c) a common coupled fixed point of the mappings $f : X \times X \to X$ and $g : X \to X$ if

$$\begin{aligned} x &= f(x, y) = g(x), \\ y &= f(y, x) = g(y). \end{aligned} \tag{5}$$

Definition 9 (see [27]). An element $x \in X$ is called a common fixed point of the mappings $f : X \times X \to X$ and $g : X \to X$ if

$$x = g(x) = f(x, x). \tag{6}$$

Definition 10 (see [34]). The mappings $f : X \times X \to X$ and $g : X \to X$ are called compatible if

$$\begin{aligned} \lim_{n \to \infty} M(gf(x_n, y_n), f(gx_n, gy_n), t) &= 1, \\ \lim_{n \to \infty} M(gf(y_n, x_n), f(gy_n, gx_n), t) &= 1, \end{aligned} \tag{7}$$

for all $t > 0$, whenever $\{x_n\}$ and $\{y_n\}$ are sequences in X such that

$$\begin{aligned} \lim_{n \to \infty} f(x_n, y_n) &= \lim_{n \to \infty} gx_n = \alpha, \\ \lim_{n \to \infty} f(y_n, x_n) &= \lim_{n \to \infty} gy_n = \beta, \end{aligned} \tag{8}$$

for some $\alpha, \beta \in X$.

Now we introduce the following notions.

Definition 11. The mappings $f : X \times X \to X$ and $g : X \to X$ are said to be reciprocally continuous if, for sequences $\{x_n\}$, $\{y_n\}$ in X, one has

$$
\begin{aligned}
\lim_{n \to \infty} f(gx_n, gy_n) &= f(\alpha, \beta), \\
\lim_{n \to \infty} gf(x_n, y_n) &= g\alpha, \\
\lim_{n \to \infty} f(gy_n, gx_n) &= f(\beta, \alpha), \\
\lim_{n \to \infty} gf(y_n, x_n) &= g\beta,
\end{aligned}
\tag{9}
$$

whenever

$$
\begin{aligned}
\lim_{n \to \infty} f(x_n, y_n) &= \lim_{n \to \infty} gx_n = \alpha, \\
\lim_{n \to \infty} f(y_n, x_n) &= \lim_{n \to \infty} gy_n = \beta,
\end{aligned}
\tag{10}
$$

for some $\alpha, \beta \in X$.

If two self-mappings are continuous, then they are obviously reciprocally continuous, but the converse is not true. Moreover, in the setting of common fixed point theorems for compatible pairs of self mappings satisfying contractive conditions, continuity of one of the mappings implies their reciprocal continuity but not conversely (see [38]).

Definition 12. The mappings $f : X \times X \to X$ and $g : X \to X$ are said to be subsequentially continuous if and only if there exist sequences $\{x_n\}$, $\{y_n\}$ in X such that

$$
\begin{aligned}
\lim_{n \to \infty} f(x_n, y_n) &= \lim_{n \to \infty} gx_n = \alpha, \\
\lim_{n \to \infty} f(y_n, x_n) &= \lim_{n \to \infty} gy_n = \beta,
\end{aligned}
\tag{11}
$$

for some $\alpha, \beta \in X$, and

$$
\begin{aligned}
\lim_{n \to \infty} f(gx_n, gy_n) &= f(\alpha, \beta), \\
\lim_{n \to \infty} gf(x_n, y_n) &= g\alpha, \\
\lim_{n \to \infty} f(gy_n, gx_n) &= f(\beta, \alpha), \\
\lim_{n \to \infty} gf(y_n, x_n) &= g\beta.
\end{aligned}
\tag{12}
$$

One can easily check that if two self mappings f and g are both continuous, hence also reciprocally continuous mappings but f and g are not sub-sequentially continuous (see [38, Example 1]).

Definition 13. The mappings $f : X \times X \to X$ and $g : X \to X$ are said to be subcompatible if and only if there exist sequences $\{x_n\}$, $\{y_n\}$ in X such that

$$
\begin{aligned}
\lim_{n \to \infty} f(x_n, y_n) &= \lim_{n \to \infty} gx_n = \alpha, \\
\lim_{n \to \infty} f(y_n, x_n) &= \lim_{n \to \infty} gy_n = \beta,
\end{aligned}
\tag{13}
$$

for some $\alpha, \beta \in X$, and

$$
\begin{aligned}
\lim_{n \to \infty} M(f(gx_n, gy_n), gf(x_n, y_n), t) &= 1, \\
\lim_{n \to \infty} M(f(gy_n, gx_n), gf(y_n, x_n), t) &= 1,
\end{aligned}
\tag{14}
$$

for all $t > 0$.

3. Results

In this section, we state and prove our fixed point results.

Theorem 14. *Let $(X, M, *)$ be a fuzzy metric space, where $*$ is a continuous t-norm of H-type such that $M(x, y, t) \to 1$ as $t \to \infty$, for all $x, y \in X$. Let $A, B : X \times X \to X$ and $S, T : X \to X$ be four mappings such that*

(a) *the pairs (A, S) and (B, T) are compatible and subsequentially continuous;*

(b) *there exists $\phi \in \Phi$ such that*

$$
\begin{aligned}
M(A(x, y), B(u, v), \phi(t)) \\
\geq M(Sx, Tu, t) * M(Sy, Tv, t),
\end{aligned}
\tag{15}
$$

for all $x, y, u, v \in X$ and $t > 0$.

Then there exists a unique point α in X such that $\alpha = S\alpha = T\alpha = A(\alpha, \alpha) = B(\alpha, \alpha)$.

Proof. Since the mappings A and S are subsequentially continuous and compatible, there exist sequences $\{x_n\}$, $\{y_n\}$ in X such that

$$
\begin{aligned}
\lim_{n \to \infty} A(x_n, y_n) &= \lim_{n \to \infty} Sx_n = \alpha, \\
\lim_{n \to \infty} A(y_n, x_n) &= \lim_{n \to \infty} Sy_n = \beta,
\end{aligned}
\tag{16}
$$

for all $\alpha, \beta \in X$, and

$$
\begin{aligned}
\lim_{n \to \infty} M(A(Sx_n, Sy_n), SA(x_n, y_n), t) &= 1, \\
\lim_{n \to \infty} M(A(Sy_n, Sx_n), SA(y_n, x_n), t) &= 1,
\end{aligned}
\tag{17}
$$

that is $A(\alpha, \beta) = S\alpha$ and $A(\beta, \alpha) = S\beta$. Similarly, with respect to the pair (B, T), there exist sequences $\{x_n'\}$, $\{y_n'\}$ in X such that

$$
\begin{aligned}
\lim_{n \to \infty} B(x_n', y_n') &= \lim_{n \to \infty} Tx_n' = \alpha', \\
\lim_{n \to \infty} B(y_n', x_n') &= \lim_{n \to \infty} Ty_n' = \beta',
\end{aligned}
\tag{18}
$$

for all $\alpha', \beta' \in X$, and

$$
\begin{aligned}
\lim_{n \to \infty} M(B(Tx_n', Ty_n'), TB(x_n', y_n'), t) &= 1, \\
\lim_{n \to \infty} M(B(Ty_n', Tx_n'), TB(y_n', x_n'), t) &= 1,
\end{aligned}
\tag{19}
$$

that is $B(\alpha', \beta') = T\alpha'$ and $B(\beta', \alpha') = T\beta'$. Hence $(\alpha, \beta) \in X \times X$ is a coupled coincidence point of the pair (A, S),

whereas $(\alpha', \beta') \in X \times X$ is a coupled coincidence point of the pair (B, T).

Now we assert that $(\alpha, \beta) = (\alpha', \beta')$, that is, $\alpha = \alpha'$ and $\beta = \beta'$. Since $*$ is a t-norm of H-type, for any $\lambda > 0$, there exists an $\mu > 0$ such that

$$\underbrace{(1 - \mu) * (1 - \mu) * \cdots * (1 - \mu)}_{p} \geq 1 - \lambda, \tag{20}$$

for all $p \in \mathbb{N}$.

Since $M(x, y, \cdot)$ is continuous and $\lim_{t \to \infty} M(x, y, t) = 1$ for all $x, y \in X$, there exists $t_0 > 0$ such that $M(\alpha, \alpha', t_0) \geq 1 - \mu$ and $M(\beta, \beta', t_0) \geq 1 - \mu$.

On the other hand, since $\phi \in \Phi$, by condition $(\phi\text{-}3)$, we have $\sum_{n=1}^{\infty} \phi^n(t_0) < \infty$. Then for any $t > 0$, there exists $n_0 \in \mathbb{N}$ such that $t > \sum_{p=n_0}^{\infty} \phi^p(t_0)$. On using inequality (15) with $x = x_n$, $y = y_n$, $u = x'_n$, and $v = y'_n$, we have

$$\begin{aligned}
M\left(A\left(x_n, y_n\right), B\left(x'_n, y'_n\right), \phi\left(t_0\right)\right) \\
\geq M\left(Sx_n, Tx'_n, t_0\right) * M\left(Sy_n, Ty'_n, t_0\right).
\end{aligned} \tag{21}$$

Letting $n \to \infty$, we get

$$M\left(\alpha, \alpha', \phi\left(t_0\right)\right) \geq M\left(\alpha, \alpha', t_0\right) * M\left(\beta, \beta', t_0\right). \tag{22}$$

Again using inequality (15) with $x = y_n$, $y = x_n$, $u = y'_n$, and $v = x'_n$, we have

$$\begin{aligned}
M\left(A\left(y_n, x_n\right), B\left(y'_n, x'_n\right), \phi\left(t_0\right)\right) \\
\geq M\left(Sy_n, Ty'_n, t_0\right) * M\left(Sx_n, Tx'_n, t_0\right).
\end{aligned} \tag{23}$$

Letting $n \to \infty$, we get

$$M\left(\beta, \beta', \phi\left(t_0\right)\right) \geq M\left(\beta, \beta', t_0\right) * M\left(\alpha, \alpha', t_0\right). \tag{24}$$

From (22) and (24), we obtain

$$\begin{aligned}
M\left(\alpha, \alpha', \phi\left(t_0\right)\right) * M\left(\beta, \beta', \phi\left(t_0\right)\right) \\
\geq \left[M\left(\alpha, \alpha', t_0\right)\right]^2 * \left[M\left(\beta, \beta', t_0\right)\right]^2.
\end{aligned} \tag{25}$$

In general, for all $n \in \mathbb{N}$, we have

$$\begin{aligned}
M\left(\alpha, \alpha', \phi^n\left(t_0\right)\right) * M\left(\beta, \beta', \phi^n\left(t_0\right)\right) \\
\geq \left[M\left(\alpha, \alpha', \phi^{n-1}\left(t_0\right)\right)\right]^2 * \left[M\left(\beta, \beta', \phi^{n-1}\left(t_0\right)\right)\right]^2 \\
\geq \left[M\left(\alpha, \alpha', t_0\right)\right]^{2^n} * \left[M\left(\beta, \beta', t_0\right)\right]^{2^n}.
\end{aligned} \tag{26}$$

Then, we have

$$\begin{aligned}
M\left(\alpha, \alpha', t\right) * M\left(\beta, \beta', t\right) \\
\geq \left[M\left(\alpha, \alpha', \sum_{p=n_0}^{\infty} \phi^p\left(t_0\right)\right)\right] \\
* \left[M\left(\beta, \beta', \sum_{p=n_0}^{\infty} \phi^p\left(t_0\right)\right)\right] \\
\geq \left[M\left(\alpha, \alpha', \phi^{n_0}\left(t_0\right)\right)\right] \\
* \left[M\left(\beta, \beta', \phi^{n_0}\left(t_0\right)\right)\right] \\
\geq \left[M\left(\alpha, \alpha', t_0\right)\right]^{2^{n_0}} * \left[M\left(\beta, \beta', t_0\right)\right]^{2^{n_0}} \\
\geq \underbrace{(1 - \mu) * (1 - \mu) * \cdots * (1 - \mu)}_{2^{2n_0}} \\
\geq 1 - \lambda.
\end{aligned} \tag{27}$$

So for any $\lambda > 0$, we have

$$M\left(\alpha, \alpha', t\right) * M\left(\beta, \beta', t\right) \geq 1 - \lambda, \tag{28}$$

for all $t > 0$, and so $\alpha = \alpha'$ and $\beta = \beta'$. Therefore we have

$$\begin{aligned}
A\left(\alpha, \beta\right) = S\alpha, \qquad A\left(\beta, \alpha\right) = S\beta, \\
B\left(\alpha, \beta\right) = T\alpha, \qquad B\left(\beta, \alpha\right) = T\beta.
\end{aligned} \tag{29}$$

Next, we show that $S\alpha = T\alpha$ and $S\beta = T\beta$. Since $*$ is a t-norm of H-type, for any $\lambda > 0$, there exists an $\mu > 0$ such that

$$\underbrace{(1 - \mu) * (1 - \mu) * \cdots * (1 - \mu)}_{p} \geq 1 - \lambda, \tag{30}$$

for all $p \in \mathbb{N}$.

Since $M(x, y, \cdot)$ is continuous and $\lim_{t \to +\infty} M(x, y, t) = 1$ for all $x, y \in X$, there exists $t_0 > 0$ such that $M(S\alpha, T\alpha, t_0) \geq 1 - \mu$ and $M(S\beta, T\beta, t_0) \geq 1 - \mu$.

Since $\phi \in \Phi$, by condition $(\phi\text{-}3)$, we have $\sum_{n=1}^{\infty} \phi^n(t_0) < \infty$. Then for any $t > 0$, there exists $n_0 \in \mathbb{N}$ such that $t > \sum_{p=n_0}^{\infty} \phi^p(t_0)$. On using inequality (15) with $x = u = \alpha$, $y = v = \beta$, we have

$$\begin{aligned}
M\left(A\left(\alpha, \beta\right), B\left(\alpha, \beta\right), \phi\left(t_0\right)\right) \\
\geq M\left(S\alpha, T\alpha, t_0\right) * M\left(S\beta, T\beta, t_0\right),
\end{aligned} \tag{31}$$

and so

$$M\left(S\alpha, T\alpha, \phi\left(t_0\right)\right) \geq M\left(S\alpha, T\alpha, t_0\right) * M\left(S\beta, T\beta, t_0\right). \tag{32}$$

Similarly, we can obtain

$$M\left(S\beta, T\beta, \phi\left(t_0\right)\right) \geq M\left(S\beta, T\beta, t_0\right) * M\left(S\alpha, T\alpha, t_0\right). \tag{33}$$

From (32) and (33), we have

$$\begin{aligned}
M\left(S\alpha, T\alpha, \phi\left(t_0\right)\right) * M\left(S\beta, T\beta, \phi\left(t_0\right)\right) \\
\geq \left[M\left(S\alpha, T\alpha, t_0\right)\right]^2 * \left[M\left(S\beta, T\beta, t_0\right)\right]^2.
\end{aligned} \tag{34}$$

In general, for all $n \in \mathbb{N}$, we get

$$M\left(S\alpha, T\alpha, \phi^n\left(t_0\right)\right) * M\left(S\beta, T\beta, \phi^n\left(t_0\right)\right)$$

$$\geq \left[M\left(S\alpha, T\alpha, \phi^{n-1}\left(t_0\right)\right)\right]^2 * \left[M\left(S\beta, T\beta, \phi^{n-1}\left(t_0\right)\right)\right]^2$$

$$\geq \left[M\left(S\alpha, T\alpha, t_0\right)\right]^{2^n} * \left[M\left(S\beta, T\beta, t_0\right)\right]^{2^n}. \tag{35}$$

Then, we have

$$M\left(S\alpha, T\alpha, t\right) * M\left(S\beta, T\beta, t\right)$$

$$\geq \left[M\left(S\alpha, T\alpha, \sum_{p=n_0}^{\infty} \phi^p\left(t_0\right)\right)\right]$$

$$* \left[M\left(S\beta, T\beta, \sum_{p=n_0}^{\infty} \phi^p\left(t_0\right)\right)\right]$$

$$\geq \left[M\left(S\alpha, T\alpha, \phi^{n_0}\left(t_0\right)\right)\right]$$

$$* \left[M\left(S\beta, T\beta, \phi^{n_0}\left(t_0\right)\right)\right] \tag{36}$$

$$\geq \left[M\left(S\alpha, T\alpha, t_0\right)\right]^{2^{n_0}}$$

$$* \left[M\left(S\beta, T\beta, t_0\right)\right]^{2^{n_0}}$$

$$\geq \underbrace{(1-\mu) * (1-\mu) * \cdots * (1-\mu)}_{2^{2n_0}}$$

$$\geq 1 - \lambda.$$

So for any $\lambda > 0$, we obtain

$$M\left(S\alpha, T\alpha, t\right) * M\left(S\beta, T\beta, t\right) \geq 1 - \lambda, \tag{37}$$

for all $t > 0$, and hence $S\alpha = T\alpha$ and $S\beta = T\beta$. Therefore

$$S\alpha = T\alpha = A\left(\alpha, \beta\right) = B\left(\alpha, \beta\right),$$

$$S\beta = T\beta = A\left(\beta, \alpha\right) = B\left(\beta, \alpha\right). \tag{38}$$

Now we show that $S\alpha = \alpha$ and $S\beta = \beta$. Since $*$ is a t-norm of H-type, for any $\lambda > 0$, there exists an $\mu > 0$ such that

$$\underbrace{(1-\mu) * (1-\mu) * \cdots * (1-\mu)}_{p} \geq 1 - \lambda, \tag{39}$$

for all $p \in \mathbb{N}$.

Since $M(x, y, \cdot)$ is continuous and $\lim_{t \to +\infty} M(x, y, t) = 1$ for all $x, y \in X$, there exists $t_0 > 0$ such that $M(S\alpha, \alpha, t_0) \geq 1 - \mu$ and $M(S\beta, \beta, t_0) \geq 1 - \mu$.

On the other hand, since $\phi \in \Phi$, by condition (ϕ-3) we have $\sum_{n=1}^{\infty} \phi^n(t_0) < \infty$. Then for any $t > 0$, there exists $n_0 \in \mathbb{N}$ such that $t > \sum_{p=n_0}^{\infty} \phi^p(t_0)$. On using inequality (15) with $x = \alpha, y = \beta, u = x_n', v = y_n'$, we have

$$M\left(A\left(\alpha, \beta\right), B\left(x_n', y_n'\right), \phi\left(t_0\right)\right)$$

$$\geq M\left(S\alpha, Tx_n', t_0\right) * M\left(S\beta, Ty_n', t_0\right). \tag{40}$$

Letting $n \to \infty$, we obtain

$$M\left(S\alpha, \alpha, \phi\left(t_0\right)\right) \geq M\left(S\alpha, \alpha, t_0\right) * M\left(S\beta, \beta, t_0\right). \tag{41}$$

Similarly, we can get

$$M\left(S\beta, \beta, \phi\left(t_0\right)\right) \geq M\left(S\beta, \beta, t_0\right) * M\left(S\alpha, \alpha, t_0\right). \tag{42}$$

Consequently, from (41) and (42), we have

$$M\left(S\alpha, \alpha, \phi\left(t_0\right)\right) * M\left(S\beta, \beta, \phi\left(t_0\right)\right)$$

$$\geq \left[M\left(S\alpha, \alpha, t_0\right)\right]^2 * \left[M\left(S\beta, \beta, t_0\right)\right]^2. \tag{43}$$

In general, for all $n \in \mathbb{N}$, we get

$$M\left(S\alpha, \alpha, \phi^n\left(t_0\right)\right) * M\left(S\beta, \beta, \phi^n\left(t_0\right)\right)$$

$$\geq \left[M\left(S\alpha, \alpha, \phi^{n-1}\left(t_0\right)\right)\right]^2 * \left[M\left(S\beta, \beta, \phi^{n-1}\left(t_0\right)\right)\right]^2$$

$$\geq \left[M\left(S\alpha, \alpha, t_0\right)\right]^{2^n} * \left[M\left(S\beta, \beta, t_0\right)\right]^{2^n}. \tag{44}$$

Then, we have

$$M\left(S\alpha, \alpha, t\right) * M\left(S\beta, \beta, t\right)$$

$$\geq \left[M\left(S\alpha, \alpha, \sum_{p=n_0}^{\infty} \phi^p\left(t_0\right)\right)\right]$$

$$* \left[M\left(S\beta, \beta, \sum_{p=n_0}^{\infty} \phi^p\left(t_0\right)\right)\right]$$

$$\geq \left[M\left(S\alpha, \alpha, \phi^{n_0}\left(t_0\right)\right)\right]$$

$$* \left[M\left(S\beta, \beta, \phi^{n_0}\left(t_0\right)\right)\right] \tag{45}$$

$$\geq \left[M\left(S\alpha, \alpha, t_0\right)\right]^{2^{n_0}}$$

$$* \left[M\left(S\beta, \beta, t_0\right)\right]^{2^{n_0}}$$

$$\geq \underbrace{(1-\mu) * (1-\mu) * \cdots * (1-\mu)}_{2^{2n_0}}$$

$$\geq 1 - \lambda.$$

Therefore for any $\lambda > 0$, we obtain

$$M\left(S\alpha, \alpha, t\right) * M\left(S\beta, \beta, t\right) \geq 1 - \lambda, \tag{46}$$

for all $t > 0$ and so $S\alpha = \alpha$ and $S\beta = \beta$. Thus

$$\alpha = S\alpha = T\alpha = A\left(\alpha, \beta\right) = B\left(\alpha, \beta\right),$$

$$\beta = S\beta = T\beta = A\left(\beta, \alpha\right) = B\left(\beta, \alpha\right). \tag{47}$$

Finally, we assert that $\alpha = \beta$. Since $*$ is a t-norm of H-type, for any $\lambda > 0$, there exists an $\mu > 0$ such that

$$\underbrace{(1-\mu) * (1-\mu) * \cdots * (1-\mu)}_{p} \geq 1 - \lambda, \tag{48}$$

for all $p \in \mathbb{N}$.

Since $M(x, y, \cdot)$ is continuous and $\lim_{t \to +\infty} M(x, y, t) = 1$ for all $x, y \in X$, there exists $t_0 > 0$ such that $M(\alpha, \beta, t_0) \geq 1 - \mu$.

Also, since $\phi \in \Phi$, by condition (ϕ-3), we have $\sum_{n=1}^{\infty} \phi^n(t_0) < \infty$. Then for any $t > 0$, there exists $n_0 \in \mathbb{N}$ such that $t > \sum_{p=n_0}^{\infty} \phi^p(t_0)$. On using inequality (15) with $x = v = \alpha$, $y = u = \beta$, we have

$$M(A(\alpha, \beta), B(\beta, \alpha), \phi(t_0)) \geq M(S\alpha, T\beta, t_0) * M(S\beta, T\alpha, t_0), \tag{49}$$

and so

$$M(\alpha, \beta, \phi(t_0)) \geq M(\alpha, \beta, t_0) * M(\beta, \alpha, t_0). \tag{50}$$

Thus we have

$$M(\alpha, \beta, t) \geq M\left(\alpha, \beta, \sum_{p=n_0}^{\infty} \phi^p(t_0)\right)$$
$$\geq M(\alpha, \beta, \phi^{n_0}(t_0))$$
$$\geq [M(\alpha, \beta, t_0)]^{2^{n_0}} * [M(\beta, \alpha, t_0)]^{2^{n_0}} \tag{51}$$
$$\geq \underbrace{(1 - \mu) * (1 - \mu) * \cdots * (1 - \mu)}_{2^{2n_0}}$$
$$\geq 1 - \lambda,$$

which implies that $\alpha = \beta$. Therefore, we proved that there exists α in X such that

$$\alpha = S\alpha = T\alpha = A(\alpha, \alpha) = B(\alpha, \alpha). \tag{52}$$

The uniqueness of such a point follows immediately from inequality (15) and so we omit the details. □

Remark 15. The conclusion of Theorem 14 remains true if we substitute condition (a) with the following condition:

(a′) the pairs (A, S) and (B, T) are subcompatible and reciprocally continuous.

From Theorem 14, taking $A = B$ and $S = T$, we deduce the following natural result.

Corollary 16. *Let $(X, M, *)$ be a fuzzy metric space, where $*$ is a continuous t-norm of H-type such that $M(x, y, t) \to 1$ as $t \to \infty$, for all $x, y \in X$. Let $A : X \times X \to X$ and $S : X \to X$ be compatible and subsequentially continuous (alternately subcompatible and reciprocally continuous) mappings such that*

$$M(A(x, y), A(u, v), \phi(t)) \geq M(Sx, Su, t) * M(Sy, Sv, t), \tag{53}$$

for all $x, y, u, v \in X$, $\phi \in \Phi$ and $t > 0$. Then there exists a unique point α in X such that $\alpha = S\alpha = A(\alpha, \alpha)$.

Next, we illustrate our results providing the following examples.

Example 17. Let $X = [0, +\infty)$, $a * b = ab$ for all $a, b \in [0, 1]$ and $\psi(s) = s/(s + 1)$ for all $s \in \mathbb{R}^+$. Then $(X, M, *)$ is a fuzzy metric space, where

$$M(x, y, t) = [\psi(t)]^{|x-y|}, \tag{54}$$

for all $x, y \in X$ and $t > 0$. Let $\phi(s) = s/2$, and let the mappings $A : X \times X \to X, S : X \to X$ be defined as

$$A(x, y) = \begin{cases} 3x + 3y - 5, & \text{if } x, y \in (1, \infty), \\ \dfrac{x+y}{6}, & \text{otherwise,} \end{cases}$$
$$S(x) = \begin{cases} 3x - 2, & \text{if } x \in (1, \infty), \\ \dfrac{x}{6}, & \text{if } x \in [0, 1]. \end{cases} \tag{55}$$

In view of Definition 10, to prove compatibility, we have only to consider sequences $\{x_n\}$ and $\{y_n\}$ converging to zero from the right. In such case we have

$$\lim_{n \to \infty} A(x_n, y_n) = 0 = \lim_{n \to \infty} S(x_n),$$
$$\lim_{n \to \infty} A(y_n, x_n) = 0 = \lim_{n \to \infty} S(y_n). \tag{56}$$

Next, we get

$$\lim_{n \to \infty} A(Sx_n, Sy_n) = 0 = A(0, 0),$$
$$\lim_{n \to \infty} SA(x_n, y_n) = 0 = S(0),$$
$$\lim_{n \to \infty} A(Sy_n, Sx_n) = 0 = A(0, 0),$$
$$\lim_{n \to \infty} SA(y_n, x_n) = 0 = S(0). \tag{57}$$

Consequently

$$\lim_{n \to \infty} M(A(Sx_n Sy_n), SA(x_n, y_n), t) = 1,$$
$$\lim_{n \to \infty} M(A(Sy_n Sx_n), SA(y_n, x_n), t) = 1, \tag{58}$$

for all $t > 0$.

On the other hand, to prove subsequential continuity, in view of Definition 12, we have only to consider sequences $\{x_n\}$ and $\{y_n\}$ converging to one from the right. In such case we have

$$\lim_{n \to \infty} A(x_n, y_n) = 1 = \lim_{n \to \infty} S(x_n),$$
$$\lim_{n \to \infty} A(y_n, x_n) = 1 = \lim_{n \to \infty} S(y_n). \tag{59}$$

Also, note that, for the same sequences, we get

$$\lim_{n \to \infty} A(Sx_n, Sy_n) = 1 \neq A(1, 1),$$
$$\lim_{n \to \infty} SA(x_n, y_n) = 1 \neq S(1),$$
$$\lim_{n \to \infty} A(Sy_n, Sx_n) = 1 \neq A(1, 1),$$
$$\lim_{n \to \infty} SA(y_n, x_n) = 1 \neq S(1), \tag{60}$$

but

$$\lim_{n\to\infty} M\left(A\left(Sx_n, Sy_n\right), SA\left(x_n, y_n\right), t\right) = 1,$$
$$\lim_{n\to\infty} M\left(A\left(Sy_n, Sx_n\right), SA\left(y_n, x_n\right), t\right) = 1. \tag{61}$$

Thus, the mappings A and S are compatible as well as subsequentially continuous but not reciprocally continuous. Next, by a routine calculation, one can verify that condition (53) holds true. For instance, for all $t > 0$ and $x, y, u, v \in [0, 1]$, we have

$$M\left(A\left(x, y\right), A\left(u, v\right), \phi\left(t\right)\right)$$
$$= M\left(A\left(x, y\right), A\left(u, v\right), \left(\frac{t}{2}\right)\right)$$
$$= \left[\psi\left(\frac{t}{2}\right)\right]^{|x-u+y-v|/6}$$
$$\geq \left[\psi\left(\frac{t}{2}\right)\right]^{|x-u|/6} \cdot \left[\psi\left(\frac{t}{2}\right)\right]^{|y-v|/6}$$
$$= \left[\frac{t}{t+2}\right]^{|x-u|/6} \cdot \left[\frac{t}{t+2}\right]^{|y-v|/6} \tag{62}$$
$$\geq \left[\frac{t}{t+1}\right]^{|x-u|/6} \cdot \left[\frac{t}{t+1}\right]^{|y-v|/6}$$
$$= \left[\psi\left(t\right)\right]^{|x-u|/6} \cdot \left[\psi\left(t\right)\right]^{|y-v|/6}$$
$$= M\left(Sx, Su, t\right) \cdot M\left(Sy, Sv, t\right)$$
$$= M\left(Sx, Su, t\right) * M\left(Sy, Sv, t\right).$$

Therefore, all the conditions of **Corollary 16** are satisfied and $(0,0)$ is the unique common fixed point of the pair (A, S). It is noted that this example cannot be covered by those fixed point theorems which involve compatibility and reciprocal continuity both.

Example 18. In the setting of **Example 17** (besides retaining the rest), let $X = (-\infty, \infty)$, and let the mappings $A : X \times X \to X, S : X \to X$ be defined as

$$A\left(x, y\right) = \begin{cases} \dfrac{x+y}{4}, & \text{if } x, y \in (-\infty, 1), \\ 3x + 3y - 5, & \text{if } x, y \in [1, \infty), \\ \dfrac{x-y}{4}, & \text{if } x \in (-\infty, 1), \ y \in [1, \infty), \end{cases}$$

$$S\left(x\right) = \begin{cases} x + 1, & \text{if } x \in (-\infty, 1), \\ 3x - 2, & \text{if } x \in [1, \infty). \end{cases} \tag{63}$$

In view of Definitions 11 and 13, to prove reciprocal continuity and subcompatibility, we have only to consider sequences $\{x_n\}$ and $\{y_n\}$ converging to one from the right. For such

sequences, we get

$$\lim_{n\to\infty} A\left(x_n, y_n\right) = 1 = \lim_{n\to\infty} S\left(x_n\right),$$
$$\lim_{n\to\infty} A\left(y_n, x_n\right) = 1 = \lim_{n\to\infty} S\left(y_n\right). \tag{64}$$

Also, we deduce that

$$\lim_{n\to\infty} A\left(Sx_n, Sy_n\right) = 1 = A\left(1, 1\right),$$
$$\lim_{n\to\infty} SA\left(x_n, y_n\right) = 1 = S\left(1\right),$$
$$\lim_{n\to\infty} A\left(Sy_n, Sx_n\right) = 1 = A\left(1, 1\right),$$
$$\lim_{n\to\infty} SA\left(y_n, x_n\right) = 1 = S\left(1\right). \tag{65}$$

Therefore, we have

$$\lim_{n\to\infty} M\left(A\left(Sx_n, Sy_n\right), SA\left(x_n, y_n\right), t\right) = 1,$$
$$\lim_{n\to\infty} M\left(A\left(Sy_n, Sx_n\right), SA\left(y_n, x_n\right), t\right) = 1, \tag{66}$$

for all $t > 0$. Finally, to show that the mappings A and S are not compatible, it suffices to consider the particular sequences $\{x_n\} = \{1/n - 2\}_{n\in\mathbb{N}}$ and $\{y_n\} = \{1/3n - 2\}_{n\in\mathbb{N}}$ in X. In fact, in such case, we have

$$\lim_{n\to\infty} A\left(x_n, y_n\right) = -1 = \lim_{n\to\infty} S\left(x_n\right),$$
$$\lim_{n\to\infty} A\left(y_n, x_n\right) = -1 = \lim_{n\to\infty} S\left(y_n\right). \tag{67}$$

Next, we deduce that

$$\lim_{n\to\infty} A\left(Sx_n, Sy_n\right) = -\frac{1}{2} = A\left(-1, -1\right),$$
$$\lim_{n\to\infty} SA\left(x_n, y_n\right) = 0 = S\left(-1\right),$$
$$\lim_{n\to\infty} A\left(Sy_n, Sx_n\right) = -\frac{1}{2} = A\left(-1, -1\right),$$
$$\lim_{n\to\infty} SA\left(y_n, x_n\right) = 0 = S\left(-1\right). \tag{68}$$

Consequently, we obtain

$$\lim_{n\to\infty} M\left(A\left(Sx_n, Sy_n\right), SA\left(x_n, y_n\right), t\right) \neq 1,$$
$$\lim_{n\to\infty} M\left(A\left(Sy_n, Sx_n\right), SA\left(y_n, x_n\right), t\right) \neq 1, \tag{69}$$

for all $t > 0$. Thus, the mappings A and S are reciprocally continuous as well as subcompatible but not compatible. Next, by a routine calculation, one can verify that condition

(53) holds true. For instance, for all $t > 0$ and $x, y, u, v \in [1, \infty)$, we have

$$
\begin{aligned}
& M\left(A\left(x, y\right), A\left(u, v\right), \phi\left(t\right)\right) \\
&= M\left(A\left(x, y\right), A\left(u, v\right), \left(\frac{t}{2}\right)\right) \\
&= \left[\psi\left(\frac{t}{2}\right)\right]^{|3x-3u+3y-3v|} \\
&\geq \left[\psi\left(\frac{t}{2}\right)\right]^{3|x-u|} \cdot \left[\psi\left(\frac{t}{2}\right)\right]^{3|y-v|} \\
&= \left[\frac{t}{t+2}\right]^{3|x-u|} \cdot \left[\frac{t}{t+2}\right]^{3|y-v|} \\
&\geq \left[\frac{t}{t+1}\right]^{3|x-u|} \cdot \left[\frac{t}{t+1}\right]^{3|y-v|} \\
&= \left[\psi\left(t\right)\right]^{3|x-u|} \cdot \left[\psi\left(t\right)\right]^{3|y-v|} \\
&= M\left(Sx, Su, t\right) \cdot M\left(Sy, Sv, t\right) \\
&= M\left(Sx, Su, t\right) * M\left(Sy, Sv, t\right).
\end{aligned}
\tag{70}
$$

Therefore, all the conditions of Corollary 16 are satisfied, and $(1, 1)$ is the unique common fixed point of the pair (A, S). It is also noted that this example cannot be covered by those fixed point theorems which involve compatibility and reciprocal continuity both.

Remark 19. The conclusions of Theorem 14 and Corollary 16 remain true if we assume $\phi(s) = ks$, where $k \in (0, 1)$.

4. Conclusion

Theorem 14 is proved for two pairs of compatible and subsequentially continuous (alternately subcompatible and reciprocally continuous) mappings in fuzzy metric spaces, wherein conditions on completeness (or closedness) of the underlying space (or subspaces) together with conditions on continuity in respect to anyone of the involved mappings are relaxed. Theorem 14 improves the results of Jain et al. [39, Theorem 3.2, Corollary 3.2, Theorem 3.3, Theorem 3.4, Theorem 4.1] and Hu [34, Theorem 1]. A natural result is also obtained for a pair of mappings (see Corollary 16). Finally, Examples 17 and 18 are furnished to demonstrate the usefulness of Corollary 16. In view of Remark 19, Theorem 14 and Corollary 16 improve the results of Sedghi et al. [32, Theorem 2.5, Corollary 2.6] and Jain et al. [39, Corollary 3.1].

Acknowledgments

References

[1] L. A. Zadeh, "Fuzzy sets," *Information and Computation*, vol. 8, pp. 338–353, 1965.

[2] I. Kramosil and J. Michalek, "Fuzzy metric and statistical metric spaces," *Kybernetika*, vol. 11, no. 5, pp. 336–344, 1975.

[3] M. Grabiec, "Fixed points in fuzzy metric spaces," *Fuzzy Sets and Systems*, vol. 27, no. 3, pp. 385–389, 1988.

[4] P. Balasubramaniam, S. Muralisankar, and R. P. Pant, "Common fixed points of four mappings in a fuzzy metric space," *Journal of Fuzzy Mathematics*, vol. 10, no. 2, pp. 379–384, 2002.

[5] Y. J. Cho, "Fixed points in fuzzy metric spaces," *Journal of Fuzzy Mathematics*, vol. 5, no. 4, pp. 949–962, 1997.

[6] J.-X. Fang, "On fixed point theorems in fuzzy metric spaces," *Fuzzy Sets and Systems*, vol. 46, no. 1, pp. 107–113, 1992.

[7] A. George and P. Veeramani, "On some results in fuzzy metric spaces," *Fuzzy Sets and Systems*, vol. 64, no. 3, pp. 395–399, 1994.

[8] P. V. Subrahmanyam, "A common fixed point theorem in fuzzy metric spaces," *Information Sciences*, vol. 83, no. 3-4, pp. 109–112, 1995.

[9] R. Vasuki, "Common fixed points for R-weakly commuting maps in fuzzy metric spaces," *Indian Journal of Pure and Applied Mathematics*, vol. 30, no. 4, pp. 419–423, 1999.

[10] S. N. Mishra, N. Sharma, and S. L. Singh, "Common fixed points of maps on fuzzy metric spaces," *International Journal of Mathematics and Mathematical Sciences*, vol. 17, no. 2, pp. 253–258, 1994.

[11] G. Jungck, "Compatible mappings and common fixed points," *International Journal of Mathematics and Mathematical Sciences*, vol. 9, no. 4, pp. 771–779, 1986.

[12] B. Singh and S. Jain, "Semicompatibility and fixed point theorems in fuzzy metric space using implicit relation," *International Journal of Mathematics and Mathematical Sciences*, vol. 2005, no. 16, pp. 2617–2629, 2005.

[13] H. Bouhadjera and C. Godet-Thobie, "Common fixed point theorems forpairs of subcompatible maps," http://arxiv.org/abs/0906.3159.

[14] H. Bouhadjera and C. Godet-Thobie, "Common fixed point theorems for pairs of subcompatible maps," http://arxiv.org/abs/0906.3159v2.

[15] D. Gopal and M. Imdad, "Some new common fixed point theorems in fuzzy metric spaces," *Annali dell'Universita di Ferrara*, vol. 57, no. 2, pp. 303–316, 2011.

[16] M. Imdad, J. Ali, and M. Tanveer, "Remarks on some recent metrical common fixed point theorems," *Applied Mathematics Letters*, vol. 24, no. 7, pp. 1165–1169, 2011.

[17] M. Abbas, I. Altun, and D. Gopal, "Common fixed point theorems for non compatible mappings in fuzzy metric spaces," *Bulletin of Mathematical Analysis and Applications*, vol. 1, no. 2, pp. 47–56, 2009.

[18] C. di Bari and C. Vetro, "A fixed point theorem for a family of mappings in a fuzzy metric space," *Rendiconti del Circolo Matematico di Palermo*, vol. 52, no. 2, pp. 315–321, 2003.

[19] S. Chauhan, S. Bhatnagar, and S. Radenović, "Common fixed point theorems for weakly compatible mappings in fuzzy metric spaces," *Le Matematiche*, vol. 68, no. 1, pp. 87–98, 2013.

[20] M. Imdad and J. Ali, "Some common fixed point theorems in fuzzy metric spaces," *Mathematical Communications*, vol. 11, no. 2, pp. 153–163, 2006.

[21] S. Kumar and S. Chauhan, "Common fixed point theorems using implicit relation and property (E.A) in fuzzy metric spaces," *Annals of Fuzzy Mathematics and Informatics*, vol. 5, no. 1, pp. 107–114, 2013.

[22] D. Miheţ, "A Banach contraction theorem in fuzzy metric spaces," *Fuzzy Sets and Systems*, vol. 144, no. 3, pp. 431–439, 2004.

[23] D. Miheţ, "Fixed point theorems in fuzzy metric spaces using property E.A," *Nonlinear Analysis*, vol. 73, no. 7, pp. 2184–2188, 2010.

[24] D. O'Regan and M. Abbas, "Necessary and sufficient conditions for common fixed point theorems in fuzzy metric space," *Demonstratio Mathematica*, vol. 42, no. 4, pp. 887–900, 2009.

[25] B. D. Pant and S. Chauhan, "Common fixed point theorems for two pairs of weakly compatible mappings in Menger spaces and fuzzy metric spaces," *Scientific Studies and Research*, vol. 21, no. 2, pp. 81–96, 2011.

[26] C. Vetro and P. Vetro, "Common fixed points for discontinuous mappings in fuzzy metric spaces," *Rendiconti del Circolo Matematico di Palermo*, vol. 57, no. 2, pp. 295–303, 2008.

[27] T. G. Bhaskar and V. Lakshmikantham, "Fixed point theorems in partially ordered metric spaces and applications," *Nonlinear Analysis*, vol. 65, no. 7, pp. 1379–1393, 2006.

[28] V. Lakshmikantham and L. Ćirić, "Coupled fixed point theorems for nonlinear contractions in partially ordered metric spaces," *Nonlinear Analysis*, vol. 70, no. 12, pp. 4341–4349, 2009.

[29] D. Đorić, Z. Kadelburg, and S. Radenović, "Coupled fixed point results for mappings without mixed monotone property," *Applied Mathematics Letters*, vol. 25, no. 11, pp. 1803–1808, 2012.

[30] Z. Golubović, Z. Kadelburg, and S. Radenović, "Coupled coincidence points of mappings in ordered partial metric spaces," *Abstract and Applied Analysis*, vol. 2012, Article ID 192581, 18 pages, 2012.

[31] Z. Kadelburg and S. Radenović, "Coupled fixed point results under TVS-cone metric and *w*-cone-distance," *Advances in Fixed Point Theory*, vol. 2, no. 1, pp. 29–46, 2012.

[32] S. Sedghi, I. Altun, and N. Shobe, "Coupled fixed point theorems for contractions in fuzzy metric spaces," *Nonlinear Analysis*, vol. 72, no. 3-4, pp. 1298–1304, 2010.

[33] J.-X. Fang, "Common fixed point theorems of compatible and weakly compatible maps in Menger spaces," *Nonlinear Analysis*, vol. 71, no. 5-6, pp. 1833–1843, 2009.

[34] X.-Q. Hu, "Common coupled fixed point theorems for contractive mappings in fuzzy metric spaces," *Fixed Point Theory and Applications*, vol. 2011, Article ID 363716, 14 pages, 2011.

[35] X.-H. Zhu and J.-Z. Xiao, "Note on "Coupled fixed point theorems for contractions in fuzzy metric spaces"," *Nonlinear Analysis*, vol. 74, no. 16, pp. 5475–5479, 2011.

[36] B. Schweizer and A. Sklar, *Probabilistic Metric Spaces*, North-Holland Series in Probability and Applied Mathematics, North-Holland, New York, NY, USA, 1983.

[37] O. Hadžić and E. Pap, *Fixed Point Theory in Probabilistic Metric Spaces*, vol. 536 of *Mathematics and Its Applications*, Kluwer Academic, Dodrecht, The Netherlands, 2001.

[38] R. P. Pant and R. K. Bisht, "Common fixed point theorems under a new continuity condition," *Annali dell'Universitá di Ferrara*, vol. 58, no. 1, pp. 127–141, 2012.

[39] M. Jain, S. Kumar, and R. Chugh, "Coupled fixed point theorems for weak compatible mappings in fuzzy metric spaces," *Annals of Fuzzy Mathematics and Informatics*, vol. 5, no. 2, pp. 321–336, 2013.

Research Article

Generating Suitable Basic Functions Used in Image Reconstruction by F-Transform

Pavel Vlašánek

Department of Informatics and Computers, University of Ostrava, 30. Dubna 22, 701 03 Ostrava, Czech Republic

Correspondence should be addressed to Pavel Vlašánek; pavel.vlasanek@osu.cz

Received 5 July 2013; Accepted 12 July 2013

Academic Editor: Salvatore Sessa

Image reconstruction technique based on F-transform uses clearly defined basic functions. These functions have strong impact on the quality of reconstruction. We can use some predefined shape and radius, but also we can create a new one from the scratch. The aim of this paper is to analyze the creating process and based on that find best basic function for input set of damaged testing images.

1. Introduction

Image reconstruction aims at recovering damaged parts. In real situation this damage can be caused by various sources on various surfaces. Input information has to be digitalized as a first step and after that divided on damaged and nondamaged parts. Typical situation lays on photography. We can distinguish among many types of damage like stains, scratches, text, or noise. We can say that every kind of damage covers typical way of damaging process. Unwanted time or date stamp is covered by *text*. Scratches, cracks, and folds are covered by *inpaint*. These are shown in Figure 1 which includes also *noise*.

Target of reconstruction is removing damaged parts from input image and replacing them by the parts with recomputed values. These values are computed from the neighborhood ones. The technique mentioned in this paper is based on F-transform which brings particular way of valuation neighborhood pixels and their usage in the computation [1, 2]. Other methods [3, 4] differ by the choice at the technique.

In this paper, we will focus on the valuation part of the computation. Quality of reconstruction will be measured by RMSE value (RMSE stands for the root mean square error). In Figure 2 you can see damaged input images and reconstructed ones with usage of the ideal basic function described later. We will analyse influence of changing parameter on target quality.

2. F-Transform

In image reconstruction, a discrete version of the F-transform is used. Details can be seen in [5, 6]. In this section two-dimensional (2D) variant and also conditions for proper functioning will be briefly introduced.

2.1. Fuzzy Partition with Ruspini Condition. Let $x_1 < \cdots < x_n$ be fixed nodes within $[a, b]$ such that $x_1 = a$, $x_n = b$ and $n \geq 2$. We say that the fuzzy sets $A_1, \ldots, A_n$, identified with their membership functions defined on $[a, b]$, establish a fuzzy partition with Ruspini condition of $[a, b]$ if they fulfill the following conditions for $k = 1, \ldots, n$:

(1) A_k: $[a, b] \rightarrow [0, 1]$, $A_k(x_k) = 1$;

(2) $A_k(x) = 0$ if $x \notin (x_{k-1}, x_{k+1})$, where for uniformity of notation, we set $x_0 = a$ and $x_{n+1} = b$;

(3) $A_k(x)$ is continuous;

(4) $A_k(x)$, for $k = 2, \ldots, n$, increases on $[x_{k-1}, x_k]$, and $A_k(x)$, for $k = 1, \ldots, n - 1$, strictly decreases on $[x_k, x_{k+1}]$;

(5) for all $x \in [a, b]$,

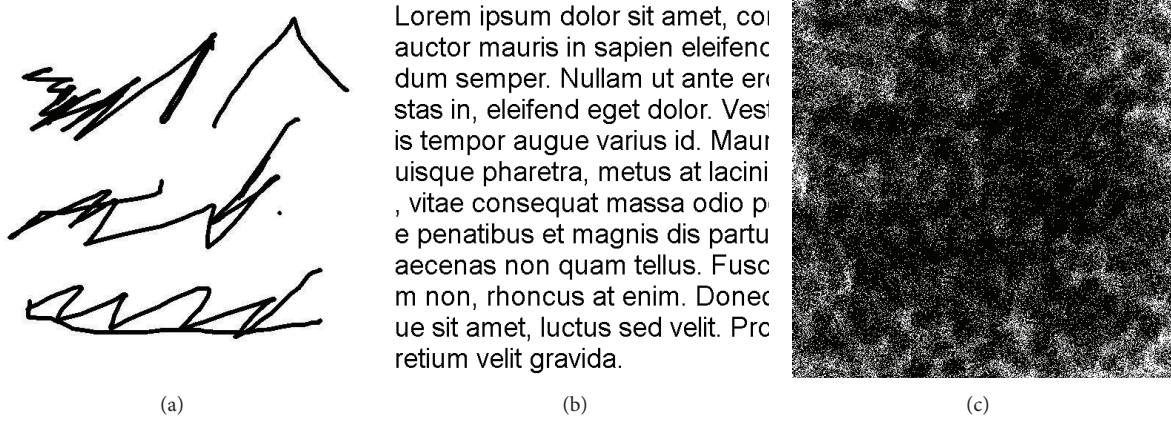$$\sum_{k=1}^{n} A_k(x) = 1. \tag{1}$$

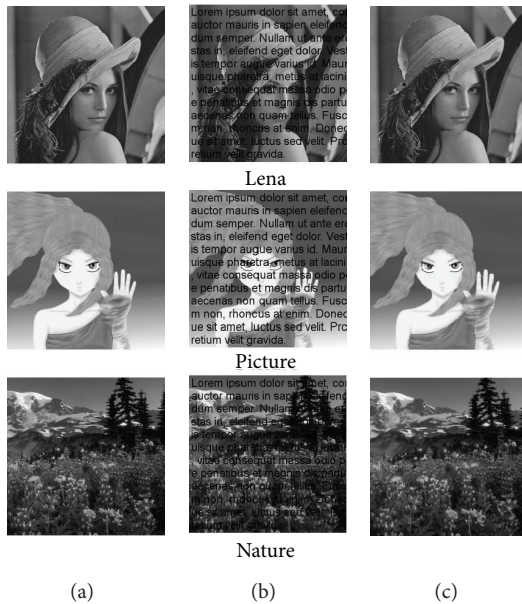FIGURE 1: (a) Inpaint damage; (b) text damage; (c) noise damage.

FIGURE 2: (a) Original image; (b) damaged image; (c) reconstructed image.

The condition (1) is known as the *Ruspini condition*. The membership functions $A_1, \ldots, A_n$ are called *basic functions*. A point $x \in [a, b]$ is *covered* by basic function A_k if $A_k(x) > 0$.

2.2. Shape of the Basic Function. The shape of the basic functions is not predetermined, and therefore, it can be chosen according to additional requirements (e.g., smoothness). Let us give examples of various fuzzy partitions with the Ruspini condition. In Figure 3, two such partitions with triangular and cosine basic functions are shown. The formulas given below represent generic fuzzy partitions with the Ruspini condition and triangular functions:

$$A_1(x) = \begin{cases} 1 - \dfrac{(x - x_1)}{h_1}, & x \in [x_1, x_2], \\ 0, & \text{otherwise}, \end{cases}$$

$$A_k(x) = \begin{cases} \dfrac{(x - x_{k-1})}{h_{k-1}}, & x \in [x_{k-1}, x_k], \\ 1 - \dfrac{(x - x_k)}{h_k}, & x \in [x_k, x_{k+1}], \\ 0, & \text{otherwise}, \end{cases}$$

$$A_n(x) = \begin{cases} \dfrac{(x - x_{n-1})}{h_{n-1}}, & x \in [x_{n-1}, x_n], \\ 0, & \text{otherwise}, \end{cases} \tag{2}$$

where $k = 2, \ldots, n - 1$ and $h_k = x_{k+1} - x_k$.

We say that a Ruspini partition of $[a, b]$ is *h-uniform* if its nodes $x_1, \ldots, x_n$, where $n \geq 3$, are h-equidistant; that is, $x_k = a + h(k - 1)$, for $k = 1, \ldots, n$, where $h = (b - a)/(n - 1)$, and two additional properties are met:

(6) $A_k(x_k - x) = A_k(x_k + x)$, for all $x \in [0, h]$, $k = 2, \ldots, n - 1$;

(7) $A_k(x) = A_{k-1}(x - h)$, for all $k = 2, \ldots, n - 1$ and $x \in [x_k, x_{k+1}]$, and $A_{k+1}(x) = A_k(x - h)$, for all $k = 2, \ldots, n - 1$ and $x \in [x_k, x_{k+1}]$.

An h-uniform fuzzy partition of $[a, b]$ can be determined by the so called *generating function* A_0: $[-1, 1] \rightarrow [0, 1]$, which is assumed to be *even* (The function A_0: $[-1, 1] \rightarrow \mathbb{R}$ is even if for all $x \in [0, 1]$, $A_0(-x) = A_0(x)$), continuous, have a bell shape, and fulfill $A_0(0) = 1$. Basic functions A_k of an h-uniform fuzzy partition with generating function A_0 are shifted copies of A_0 in the sense that

$$A_1(x) = \begin{cases} A_0\left(\dfrac{x - x_1}{h}\right), & x \in [x_1, x_2], \\ 0, & \text{otherwise}, \end{cases} \tag{3}$$
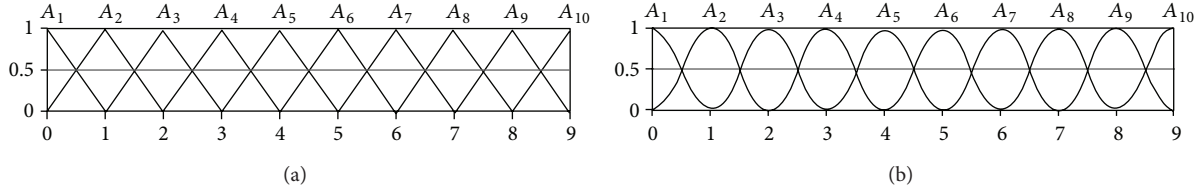
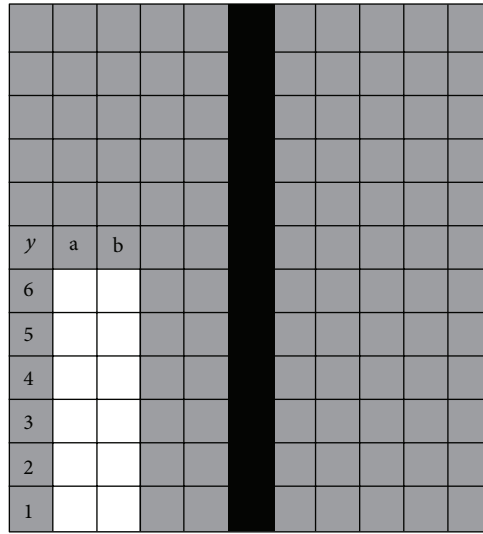FIGURE 3: (a) Ruspini partitions with triangular basic function; (b) Ruspini partitions with cosine basic function.

FIGURE 4: Template for basic function definition.

and for $k = 2, \ldots, n-1$,

$$
A_k(x) = \begin{cases} A_0\left(\dfrac{x - x_k}{h}\right), & x \in [x_{k-1}, x_{k+1}], \\ 0, & \text{otherwise}, \end{cases}
$$

$$
A_n(x) = \begin{cases} A_0\left(\dfrac{x - x_n}{h}\right), & x \in [x_n - 1, x_n], \\ 0, & \text{otherwise}. \end{cases} \tag{4}
$$

As an example, we notice that the function $A_0(x) = 1 - |x|$ is a generating function for any h-uniform triangular partition. In the sequel, we will be using h-uniform fuzzy partitions only and refer to h as to a *radius* of partition [7].

2.3. Discrete 2D F-Transform.

We say that the $n \times m$-matrix of real numbers $[U_{kl}]$ is called *the (discrete) F-transform* of u with respect to $\{A_1, \ldots, A_n\}$ and $\{B_1, \ldots, B_m\}$ if for all $k = 1, \ldots, n, \ l = 1, \ldots, m,$

$$
U_{kl} = \frac{\sum_{j=1}^{M} \sum_{i=1}^{N} u\left(p_i, q_j\right) A_k\left(p_i\right) B_l\left(q_j\right)}{\sum_{j=1}^{M} \sum_{i=1}^{N} A_k\left(p_i\right) B_l\left(q_j\right)}. \tag{5}
$$

The elements U_{kl} are called components of the F-transform.

The *inverse F-transform* is defined as follows:

$$
\widehat{u}(i, j) = \sum_{k=1}^{n} \sum_{l=1}^{m} U_{kl} A_k(i) B_l(j). \tag{6}
$$

We use discrete basic functions A_k and B_l. Our results show that sufficient image reconstruction is enough to use maximal radius 4. Discrete basic function with respect to Ruspini condition is building on top of template in Figure 4.

You can see white squares in Figure 4. These squares can be marked as parts of the basic function. One marked per column. After that is automatically computed mirrored part of the basic function as can be seen in Figure 5. We choose $y = 4$ for the column a. Value in column 10 is the same, and because of Ruspini condition, values in columns 5 and 7 are easily computable as

$$
f(y_5) = 1 - f(y_a),
$$
$$
f(y_7) = 1 - f(y_a) = f(y_5). \tag{7}
$$

Because of using Ruspini condition, we can use copies of the basic function for covering the whole range. Height of the template determines values $f(y)$ on the y axis. For better usability we choose value 0 for first row, 1 for last one, and twice 0.5 on the middle. Two basic functions with marked values can be seen in Figure 6.

(a)   (b)
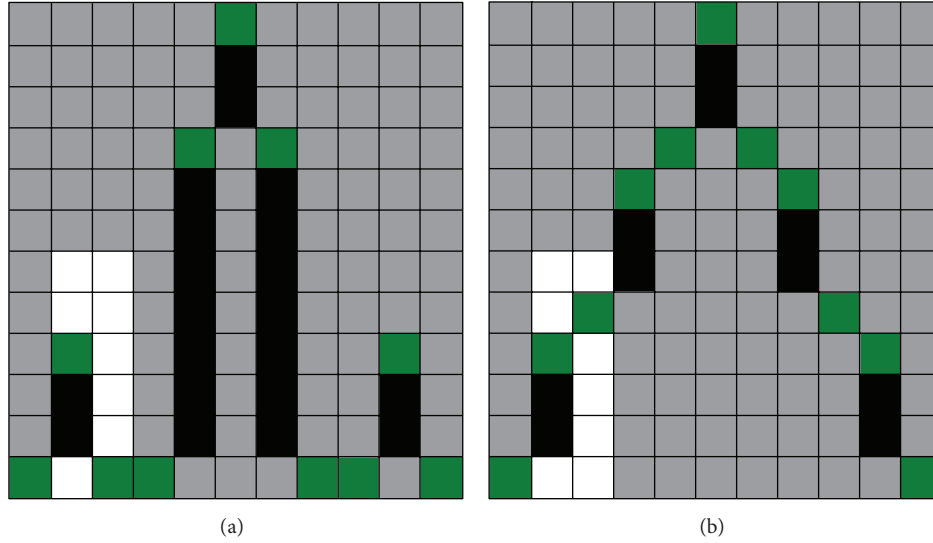
FIGURE 5: (a) Result after selection of fourth pixel in a column; (b) result after selection of fifth pixel in b column.
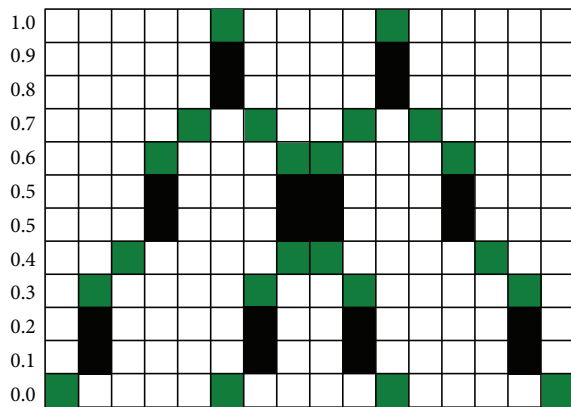

FIGURE 6: Template for basic function definition.

The overlapping part of basic functions have functional values equal 1 in each column. For better visualization, black vertical lines are also plotted.

3. Influence of Basic Functions

Shapes of the basic functions can be *nondecreasing*, *oscillating*, or *nonincreasing*. Differences and influences on computation are described in [8]. We choose basic functions with radius 2 in the first step of reconstruction and radius 4 in the second step because of fully sufficient usage on the input set of testing images. In this paper, we focus on building shape of basic function step by step based on results provided by RMSE. We identified two ways of this process which will be demonstrated on template in Figure 4 where max = 6.

Column by Column. Find the best value for current column and continue with next column:

(1) choose radius $r = 2$,

(2) choose active column as $c = $ "a,"

(3) choose current row as $y = 1$,

(4) based on those values create a basic function by mirroring and with respect to Ruspini condition formula (7),

(5) use the basic function for image reconstruction,

(6) compare reconstructed image with original undamaged one by RMSE,

(7) if $y = $ max, then $r = 4$, $c = $ "b" and continue by step 3,

(8) change current row as $y = y + 1$,

(9) continue by step 4.

Radius by Radius. Find the best value for current radius and continue with next radius:

(1) choose current radius as $r = 2$,

(2) choose current column as $c = $ "a,"

(3) choose current row as $y = 1$,

(4) based on those values create a basic function,

(5) use the basic function for image reconstruction,

(6) compare reconstructed image with the original undamaged by RMSE,

(7) if $y = $ max and $r = 4$, then $c = $ "b" and continue by step 3,

(8) if $y = $ max, then $r = 4$ and continue by step 3,

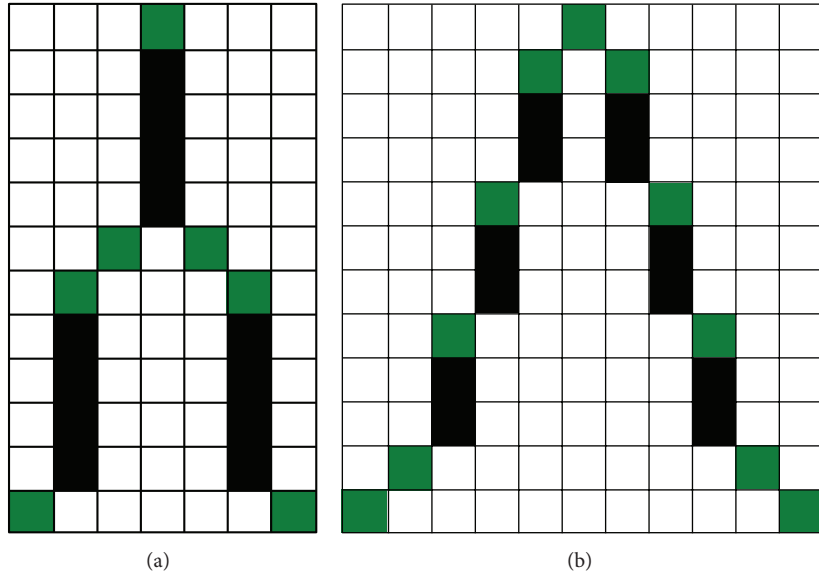(9) choose current row as $y = y + 1$,

(10) continue by step 4.

Figure 7: (a) Basic function for radius 2; (b) basic function for radius 4.

Table 1: RMSE values of the *column by column* basic function creation.

y	a	b	a	b	a	b
	Lena		Picture		Nature	
1	62.99	5.16	46.72	4.01	71.25	7.55
2	49.99	5.04	36.63	3.89	56.39	7.39
3	49.98	4.97	36.62	3.82	56.37	7.30
4	49.97	4.93	36.62	3.79	56.36	7.27
5	49.97	4.92	36.61	3.80	56.35	7.27
6	49.96	4.95	36.61	3.84	56.35	7.32

Table 2: RMSE values of the *radius by radius* basic function creation.

a/b	1	2	3	4	5	6
			Lena			
1	6.12	5.71	5.58	5.51	5.50	5.52
2	5.16	4.97	4.85	4.79	4.78	4.81
3	5.12	4.96	4.86	4.81	4.80	4.83
4	5.11	4.97	4.88	4.83	4.83	4.86
5	5.13	5.00	4.92	4.87	4.87	4.90
6	5.16	5.04	5.97	4.93	4.92	4.95
			Picture			
1	4.93	4.32	4.21	4.16	4.15	4.19
2	3.93	3.76	3.65	3.61	3.61	3.65
3	3.91	3.76	3.67	3.63	3.64	3.68
4	3.92	3.79	3.71	3.67	3.68	3.72
5	3.96	3.83	3.76	3.73	3.73	3.77
6	4.01	3.89	3.82	3.80	3.80	3.84
			Nature			
1	8.50	7.68	7.45	7.33	7.30	7.33
2	7.63	7.33	7.16	7.07	7.06	7.10
3	7.53	7.30	7.15	7.09	7.09	7.13
4	7.50	7.30	7.18	7.13	7.14	7.19
5	7.51	7.34	7.23	7.19	7.20	7.25
6	7.55	7.39	7.30	7.27	7.27	7.32

First way *column by column* is computed in Table 1. You can see that there is for column a best RMSE value for $y = 6$. It means that we choose sixth row for column a. Next column b is the best RMSE value in row $y = 5$ for the *Lena* and *Nature* images and $y = 4$ for the *Picture* image. We choose basic function with values $y = 6$ for column a and $y = 5$ for column b. This function is in Figure 8.

Second way of basic function creation *radius by radius* is computed in Table 2. From the table comes that the best value is $y = 2$ for a and $y = 5$ for column b. This basic function is shown in Figure 7.

4. Conclusion

As a result we can say that step by step process converges to oscillating or linear shape. *Column by column* way is the best solution oscillating basic function. Value $y = 6$ for column a and $y = 5$ for column b provides RMSE values 4.92 for *Lena*, 3.80 for *Picture*, and 7.27 for *Nature*. Because of very close results for *Picture* image between $b = 4$ and $b = 5$, we choose value $b = 5$ for all of them. *Radius by radius* is the best linear function with $y = 2$ for column a and $y = 5$ for column b. For *Lena* RMSE is equal to 4.78, for *Picture* is equal to 3.61, and for *Nature* is equal to 7.06.
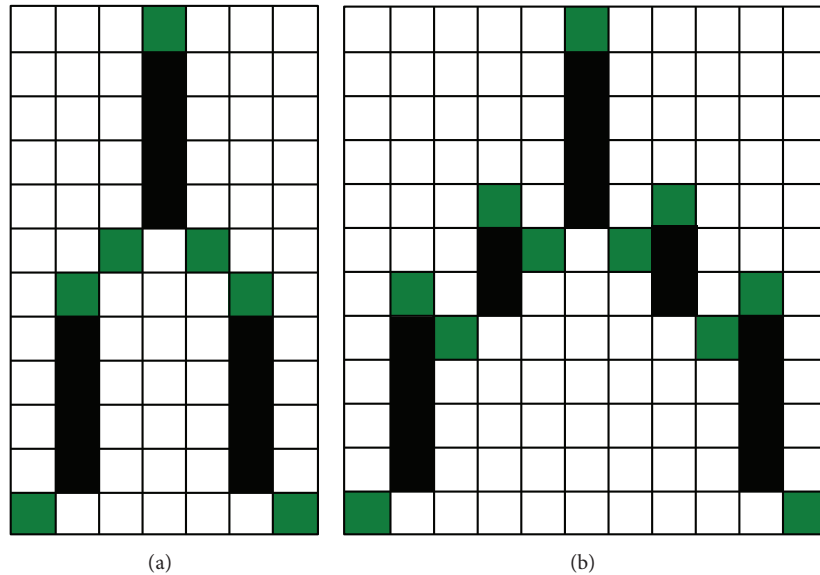
(a)   (b)

FIGURE 8: (a) Basic function for radius 2; (b) basic function for radius 4.

Acknowledgment

References

[1] P. Vlasanek, I. Perfilieva, and M. Wrublova, "Fuzzy transform for image reconstruction, Uncertainty modeling in knowledge engineering and decision making," in *Proceedings of the 10th International FLINS Conference*, pp. 615–620, World Scientific, Istanbul, Turkey, August 2012.

[2] P. Vlasanek and I. Perfilieva, "Image reconstruction with usage of the F-Transform," in *Proceedings of the Advances in Intelligent Systems and Computing, Interna- tional Joint Conference (CISIS'12-ICEUTE'12-SOCO '12)*, A. Herrero, V. Snášel, A. Abraham et al., Eds., vol. 189, pp. 507–514, Springer, 2012.

[3] J. A. Parker, R. V. Kenyon, and D. E. Troxel, "Comparison of interpolating methods for image resampling," *IEEE Transactions on Medical Imaging*, vol. MI-2, no. 1, pp. 31–39, 1983.

[4] K. Uhlir and V. Skala, "Radial basis function use for the restoration of damaged images," in *Computer Vision and Graphics*, K. Wojciechowski, B. Smolka, H. Palus et al., Eds., vol. 32, pp. 839–844, Kluwer Academic, 2006.

[5] F. Di Martino, V. Loia, I. Perfilieva, and S. Sessa, "An image coding/decoding method based on direct and inverse fuzzy transforms," *International Journal of Approximate Reasoning*, vol. 48, no. 1, pp. 110–131, 2008.

[6] I. Perfilieva, "Fuzzy transforms: theory and applications," *Fuzzy Sets and Systems*, vol. 157, no. 8, pp. 993–1023, 2006.

[7] I. Perfilieva and P. Vlasanek, Image Reconstruction by means of F-transform, Elsevier Editorial System for Knowledge-Based Systems, 2013.

[8] P. Vlasanek and I. Perfilieva, "Influence of various types of basic functions on image reconstruction using F-transform," *European Society for Fuzzy Logic and Technology*. In press.

Research Article

Coding B-Frames of Color Videos with Fuzzy Transforms

Ferdinando Di Martino and Salvatore Sessa

Università degli Studi di Napoli Federico II, Dipartimento di Architettura, Via Toledo 402, 80134 Napoli, Italy

Correspondence should be addressed to Salvatore Sessa; sessa@unina.it

Received 24 May 2013; Accepted 26 June 2013

Academic Editor: Irina Perfilieva

We use a new method based on discrete fuzzy transforms for coding/decoding frames of color videos in which we determine dynamically the GOP sequences. Frames can be differentiated into intraframes, predictive frames, and bidirectional frames, and we consider particular frames, called Δ-frames (resp., R-frames), for coding P-frames (resp., B-frames) by using two similarity measures based on Lukasiewicz t-norm; moreover, a preprocessing phase is proposed to determine similarity thresholds for classifying the above types of frame. The proposed method provides acceptable results in terms of quality of the reconstructed videos to a certain extent if compared with classical-based F-transforms method and the standard MPEG-4.

1. Introduction

A video can be considered as a sequence of frames of sizes $N \times M$; a frame is an image that can be compressed by using a lossy compression method. We can classify each frame as intraframe (for short, I-frame), predictive frame (for short, P-frame), and bidirectional frame (for short, B-frame) which is more compressible than I-frame. A B-frame can be predicted or interpolated from an earlier and/or later frame. In order to avoid a growing propagation error, a B-frame is not used as a reference to make further predictions in most encoding standards except in AVC [1]. A frame can be considered as a P-frame if it is "similar" to the previous I-frame in the frame sequence; otherwise, it must be considered as a new I-frame. This similarity relation between a P-frame and the previous I-frame is fundamental in video-compression processes because a P-frame has values in its pixels very close to the pixels of the previous I-frame. This suggests to define a frame containing differences between a P-frame and the previous I-frame, called Δ-frame which has a low quantity of information and hence it can be coded with a low compression rate. A P-frame is decoded via the previous I-frame and the Δ-frame. In the MPEG-4 method [2, 3], that adopts the JPEG technique [4] for coding/decoding frames, the I-frames, P-frames, and B-frames are arranged in a Group of Picture (for short, GOP) sequence. A B-frame

is reconstructed by using either the previous or successive I-frame. Here the results of [5] are improved by using a technique based on F-transforms for coding B-frames. For convenience, we assume that the first frame of a video is an I-frame. We assign an ID number to each frame of the video. Then we can say that the kth frame is a B-frame or a P-frame if it is "very similar" to the previous ith I-frame in the sense that its similarity $\mathrm{Sim}(i, k)$ a parameter defined on the Lukasiewicz t-norm (see formula (12)) is greater than a threshold value $\mathrm{Sim}P$ [5]; otherwise the kth frame is assumed to be a new I-frame as the first frame of the successive GOP sequence.

The first algorithm is used for determining the GOP sequences; the second algorithm is used for determining the type of P-frame or B-frame. The first frame of the GOP sequence is always an I-frame and the last frame is a P-frame. The function "analyze GOP sequence (ID1, ID2)" reported in Algorithm 1 describes this process, where ID1 is the ID of the first I-frame and ID2 is the ID of the last P-frame in the GOP sequence. This function is used for determining if the kth frame in the GOP sequence, where $\mathrm{ID1} < k < \mathrm{ID2}$, is a B-frame or a P-frame. We define a threshold similarity $\mathrm{Sim}B$, and we compare it with the frame whose ID is formed from the integer $[Ms]$ contained in the mean Ms of the previous I-frame or P-frame and the kth frame by obtaining a similarity value $\mathrm{Sim}(k, [Ms])$. In the array element $\mathrm{NP}[k]$ we insert the ID number of the last frame after the kth frame for which

$\mathrm{Sim}(k, [Ms]) < \mathrm{Sim}B$ holds. The variable i contains the ID number of the previous I-frame or P-frame; it is initially called ID1; the variable w points to the last frame in the GOP sequence; it is called ID2.

Algorithm 1 (analyze GOP sequence (ID1, ID2)). Pseudo-code for determining a GOP sequence

(1) i = ID of the first I-frame $//i$ is the ID of first frame of the video

(2) w = number of frames $//w$ is the ID of the last P-frame of the video

(3) $k = i + 1$

(4) IF $k < w$

(5) Calculate the similarity $\mathrm{Sim}(i, k)$ between the kth frame and the ith frame

(6) If $\mathrm{Sim}(i, k) < \mathrm{Sim}P$,

    (a) the kth frame is a B-frame or a P-frame and is inserted in the GOP sequence

    (b) $k = k + 1$

(7) Else

    (a) analyse GOP sequence $(i, k - 1)$

    (b) $i = k$

    (c) go to (3)

(8) End.

Algorithm 2. Pseudo-code for determining type of frames

(1) i = ID1$//i$ is the ID of the first frame of the GOP sequence

(2) w = ID2$//w$ is the ID of the last P-frame of the GOP sequence

(3) For each k in $[i + 1, w - 1]$

    $\mathrm{NP}[k] = k //\mathrm{Initialize\ NP}[k]$

(4) $s = k + 1$

(5) Create the $[Ms]$th frame as a new frame whose normalized pixels are obtained as the mean between the normalized pixels of the ith and sth frames

(6) Calculate the similarity $\mathrm{Sim}(k, [Ms])$ between the kth and $[Ms]$th frames. If $\mathrm{Sim}(k, [Ms]) < \mathrm{Sim}B$,

    (a) $\mathrm{NP}[k] = s - 1$

    (b) Else $s = s + 1$

    (c) go to step (6)

(7) next for

(8) $\mathrm{NPMin} = \min(\mathrm{NP}[k])$

(9) The frames between the ith and NPMin-th frames are labelled as B-frames

(10) The NPMin-th frame is labelled as a P-frame

(11) If NPmin $< w$ then

    (a) i = NPMin,

    (b) go to step (2)

(12) End.

In our approach we determine a GOP sequence at each step. The frame after the last P-frame is the I-frame of the new GOP sequence. After determining the GOP sequences of the color video, we use the F-transforms [5, 7–10] for compressing the frames. The F-transform method has been developed in [5]. In this paper each frame is converted in the YUV space. Indeed, since the human eye perceives an image mostly in the Y band (brightness) with respect to the U and V bands (chrominance), we can use a stronger compression rate for coding the image in U and V bands with respect to that one used for coding the image in the Y band, without loss of information in the reconstructed image. In [5] the authors show that the quality of the reconstructed images is better than the one obtained using the F-transform method directly in the RGB space (see also [11, 12]). The proposed method is widely discussed in Section 4. In Sections 2 and 3 the theory of F-transforms and its application are recalled for image compression, respectively. In Section 5 the results are deduced on a large color videos dataset.

2. Fuzzy Transforms

We recall from [9] some essential definitions. Let $n \geq 3$ and $x_1, x_2, \ldots, x_n$ be points (nodes) of $[a, b]$ such that $x_1 = a < x_2 < \cdots < x_n = b$. The fuzzy sets $A_1, \ldots, A_n : [a, b] \to [0, 1]$ form a fuzzy partition of $[a, b]$ if

(1) $A_i(x_i) = 1$ for any $i = 1, 2, \ldots, n$;

(2) $A_i(x) = 0$ if $x \notin (x_{i-1}, x_{i+1})$, where $i = 1, 2, \ldots, n$ and $x_0 = x_1 = a$, $x_{n+1} = x_n = b$;

(3) $A_i(x)$ is a continuous function on $[a, b]$;

(4) $A_i(x)$ is strictly increasing on the interval $[x_{i-1}, x_i]$ for $i = 2, \ldots, n$ and is strictly decreasing on the interval $[x_i, x_{i+1}]$ for $i = 1, \ldots, n - 1$;

(5) for any $x \in [a, b]$, $\sum_{i=1}^{n} A_i(x) = 1$.

We say that $\{A_1, A_2, \ldots, A_n\}$ constitute a symmetric fuzzy partition if the following hold:

(6) equidistance of the nodes, that is, $x_i = a + h \cdot (i - 1)$ for $i = 1, 2, \ldots, n$, where $h = (b - a)/(n - 1)$;

(7) $A_i(x_i - x) = A_i(x_i + x)$ for any $x \in [0, h]$ and $i = 2, \ldots, n - 1$;

(8) $A_{i+1}(x) = A_i (x - h)$ for any $x \in [x_i, x_{i+1}]$ and $i = 1, 2, \ldots, n - 1$.

Considering functions f taking values on a finite set $P = \{p_1, \ldots, p_m\} \subseteq [a, b]$, $f : P \to [0, 1]$, we suppose that P is sufficiently dense with respect to a fuzzy partition $\{A_1, A_2, \ldots, A_n\}$ of $[a, b]$, that is, if $m > n$ and for each $i = 1, \ldots, n$ there exists an index $j \in \{1, \ldots, m\}$ such that $A_i(p_j) > 0$. Now let $n, m \geq 3$, $y_1, y_2, \ldots, y_m \in [c, d]$ be other m assigned nodes such that $y_1 = c < \cdots < y_m = d$. Let $C_1, \ldots, C_m : [c, d] \to [0, 1]$ be another fuzzy partitions of $[c, d]$. Let $f : P \times Q \to [0, 1]$ be a function defined on the finite set $P \times Q = \{p_1, \ldots, p_N\} \times \{q_1, \ldots, q_M\} \subseteq [a, b] \times [c, d]$, with $N > n$ and $M > m$, where P (resp., Q) is sufficiently dense with respect to some fuzzy partition

$\{A_1, A_2, \ldots, A_n\}$ of $[a, b]$ (resp., $\{C_1, \ldots, C_m\}$ of $[c, d]$). Then $[F_{kl}]$, $F_{kl} \in [0, 1]$, $k = 1, \ldots, n$ and $l = 1, \ldots, m$, is the fuzzy matrix which is defined as discrete F-transform of f with respect to $\{A_1, A_2, \ldots, A_n\}$ and $\{C_1, \ldots, C_m\}$ if the following holds:

$$F_{kl} = \frac{\sum_{j=1}^{M} \sum_{i=1}^{N} f(p_i, q_j) A_k(p_i) C_l(q_j)}{\sum_{j=1}^{M} \sum_{i=1}^{N} A_k(p_i) C_l(q_j)}. \tag{1}$$

Afterwards we define $f_{nm}^{F} : P \times Q \rightarrow [0, 1]$ to be the inverse F-transform of f with respect to $\{A_1, A_2, \ldots, A_n\}$ and $\{C_1, \ldots, C_m\}$ as

$$f_{nm}^{F}(p_i, q_j) = \sum_{k=1}^{n} \sum_{l=1}^{m} F_{kl} A_k(p_i) C_l(q_j). \tag{2}$$

The following theorem holds.

Theorem 3. *Let $f : P \times Q \rightarrow [0, 1]$ be a function assigned on $P \times Q = \{p_1, \ldots, p_N\} \times \{q_1, \ldots, q_M\} \subseteq [a, b] \times [c, d]$. Then for every $\varepsilon > 0$, there exist two integers $n(\varepsilon)$, $m(\varepsilon)$ with $n(\varepsilon) < N$, $m(\varepsilon) < M$ and some fuzzy partitions $\{A_1, A_2, \ldots, A_{n(\varepsilon)}\}$ of $[a, b]$ and $\{C_1, C_2, \ldots, C_{m(\varepsilon)}\}$ of $[c, d]$ for which P and Q are sufficiently dense with respect to these partitions, respectively, and such that the following inequality holds for every $i = 1, \ldots, N$, $j = 1, \ldots, M$:*

$$\left| f(p_i, q_j) - f_{n(\varepsilon)m(\varepsilon)}^{F}(p_i, q_j) \right| < \varepsilon. \tag{3}$$

3. The Coding/Decoding Process

Let R be an image of sizes $N \times M$, considered as a fuzzy relation $R : (i, j) \in \{1, \ldots, N\} \times \{1, \ldots, M\} \rightarrow [0, 1]$; that is, $R(i, j) = P(i, j)/L_t$, with $P(i, j)$ being the normalized value of the pixel with respect to the length L_t of the scale used. For simplicity, let $p_i = i$, $q_j = j$, $a = c = 1$, $b = N$, and $d = M$. Let the fuzzy sets $A_1, \ldots, A_n : [1, N] \rightarrow [0, 1]$ and $C_1, \ldots, C_m : [1, M] \rightarrow [0, 1]$, with $n < N$ and $m < M$, form a fuzzy partition of $[1, N]$ and $[1, M]$, respectively. Following [8], R is subdivided in submatrices R_B of sizes $N(R_B) \times M(R_B)$, $R_B : (i, j) \in \{1, \ldots, N(R_B)\} \times \{1, \ldots, M(R_B)\} \rightarrow [0, 1]$, called blocks, coded to matrices of sizes $n(R_B) \times m(R_B)$, $(n(R_B) < N(R_B), m(R_B) < M(R_B))$ via the following discrete F-transforms $[F_{kl}^{B}]$ for every $(k, l) \in \{1, \ldots, n(R_B)\} \times \{1, \ldots, m(R_B)\}$ as

$$F_{kl}^{B} = \frac{\sum_{j=1}^{M(R_B)} \sum_{i=1}^{N(R_B)} R_B(i, j) A_k(i) C_l(j)}{\sum_{j=1}^{M(R_B)} \sum_{i=1}^{N(R_B)} A_k(i) C_l(j)}, \tag{4}$$

and decode $[F_{kl}^{B}]$ via $R_{n(R_B)m(R_B)}^{F} : (i, j) \in \{1, \ldots, N(R_B)\} \times \{1, \ldots, M(R_B)\} \rightarrow [0, 1]$ defined as

$$R_{n(R_B)m(R_B)}^{F} = \sum_{j=1}^{M(R_B)} \sum_{i=1}^{N(R_B)} F_{kl}^{B} A_k(i) C_l(j) \tag{5}$$

which approximates R_B in the sense of Theorem 3; that is, there exist, for every $\varepsilon > 0$, two integers $n(R_B, \varepsilon)$, $m(R_B, \varepsilon)$ such that the following holds for every $(i, j) \in \{1, \ldots, N(R_B)\} \times \{1, \ldots, M(R_B)\}$:

$$\left| R_B(i, j) - R_{n(R_B, \varepsilon)m(R_B, \varepsilon)}^{F}(i, j) \right| < \varepsilon. \tag{6}$$

Unfortunately the previous theorem does not suggest a method for finding such integers, and then we try to assign values to $n(R_B) = n(R_B, \varepsilon)$ and $m(R_B) = m(R_B, \varepsilon)$ for getting compression rates given by

$$\rho(R_B) = \frac{n(R_B) \cdot m(R_B)}{N(R_B) \cdot M(R_B)} \tag{7}$$

which are useful to code any original block R_B. The recomposition of the blocks $R_{n(R_B)m(R_B)}^{F}$ gives the image R^F whose PSNR with respect to the original image R is calculated via the following well-known formula:

$$\text{PSNR}(R, R^F)$$
$$= 20\log_{10} \frac{Lt}{\sqrt{\sum_{i=1}^{N} \sum_{j=1}^{M} (R(i, j) - R^F(i, j))^2 / N \times M}}. \tag{8}$$

In accordance with [8], in the proposed experiments the best results are deduced with the symmetric fuzzy partitions $A_1, \ldots, A_{n(R_B)} : [1, N(R_B)] \rightarrow [0, 1]$ and $C_1, \ldots, C_{m(R_B)} : [1, M(R_B)] \rightarrow [0, 1]$ defined as

$$A_1(i) = \begin{cases} 0.5\left(\cos\dfrac{\pi}{h}(i - 1) + 1\right) & \text{if } 1 \leq i \leq x_2, \\ 0 & \text{else}, \end{cases}$$

$$A_k(i) = \begin{cases} 0.5\left(\cos\dfrac{\pi}{h}(i - x_k) + 1\right) & \text{if } x_k \leq i \leq x_{k+1}, \\ 0 & \text{else}, \end{cases}$$

$$A_{n(R_B)}(i)$$
$$= \begin{cases} 0.5\left(\cos\dfrac{\pi}{h}\left(i - x_{n(R_B - 1)}\right) + 1\right) & \text{if } x_{n(B) - 1} \leq i \leq N(R_B), \\ 0 & \text{else}, \end{cases} \tag{9}$$

where $k = 2, \ldots, n(R_B) - 1$, $h = (N(R_B) - 1)/(n(R_B) - 1)$, $x_k = 1 + h \cdot (k - 1)$, and

$$
C_1(j) = \begin{cases} 0.5\left(\cos \dfrac{\pi}{s}(j-1) + 1\right) & \text{if } 1 \le j \le y_2, \\ 0 & \text{else,} \end{cases}
$$

$$
C_t(j) = \begin{cases} 0.5\left(\cos \dfrac{\pi}{s}(j - y_t) + 1\right) & \text{if } y_{t-1} \le j \le x_{t+1}, \\ 0 & \text{else,} \end{cases}
$$

$$
C_{m(R_B)}(j)
$$
$$
= \begin{cases} 0.5\left(\cos \dfrac{\pi}{s}\left(j - y_{m(R_B)-1}\right) + 1\right) & \text{if } y_{m(R_B)-1} \le j \le M(R_B), \\ 0 & \text{else,} \end{cases} \tag{10}
$$

where $t = 2, \ldots, m(R_B) - 1$, $s = (M(R_B) - 1)/(m(R_B) - 1)$, and $y_t = 1 + s \cdot (t - 1)$.

4. Our Proposal

The proposed process includes the following steps:

(1) each color frame, seen as a fuzzy relation, is converted from the space RGB to the space YUV;

(2) a classification of the frames is made via the previous algorithms;

(3) the compression rate $\rho_I = \rho_I(R_B)$ of the I-frames is the mean of three (possibly different) compression rates used in the three bands, that is, if any block R_B of an I-frame has sizes (say) $N_{IY}(R_B) \times M_{IY}(R_B)$ in the band Y and is coded to a block of sizes (say) $n_{IY}(R_B) \times m_{IY}(R_B)$ for which the related compression rate is given by $\rho_{IY} = \rho_{IY}(R_B) = (n_{IY}(R_B) \cdot m_{IY}(R_B)) \cdot (N_{IY}(R_B) \cdot M_{IY}(R_B))^{-}$ and the analogous meaning has the symbols ρ_{IU}, ρ_{IV}. Of course we have $\rho_I = (\rho_{IY} + \rho_{IU} + \rho_{IV})/3$. A similar meaning can be given to $\rho_\Delta = \rho_\Delta(R_B)$ (resp., $\rho_R = \rho_R(R_B)$) for Δ-frames (resp., R-frames).

A color image in the RGB space with pixels normalized in $[0, 1]$ is converted to YUV space via the formula [5]

$$
\begin{bmatrix} Y \\ U \\ V \end{bmatrix} = \begin{bmatrix} 0.299 & 0.587 & 0.114 \\ -0.169 & -0.332 & 0.500 \\ 0.500 & -0.419 & -0.0813 \end{bmatrix} \begin{bmatrix} R \\ G \\ B \end{bmatrix} + \begin{bmatrix} 0 \\ 0.5 \\ 0.5 \end{bmatrix}. \tag{11}
$$

Since no misunderstanding can arise, a frame is denoted by a capital letter instead of its ID number in a sequence of a video. In step (2), the similarity measure adopted in [5] is used for classifying the type of frame. It is based on the Lukasiewicz

t-norm between two frames F and G, with $F, G : (i, j) \in \{1, 2, \ldots, N\} \times \{1, 2, \ldots, M\} \to [0, 1]$, defined as

$$
\text{Sim}(F, G) = \left(\sum_{i=1}^{N} \sum_{j=1}^{M} \{1 - \max\{F(i, j), G(i, j)\} \right.
$$
$$
\left. + \min\{F(i, j), G(i, j)\}\} \right) \tag{12}
$$
$$
\times (N \times M)^{-1}.
$$

In the μth band ($\mu \in \{Y, U, V\}$) we will use the symbol $\text{Sim}_\mu(F, G)$. The authors [5] have shown that Lukasiewicz t-norm provides the best results with respect to other t-norms as the classical Min and the arithmetical product. For convenience, we assume that the first frame of a video is an I-frame. For determining a GOP sequence in a single band, it can be verified if the successive frame G is a B-frame or a P-frame, that is, if it is "very similar" to the preceding I-frame F in the sense that $\text{Sim}(F, G) < \text{Sim}B$, with $\text{Sim}B \in [0, 1]$ being a prefixed threshold value; otherwise G is assumed to be a new I-frame. We determine a GOP sequence in an assigned band using (12) with the following process:

(1) we consider the first frame F as an I-frame;

(2) we compare F with the successive frame G;

(3) if $\text{Sim}(F, G) < \text{Sim}P$, the frame G is a B-frame or a P-frame and is enclosed in the GOP sequence. Then we consider the successive frame G and go to step (2); otherwise G is a new I-frame. The previous frame is a P-frame and represents the last frame of the GOP sequence.

After determining the GOP sequence, we check if each frame of the sequence is a B-frame or a P-frame by using the previous algorithms. In step (3) we finally compress the frames. In order to reduce the mean compression rate for a P-frame, in [5] and references therein, the authors introduce a "difference" frame D, called Δ-frame, between a P-Frame G and I-frame F by defining $D : (i, j) \in \{1, 2, \ldots, N\} \times \{1, 2, \ldots, M\} \to [0, 1]$ as

$$
D(i, j) = \frac{[F(i, j) - G(i, j) + 1]}{2}. \tag{13}
$$

The usage of the Δ-frame has the advantage of using a stronger compression rate for the P-frames with respect to the I-frames; indeed a P-frame G has values in its pixels very close to the pixels of the previous I-frame. Hence the Δ-frame D in (13) has a low quantity of information and it can be coded with a low compression rate. Then, if D' and F' are the frames obtained after coding/decoding F and D, the frame G' (reconstruction of the frame G), with $D', F', G' : (i, j) \in \{1, 2, \ldots, N\} \times \{1, 2, \ldots, M\} \to [0, 1]$, is deduced from the membership values of F' and D' via the following formula:

$$
G'(i, j) = \frac{\max\{0, F'(i, j) - 2D'(i, j) + 1\}}{\max\{1, F'(i, j) - 2D'(i, j) + 1\}}. \tag{14}
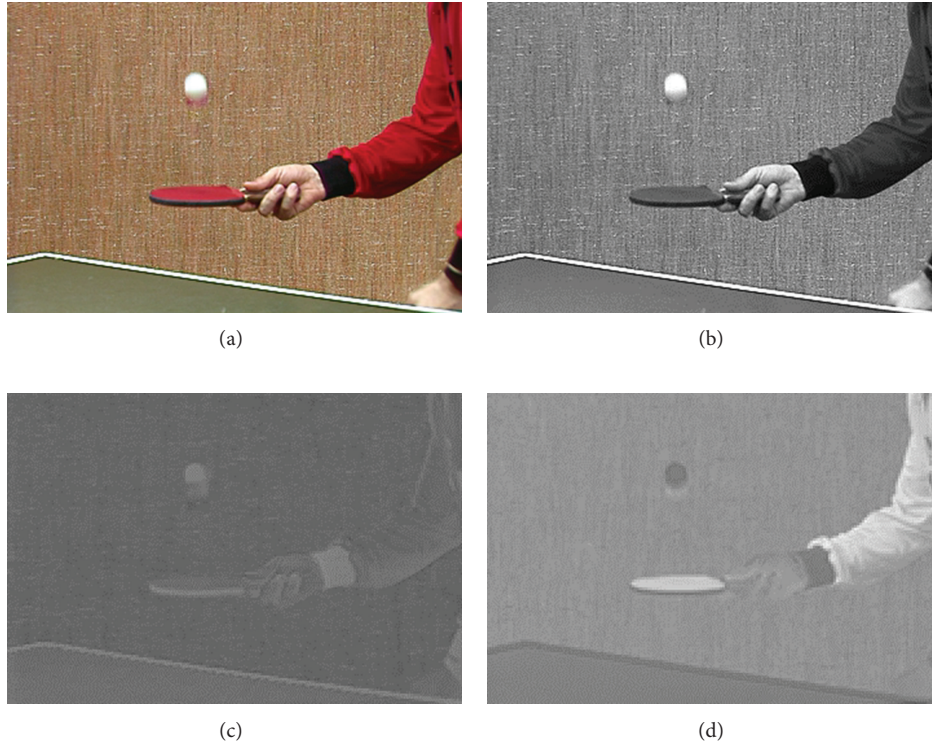$$

FIGURE 1: (a) Frame 1 of "tennis2" [6], (b) Frame 1 in Y band, (c) Frame 1 in U band, and (d) Frame 1 in V band.
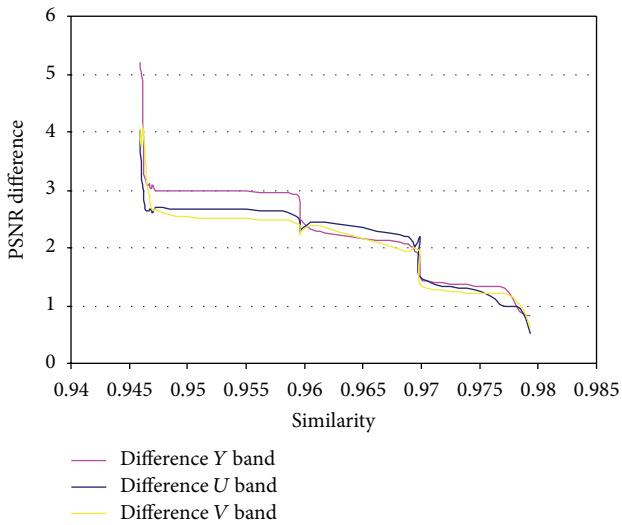

FIGURE 2: Diff(PSNR) with the similarity in Y, U, and V bands.

Now we present a new schema for coding/decoding a B-frame which is inserted in a GOP between an I-frame F and a P-frame G. Then we consider a frame R given by

$$R(i, j) = \frac{[(F(i, j) + G(i, j))/2 - B(i, j) + 1]}{2} \quad (15)$$

and we code it. Let R' be the frame obtained after decoding R, with $R' : (i, j) \in \{1, 2, \ldots, N\} \times \{1, 2, \ldots, M\} \to [0, 1]$. All the coding/decoding processes are realized via the F-transforms with the symmetric fuzzy partition given in Section 3. We reconstruct the B-frame, say B', by combining the membership values of F', G', and R' via the following formula:

$$B'(i, j) = \frac{\max\left\{0, \left[F'(i, j) + G'(i, j)\right]/2 - 2R'(i, j) + 1\right\}}{\max\left\{1, \left[F'(i, j) + G'(i, j)\right]/2 - 2R'(i, j) + 1\right\}}. \quad (16)$$

We use the formulas (14) and (16) for reconstructing the P-frames and the B-frames in the videos, respectively. In accordance with [5], we convert each image in the RGB space by using the formula

$$\begin{bmatrix} R \\ G \\ B \end{bmatrix} = \begin{bmatrix} 1 & 0 & 1.4075 \\ 1 & -0.3455 & -0.7169 \\ 1 & 1.7790 & 0 \end{bmatrix} \begin{bmatrix} Y \\ U \\ V \end{bmatrix} + \begin{bmatrix} 0.5 \\ 0.5 \\ 0.5 \end{bmatrix}. \quad (17)$$

For simplicity of presentation, in our tests here we adopt $M(R_B) = N(R_B)$, $m(R_B) = n(R_B)$. In [5] a preprocessing phase is adopted for determining the threshold $\text{Sim}P$ calculated with the following steps:
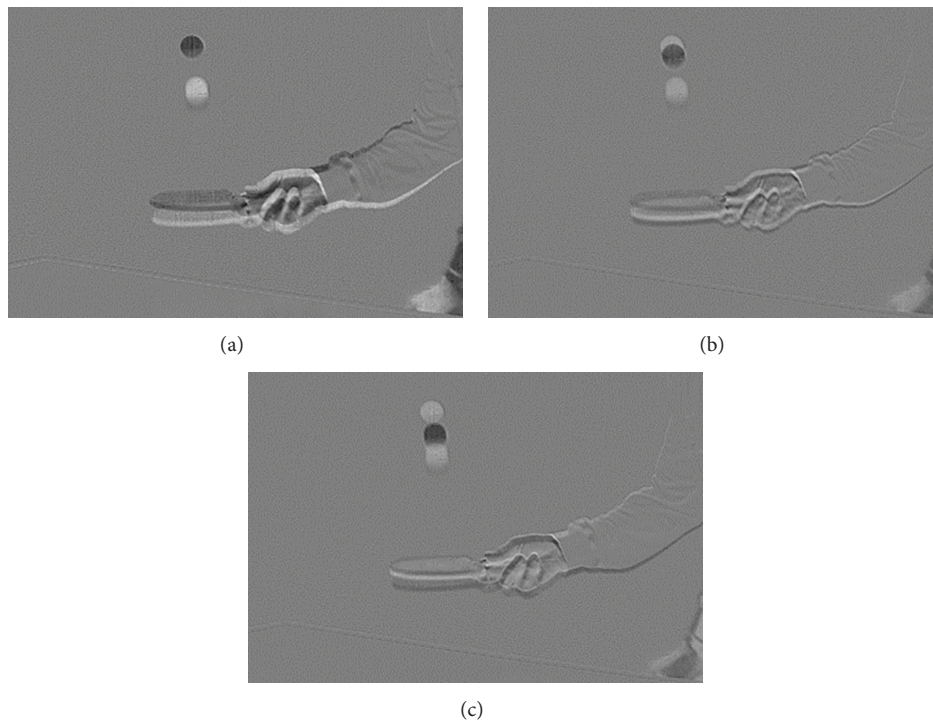
(a)

(b)

(c)

Figure 3: (a) Δ-frame from Frame 4 in Y band, (b) R-frame from Frame 2 in Y band, and (c) R-frame from Frame 3 in Y band.

(a)

(b)

(c)

(d)

Figure 4: (a) Δ-frame from Frame 6 in U band, (b) R-frame from Frame 2 in U band, (c) R-frame from Frame 3 in U band, and (d) R-frame from Frame 4 in U band.
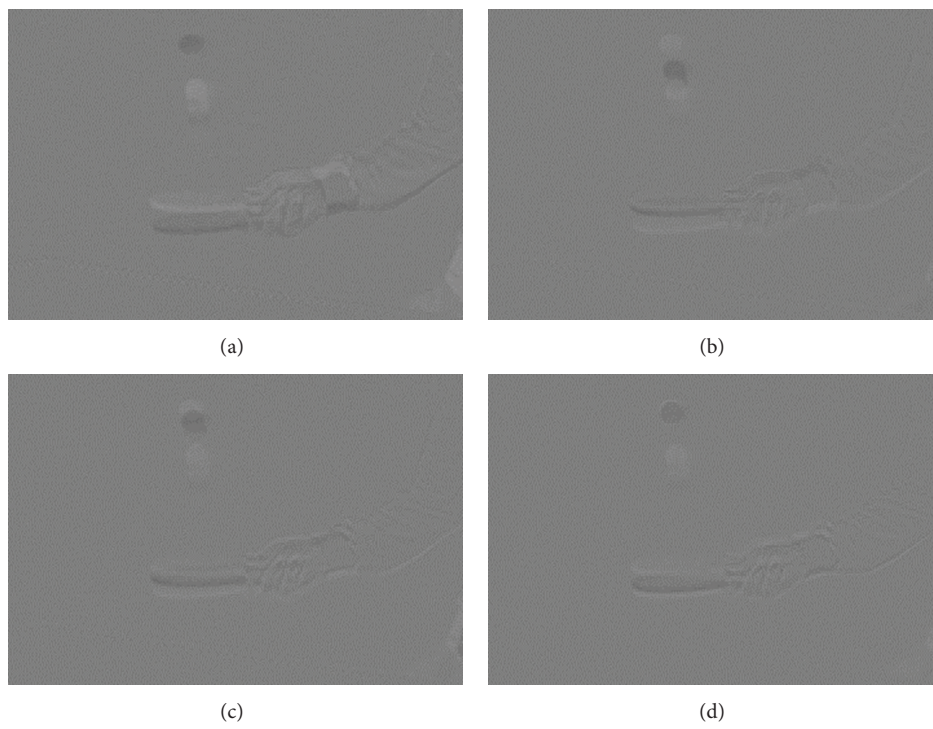
Figure 5: (a) Δ-frame from Frame 5 in V band, (b) R-frame from Frame 2 in V band, (c) R-frame from Frame 3 in V band, and (d) R-frame from Frame 4 in V band.
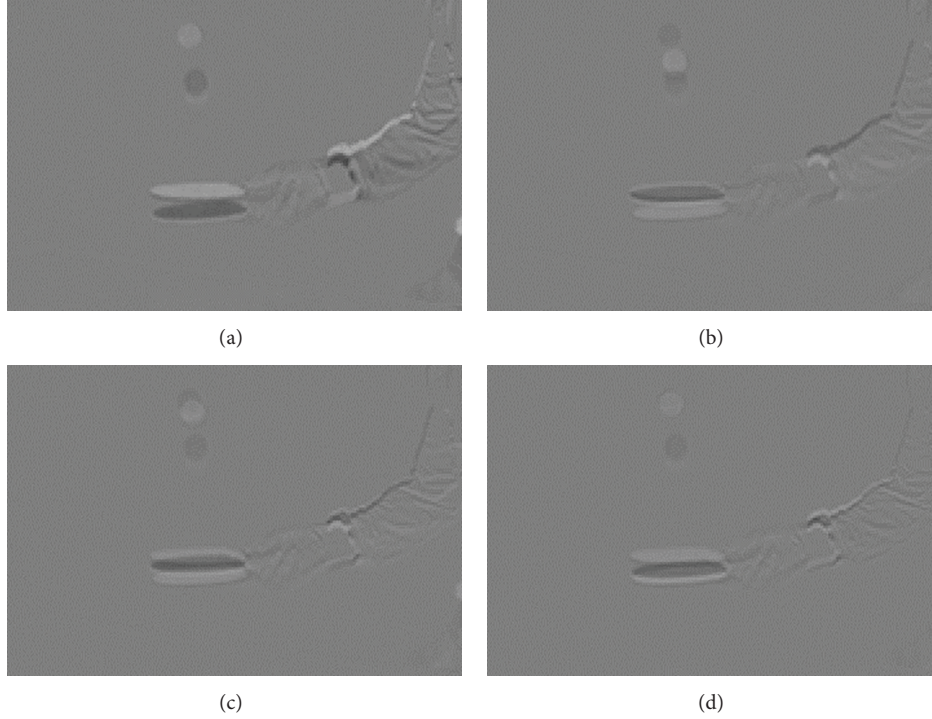
(1) if the initial frame F is considered as an I-frame, we compress F in the μth band ($\mu \in \{Y, U, V\}$) with compression rate $\rho_{I\mu}$; each successive frame is a P-frame G and we archive the similarity value $\mathrm{Sim}_\mu(F, G)$ calculated with formula (12); we compress the Δ-frame D in the μth band with compression rate equal to $\rho_{P\mu}$ (less than of $\rho_{I\mu}$) and if D' is the related decompressed frame, we derive the P-frame G' via (14);

(2) each P-frame G is also coded in the μth band with compression rate $\rho_{P\mu}$ and let G'' be the decoded P-frame by using directly the F-transforms; then we determine the difference diff(PSNR) $= |\mathrm{PSNR}(G'', G) - \mathrm{PSNR}(G', G)|$;

(3) the trend of diff(PSNR) is plotted with respect to the similarity $\mathrm{Sim}_\mu(F, G)$ in each band of the image. As similarity threshold, we assume that value of $\mathrm{Sim}_\mu(F, G)$ such that diff(PSNR) does not exceed a prefixed limit is equal to 3 (cf. [5] for details);

(4) then the threshold Sim$P$ is given by

$$\mathrm{Sim}P = \max_{G \in \mathrm{GOP}} \left\{ \max \left\{ \mathrm{Sim}_\mu(F, G) : \mu \in \{Y, U, V\} \right\} \right\} \qquad (18)$$

with F being the first I-frame of the GOP sequence. In our tests, in addition we put Sim$B$ = Sim$P$ in the preprocessing phase.

5. The Results

For brevity of discussion, we show the results obtained for the color video "tennis2" [6]. We present all the results by assuming $\rho_I \approx 0.262$ for the I-frames, $\rho_\Delta \approx 0.027$ for the Δ-frames, and $\rho_R \approx 0.020$ for the R-frames. Figures 1(a)–1(d) show the first frame of the video and the corresponding single-band images in the YUV space, respectively. As example of Diff(PSNR), Figure 2 contains the plots of Diff(PSNR) ≤ 3 for the similarity values obtained in Y, U, and V bands for which we choose $\mathrm{Sim}_Y(F, G) > 0.948 = \mathrm{Sim}P$ (as average). As examples we show some Δ-frames and R-frames in each band.

(i) *Y Band.* The first P-frame is given by the fourth frame. Figure 3(a) contains the Δ-frame obtained by using (13) from the fourth frame and the first frame (an I-frame). The second and the third frames are B-frames. Figure 3(b) (resp., Figure 3(c)) shows the R-frame obtained by using (15) from the second (resp., third) frame, the first frame (an I-frame), and the fourth frame (a P-frame).

(ii) *U Band.* The first P-frame is given by the sixth frame. Figure 4(a) contains the Δ-frame obtained by using (13) from the sixth frame and the first frame (an I-frame). The frames 2, 3, and 4 are B-frames. Figures 4(b)–4(d) show the R-frames obtained by using (15) from the first frame (an I-frame), the B-frames 2, 3, and 4, and the sixth frame (a P-frame), respectively.

(iii)*V Band.* The first P-frame is given by the fifth frame. Figure 5(a) contains the Δ-frame obtained by using (13) from
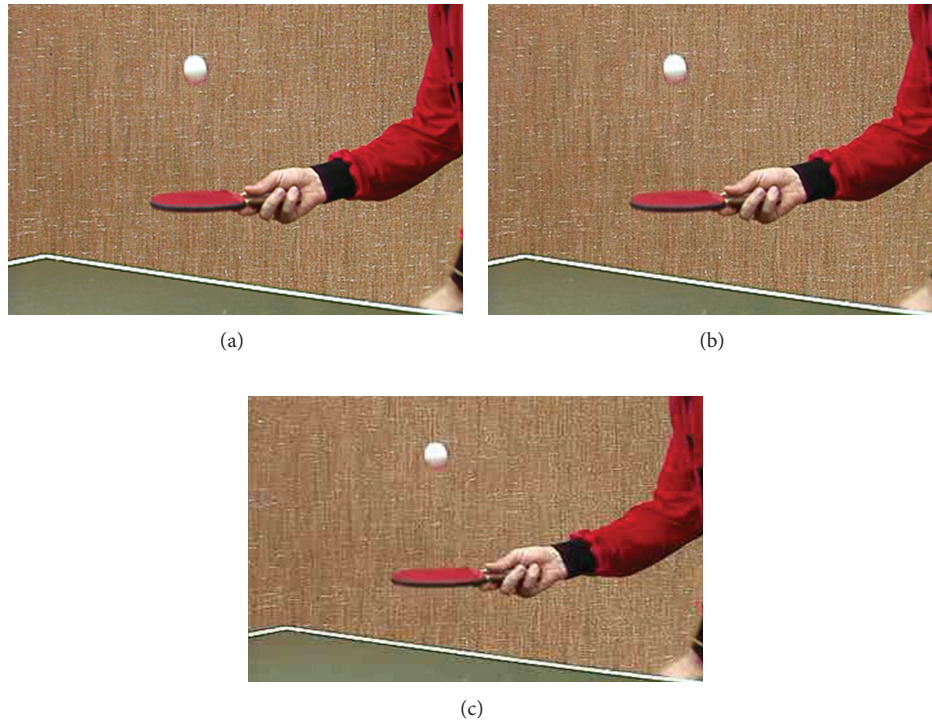
(a)

(b)

(c)

FIGURE 6: (a) Frame 2 in the proposed method, (b) Frame 2 in F-transforms, and (c) Frame 2 in MPEG-4.

TABLE 1: Results for "tennis2" [6] in the proposed method.

Parameters	Y band	U band	V band
Number of I-frames	15	7	8
Number of P-frames	31	23	23
Number of B-frames	54	70	69
Mean compression rate $\rho(B)$	0.1128	0.0236	0.0245
Mean PSNR for I-Frames	27.011	25.545	25.812
Mean PSNR for P-Frames	24.816	23.710	23.815
Mean PSNR for B-Frames	24.734	22.819	23.026

TABLE 2: Comparison with other methods for "tennis2" [6].

Parameters	Proposed method	F-transforms	MPEG-4
Mean compression rate	0.053	0.058	0.055
Mean PSNR	23.915	22.801	23.431

B-frame using similarity measures for determining the GOP sequences and the type of frames. Our method seems to be fully comparable with classical F-transforms and MPEG-4 for similar mean compression rates to a certain extent.

Acknowledgments

The authors thank the referees and the editor whose suggestions have greatly improved the contents of this paper.

References

[1] I. E. G. Richardson, *The H. 264 Advanced Videos Compression Standard*, John Wiley & Sons, Hoboken, NJ, USA, 2010.

[2] F. C. N. Pereira and T. Ebrahimi, *MPEG-4 Book*, Prentice Hall Professional, Upper Saddle River, NJ, USA, 2002.

[3] T. Sikora, *MPEG: Digital Video Coding Standards, Digital Electronics Handbook*, McGraw- Hill, New York, NY, USA, 1995.

[4] W. B. Pennebaker and J. L. Mitchell, *JPEG: Still Im Age Data Compression Standard*, Van Nostrand Reinhold, New York, NY, USA, 1993.

the sixth frame and the first frame (an I-frame). The frames 2, 3, and 4 are B-frames. Figures 5(b)–5(d) show the R-frames obtained by using (15) from the first frame (an I-frame), the B-frames 2, 3, and 4, and the fifth frame (a P-frame), respectively.

All the results obtained for the video "tennis2" are synthetized in Table 1.

Figures 6(a)–6(c) contain Frame 2 decoded with the proposed method, classical F-transforms, and MPEG-4, respectively.

In Table 2 we report the final PSNR index in the three methods.

6. Conclusions

We present a new method for coding/decoding color videos, in which we classify a frame in I-frame, P-frame, and

[5] F. Di Martino, V. Loia, and S. Sessa, "Fuzzy transforms for compression and decompression of color videos," *Information Sciences*, vol. 180, no. 20, pp. 3914–3931, 2010.

[6] http://sampl.eng.ohio-state.edu/~sampl/database.htm.

[7] F. Di Martino, V. Loia, I. Perfilieva, and S. Sessa, "An image coding/decoding method based on direct and inverse fuzzy transforms," *International Journal of Approximate Reasoning*, vol. 48, no. 1, pp. 110–131, 2008.

[8] F. Di Martino and S. Sessa, "Compression and decompression of images with discrete fuzzy transforms," *Information Sciences*, vol. 177, no. 11, pp. 2349–2362, 2007.

[9] I. Perfilieva, "Fuzzy transforms: theory and applications," *Fuzzy Sets and Systems*, vol. 157, no. 8, pp. 993–1023, 2006.

[10] I. Perfilieva and B. De Baets, "Fuzzy transforms of monotone functions with application to image compression," *Information Sciences*, vol. 180, no. 17, pp. 3304–3315, 2010.

[11] H. Nobuhara, W. Pedrycz, and K. Hirota, "Relational image compression: optimizations through the design of fuzzy coders and YUV color space," *Soft Computing*, vol. 9, no. 6, pp. 471–479, 2005.

[12] H. Nobuhara, W. Pedrycz, S. Sessa, and K. Hirota, "A motion compression/reconstruction method based on max t-norm composite fuzzy relational equations," *Information Sciences*, vol. 176, no. 17, pp. 2526–2552, 2006.

Research Article

A Fuzzy Inference System for the Conjunctive Use of Surface and Subsurface Water

Liang-Cheng Chang,[1] Hone-Jay Chu,[2] and Yi-Wen Chen[1]

[1] *Department of Civil Engineering, National Chiao Tung University, 1001 Ta Hsueh Road, Hsinchu 30050, Taiwan*
[2] *Department of Geomatics, National Cheng Kung University, No. 1 University Road, Tainan 701, Taiwan*

Correspondence should be addressed to Hone-Jay Chu; honejaychu@gmail.com

This study develops the water resources management model for conjunctive use of surface and subsurface water using a fuzzy inference system (FIS). The study applies the FIS to allocate the demands of surface and subsurface water. Subsequently, water allocations in the surface water system are simulated by using linear programming techniques, and the responses of subsurface water system with respect to pumping are forecasted by using artificial neural networks. The operating rule for the water systems is that the more abundant water system supplies more water. By using the fuzzy rule, the FIS conjunctive use model easily incorporates expert knowledge and operational polices into water resources management. The result indicates that the FIS model is more effective and efficient when compared with the decoupled conjunctive use and simulation-optimization models. Furthermore, the FIS model is an alternative way to obtain the conjunctive use policies between surface and subsurface water.

1. Introduction

The objective of the study is to develop a fuzzy rule-based method for the conjunctive use of surface and subsurface water systems. Zadeh [1] applied the fuzzy theory to mathematically deal with the imprecision and uncertainty. Fuzzy logic extends upon traditional Boolean logic and deals with the imprecision in human experience [2]. The fuzzy inference system (FIS) is an artificial intelligence technique that combines the fuzzy set, fuzzy logic, and fuzzy reasoning [1, 3–6]. The FIS utilizes linguistic variables, fuzzy rules, and fuzzy reasoning and provides a tool for knowledge representation based on degrees of membership [7]. During the past decade, the FIS application ranged from runoff forecasting to surface water supply [3–6, 8, 9]. Shrestha et al. [3] developed a FIS to determine a real-world reservoir operation. They constructed a fuzzy rule-based model to derive operation rules for a multipurpose reservoir. Their research used reservoir storages, estimated inflows, and demands as the premises and took reservoir releases as the consequences. The finding showed that the fuzzy-based structure was ordinary and time-saving in computation. Russell and Campbell [4] developed

the FIS for a simplified hydroelectric reservoir. The results also showed that fuzzy logic seemingly offered a way to improve the existing operating practices, which was relatively easy to explain and understand when compared with the complex optimization model. Panigrahi and Mujumdar [5] used a FIS for a reservoir operation model. The study incorporated expert knowledge for framing the fuzzy rule from an explicit stochastic model. Russell and Campbell [4] applied the Adaptive-Network-Based FIS (ANFIS) to water resources management and used the genetic algorithm to search the optimal reservoir operation based on a given inflow series. They used FIS for determining optimal water release according to reservoir depth and inflow. However, previous studies [3–5] mentioned that applying fuzzy logic to reservoir operation could remain limited to a single reservoir system.

Conjunctive use of surface and subsurface water is a challenging work for water resources management [10–14]. Conjunctive water management reduces the deficiencies by using subsurface water to supplement scarce surface water supply during the drought. The conjunction use enhances the reliability of water supplies by providing independent sources. Başağaoğlu and Mariño [10] developed

a simulation-optimization model of a hypothetical river basin to determine optimal operating policies for jointly using surface and subsurface water supplies. The simulation model was the response function to incorporate the transient hydraulic interaction between stream and aquifer. The response function coefficients were derived from results of the numerical simulation model. Peralta et al. [11] employed simulation-optimization models to maximize total annual allocation of surface and subsurface water yield. They used the models in attempt to satisfy temporally increasing water needs for alternative future management scenarios. Philbrick and Kitanidis [12] proposed the gradient dynamic programming to solve the minimal operating cost problem by regarding surface and subsurface storages as state variables for realizing the impact of conjunctive use. Nishikawa [15] developed a simulation-optimization model for managing water resources for the city of Santa Barbara in a five-year planning horizon. Moreover, subsurface water simulation is linked with linear programming (LP). The model addressed the cost in water supply to meet demands and control seawater intrusion. Azaiez [16] developed the model for the conjunctive use of surface and subsurface water with an artificial recharge and integrated opportunity costs for the unsatisfied demand on the limitation of the final subsurface water level. The problem was simplified to be formulated as a convex program with linear constraints. Watkins and McKinney [14] applied decomposition algorithms to conjunctively managed surface and subsurface water systems, with reference to cost functions including both discrete and nonlinear terms. The complexity had mainly arisen from integrating surface and subsurface water, that is, two reservoirs and a confined aquifer. Their study incorporated the subsurface water system into the management model using the response matrix approach. However, many studies applied the artificial neural networks (ANNs) to model hydrology field complexity [17–22] including rainfall-runoff modeling [22, 23] and groundwater flow and transport [24]. The current work trained an ANN to predict the time-varying subsurface water level in response to management alternatives [18–21]. Coppola et al. [18] trained an ANN with MODFLOW simulation data to predict subsurface water levels at locations under various pumping conditions. The ANN forecasted subsurface water levels at the next time based on management alternatives including control and state variables at the current time.

Utilizing fuzzy rules, the FIS provides a tool to incorporate human expert experience for modeling a conjunctive use of surface and subsurface water. The FIS obtained allocated demand of ground and surface water in each stage simultaneously. Then, the simulator (i.e., LP and ANN) determined the future state of system, such as reservoir storages and hydraulic heads at the next time. Moreover, the LP simulated the operation of surface water system, and the ANN predicted hydraulic head variations under time-varying pumping.

2. Methods

Figure 1 illustrates the procedure of the FIS conjunctive use model. The FIS conjunctive use model comprises the control and simulation levels. Firstly, the FIS, which is in the control level, determines the assigned demand among surface and subsurface water each time step. After determining the assigned demands, the subsurface water submodel determines the hydraulic head using ANN [19], and the surface water allocation submodel obtains the reservoir supply and future *reservoir* storage using LP [25, 26].

2.1. Fuzzy Inference System (FIS). The FIS is composed of five functional blocks [5]: (1) a rule base containing a number of fuzzy if-then rules; (2) a relational database which defines membership functions of the fuzzy set used in the fuzzy rules; (3) a fuzzification interface which transforms crisp inputs into degrees of match with linguistic values; (4) a fuzzy reasoning which performs inference operations on the rules; in FIS applications, the max-min and max product compositional operators are used most commonly because of their computational simplicity and efficiency; and (5) a defuzzification interface which transforms a combined output of fuzzy rules into a crisp value [2, 10, 22]. The current study uses the centroid method to defuzzify the aggregate fuzzy set, directly computing the real valued output as a normalized combination of membership values.

The study follows a typical process in developing the fuzzy system; for example, (1) define the linguistics variables; (2) construct the fuzzy rule structures; (3) determine the fuzzy set parameters; (4) encode the fuzzy sets, fuzzy rules, and the procedures; and (5) evaluate and tune the system [2] (Figure 2). In this study, the operation rule is the concept of water level index balance that the water system reaching the highest levels at the current time has a priority for supply at the next time [27, 28]. The FIS follows the following rule; that is, the abundant water system supplies more and the scarce water system supplies less water. In the study, the premises of the fuzzy rule are surface and subsurface water states, and the consequence is the assigned demand of each well. The kth fuzzy rule in each time step is given as:

$$\text{if} \left(\sum_i \left(V_i^t + \text{IF}_i^t \right) \text{ is } A_k \right) \text{and} \left(\overline{h}^t \text{ is } B_k \right),$$
$$\text{then} \left(\overline{D}^t \text{ is } C_k \right), \tag{1}$$

where V_i^t is the storage of the ith reservoir; IF_i^t is the inflow of the ith reservoir; $\overline{h}^t$ is the average subsurface water level in the observation wells; $\overline{D}^t$ is the assigned demand of each well in the subsurface water system; and A_k, B_k and, C_k are linguistic values in the kth rule.

The premises and consequences are assigned as the triangular membership functions as in Figure 3. Two input variables are surface water state and subsurface water state, that is, average hydraulic head in the observations. The fuzzy membership functions of the inputs are divided into five categories, that is, "*Low, Low Med., Medium, High Med. and, High.*" Triangular functions with equal base widths are the simplest possible, and these are often selected for practical applications [4]. In the study, the surface water state ranges
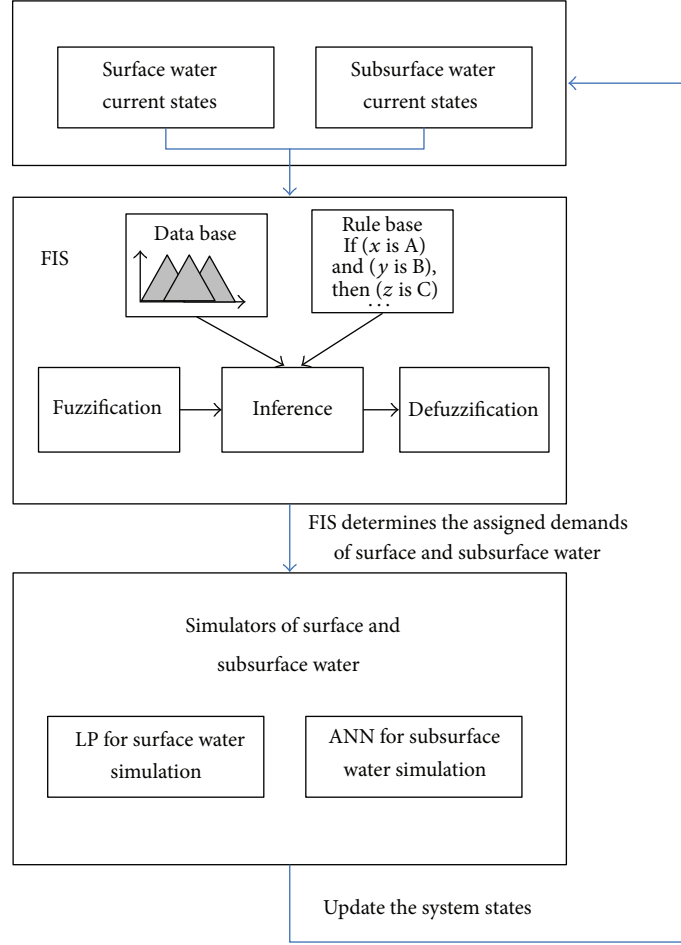
FIGURE 1: Flowchart of the FIS conjunctive use model.

from 0 to $120 \times 10^6 \, \text{m}^3$ and the average hydraulic head ranges from 70 to 94 m in the observation wells. The output variable is the assigned demand of each well from subsurface water which ranges from 0 to 0.3 cms and is divided into four categories in the membership function, that is, *Low, Low Med., Medium,* and *High*. The FIS computes the weights of each triggered rule, accumulating weights and outputs for each rule, and finally computing the weighted output for each rule [6]. Moreover, fuzzy sets provide a means of translating linguistic descriptors into a usable numerical form [26]. Table 1 shows the fuzzy rules; for example, *If* surface water state is *Low,* andsubsurface water level is *High, then* the assigned demand from subsurface water is *High*. After the FIS determines subsurface water demand, the surface water demand could be represented as

$$\widehat{D}^t = D^t - \overline{D}^t \times N_p, \tag{2}$$

where D^t is the whole water requirement in the tth time step; $\widehat{D}^t$ is the surface water assigned demand in the tth time step; and N_P is the number of pumping wells.

2.2. *Surface Water Submodel.* The surface water allocation model is represented as

$$J^t = \min_{X^t} \left[\sum_j c_{1,j} \text{SH}_j^t + \sum_i \left(c_{2,i} G_{i,k}^t + c_{3,i} Z_i^t \right) \right], \tag{3}$$

$$t = 1 \sim n; \; i, k \in N_S, \; j \in N_D$$

subject to

$$V_i^{t+1} = V_i^t + \text{IF}_i^t - X_i^t - \text{OF}_i^t, \quad i \in N_S, \tag{4}$$

$$V_i^{\min} \leq V_i^t \leq V_i^{\max}, \quad i \in N_S, \tag{5}$$

$$X_{i,j}^{\min} \leq X_{i,j}^t \leq X_{i,j}^{\max}, \quad i, j \in \Omega, \tag{6}$$

$$\sum_i X_{i,j}^t \leq \widehat{D}_j^t, \quad i \in \Omega, j \in N_D, \tag{7}$$

where SH_j^t is the shortage in demand j at the tth time step, $\text{SH}_j^t = \widehat{D}_j^t - \sum_i X_{i,j}^t$; $X_{i,j}$ means the supply from node i in demand j at time step$t$; and N_D is the demand node set; in
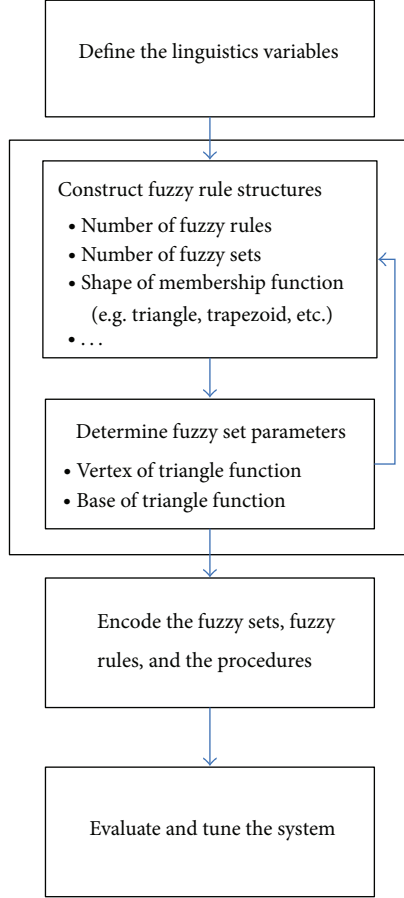
Figure 2: Procedure of developing the fuzzy system.

Table 1: Rule table for the operation in conjunctive use operation using FIS within high usage of subsurface water.

	Surface water state				
	Low	Low Med.	Medium	High Med.	High
Subsurface water state					
Low	Low	Low	Low	Low	Low
Low Med.	High	High	Low	Low	Low
Medium	High	High	Low	Low	Low
High Med.	High	High	Low	Low	Low
High	High	High	Low	Low	Low

the sum of target storage (lower limit) among the reservoirs; and V_3 is the sum of firm storage (critical limit) among the reservoirs; ω_1 and ω_2 are the rationing factors. In the study, ω_1 and ω_2 are 0.85 and 0.75.

This study uses the linear programming (LP) to simulate the surface water system in (3)~(8). The formulation is as follows. Equation (3) specifies the objective function consisting of three subobjectives which include the total shortage in each time step, the difference between the reservoir water level, and the ratio of the residual water volume to the capacity of each reservoir. Equations (4) and (5) list the mass balance equation and the demand constraint of each reservoir in each time step. Equation (6) specifies the capacity constraints for each reservoir in each time step. Equations (7) and (8) specify the constraints on the flow through the pipes and hedging rule in each time step. In the study, the model first determines the demand with the hedging rule (8), and then the LP determines the flows in the system at t while satisfying the demand with the hedging rule.

2.3. Subsurface Water Submodel. The current study uses ANN to serve as the simulator for modeling nonlinear and time-varying groundwater flow. An ANN consists of a number of neurons arranged in an input layer, an output layer, and one hidden layer. The inputs are state vectors, which are the set of hydraulic head (h^t) and the pumping rate vector (P^t). The output is the hydraulic head vector at the next time step (h^{t+1}). The subsurface water model is illustrated as follows:

$$h^{t+1} = f\left(h^t, P^t\right), \qquad (9)$$

$$P_i^t \leq \overline{D}^t, \qquad (10)$$

where h^t and h^{t+1} are subsurface water level vectors at time t and $t + 1$; P^t is the supply vector offered from the pumping well; and P_i^t is the supply at the well i in the tth time step. Equation (9) represents the subsurface water transient equation with the artificial neural networks. Equation (10) represents the demand-supply of constraint each well at time t. Pumping rate of each well is assumed to be less than or equal to assigned demand with the FIS in the study.

The ANN was trained by the back-propagation learning algorithm [29] for subsurface water table prediction. The typical processes of the ANN parameters identification such as the number of hidden layers and the neurons are listed

the study, $j = 1$. G_{ik}^t is the difference between water level index (WLI) of the reservoirs i and k at the tth time step [27, 28] and N_S is the reservoir storage node set; if $i = k$, then $G_{ik}^t = 0$ otherwise. Z_i^t is the ratio of residual volume to the capacity in reservoir i at the tth time step: $(V_i^{\max} - V_i^t)/V_i^{\max}$; c_1, c_2, and c_3 are the weight coefficients applied to the shortage, surface-water level index difference, and residual reservoir volume ratio, respectively ($c_1 = 1$, $c_2 = 10$, and $c_3 = 1$). X_i^t denotes the release from reservoir i at time step t; OF_i^t denotes spills of i reservoir at time step t; and V_i^t is the storage of the reservoir i. $V_i^{\min}$ and $V_i^{\max}$ are minimum and maximum capacity of the reservoir i. $X_{i,j}^{\min}$ and $X_{i,j}^{\max}$ are minimum and maximum discharge of the pipe from node i to j and Ω is the node set of the system network. The surface water demand considers hedging rule at time step t. The hedging rule is illustrated as follows:

$$\text{if } V_{\text{joint}}^t \geq V_2, \quad \text{then } \widehat{D}^t = \widehat{D}^t,$$

$$\text{if } V_2 > V_{\text{joint}}^t \geq V_3, \quad \text{then } \widehat{D}^t = \omega_1 \widehat{D}^t \qquad (8)$$

$$\text{if } V_{\text{joint}}^t < V_3, \quad \text{then } \widehat{D}^t = \omega_2 \widehat{D}^t,$$

where V_{joint}^t is the joint storage in all reservoirs; V_1 is the sum of maximum storage (upper limit) among the reservoirs; V_2 is

in Negnevitsky [2]. This ANN consists of a three-layer feed-forward network and one hidden layer in which the layer contains twenty neurons.

2.4. The Simulation-Optimization Model. To compare the FIS with the simulation-optimization model, this study further formulates the problem (1)~(10) into the sequential optimization problem. As previously stated, this investigation integrates sequential optimization and simulation models to solve the problem defined as follows:

$$J^t = \min_{X^t, P^t} \left[\sum_j c_{1,j} \mathrm{SH}_j^t + \sum_i \left(c_{2,i} G_{i,k}^t + c_{3,i} Z_i^t \right) + c_4 SG^t \right],$$

$$t = 1 \sim n; i, k \in N_S, j \in N_D \tag{11}$$

subject to $(4) \sim (10)$,

where SG^t represents the difference between WLI of surface and subsurface water systems at time step t and c_4 is the weight coefficient applied to WLI difference between surface and subsurface water systems ($c_4 = 10$). In the model, the pumping rates are first obtained by the heuristic optimization (i.e., genetic algorithm (GA)). Then, the release of each reservoir and next time-step states are determined by (4)~(10) using the LP and ANN.

2.5. Case Study. This study performs numerical analysis on a water supply problem to verify effectiveness of the proposed methodology. The planning horizon in the study is twenty years and each time step is ten days. Figure 4 shows the conjunctive use system including two reservoirs and an aquifer. Reservoirs 1 and 2 contain a capacity of 7.0×10^7 (m^3) and 5.0×10^7 (m^3). Reservoir operation rules will be designed to vary with periods [30]. Figures 5(a) and 5(b) are operation rule curves for Reservoirs 1 and 2, respectively. Full of water in reservoirs is assumed as the initial condition. Figure 6 shows both reservoirs inflows that reflect the hydrological dynamics of Taiwan. The inflow ratio of drought season to wet season is 0.32 (Reservoir 1) and 0.20 (Reservoir 2). Moreover, the capacity factor (i.e., effective capacity/average annual flow) of Reservoir 1 is 0.24 while that of Reservoir 2 is 0.35. Figure 7 demonstrates a hypothetical homogeneous unconfined aquifer with dimensions of 17 km by 17 km. The case contains 170×170 finite-difference meshes along with five pumping wells (red blocks) and five observation wells (black blocks). The boundary conditions on the north and south sides are no-flow boundaries. The west and east constant-head boundaries are 100 m and 80 m, respectively. Aquifer properties and simulation parameters are shown in Table 2.

3. Results and Discussion

3.1. Comparison of Decoupled and Coupled Conjunctive Use Operations. Table 3 demonstrates the series of models under the same water requirement amount, 1.5×10^7 (m^3/ten-day). Case 1 considers decoupled operation that surface

TABLE 2: Aquifer properties and simulation parameters.

Parameter	Value
Aquifer thickness (m)	110
Specific yield	0.2
Porosity	0.2
Horizontal hydraulic conductivity (m/s)	0.0001
Vertical hydraulic conductivity (m/s)	0.0001
Simulation time step length (days)	10
Maximum pumping rate (cms)	0.3

TABLE 3: Case abstract in the study.

Case number	Description
1	Decoupled conjunctive use operation
2	Conjunctive use operation using FIS within high usage of subsurface water
3	Conjunctive use operation using a simulation-optimization model
4	Conjunctive use operation using FIS within low usage of subsurface water

water is supplied in advance, and subsurface water is then supplied. Case 2 considers the conjunctive use of surface and subsurface water simultaneously by using FIS based on fuzzy rules (Table 1). Table 4 presents the water supply and shortage index (SI) [31, 32] which, proposed by the US Army Corps of Engineers, could represent the severity of the long-term water shortage from surface and subsurface water. The result shows that the 10-day and annual SI of Case 2 are lower than those of Case 1. It implies that the FIS could improve water shortage in the case study. Compared with Case 1, Case 2 decreases the shortage by 26.23%, and the FIS makes a significant drop in deficit risk. This indicates that the FIS conjunctive use of surface and subsurface water is more efficient. The FIS specifies how much water is supplied from surface and subsurface water to achieve system demand requirement. According to the fuzzy rules, water is supplied from surface water in normal time and from subsurface water during the drought. Figure 8 implies the relationship between subsurface water supply and shortage in decoupled and coupled conjunctive use models (Cases 1 and 2). Furthermore, subsurface water is supplied earlier in coupled conjunctive use model (Case 2) than in the decoupled conjunctive use model (Case 1) during the drought. The result indicates that timing of water allocation is significantly important. Considering the FIS conjunctive operation (Case 2), water supply from subsurface water in advance may reduce the impact of shortage under a long-term operation. Ponnambalam et al. [33] compared general operating rules developed by both fuzzy rules and regression-based rules. Their results demonstrate that the FIS rules perform much better than the regression rules for dealing with uncertainty of inflows. Fuzzy sets provide a nonfrequentist approach to considering uncertainty [34]. The FIS conjunctive use of surface and subsurface water can enhance the reliability of water supplies by providing

TABLE 4: The shortage indices and the supply of water system in the cases.

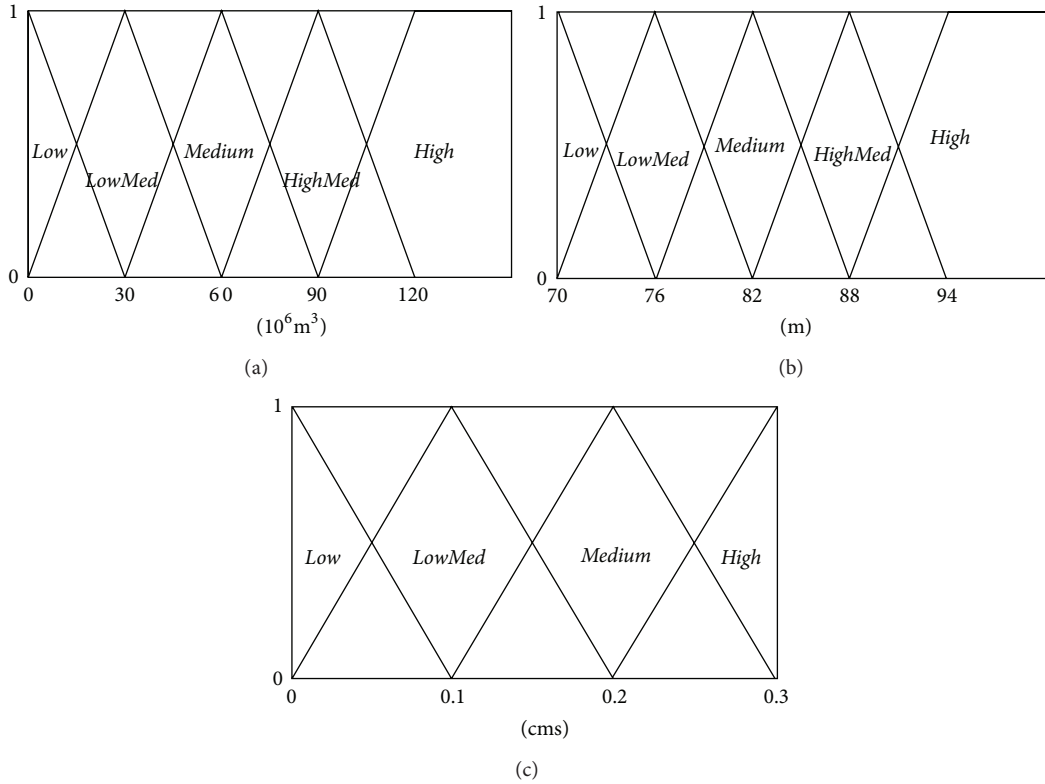| Case		1	2	3	4
10-day SI		2.09	1.44	1.50	1.84
Annual SI		0.61	0.45	0.48	0.59
Number of 10 days in shortage		262	234	241	250
Surface water (10^4 m^3)	10-day supply	1345.25	1345.07	1343.68	1347.77
	Annual supply	48429.10	48422.62	48372.49	48519.6
Subsurface water (10^4 m^3)	10-day supply	49.77	73.44	65.60	56.80
	Annual supply	1791.56	2643.77	2361.48	2044.84

(a)

(b)

(c)

FIGURE 3: Fuzzy membership function for (a) input 1: surface water state, (b) input 2: subsurface water state, and (c) output: pumping rate.
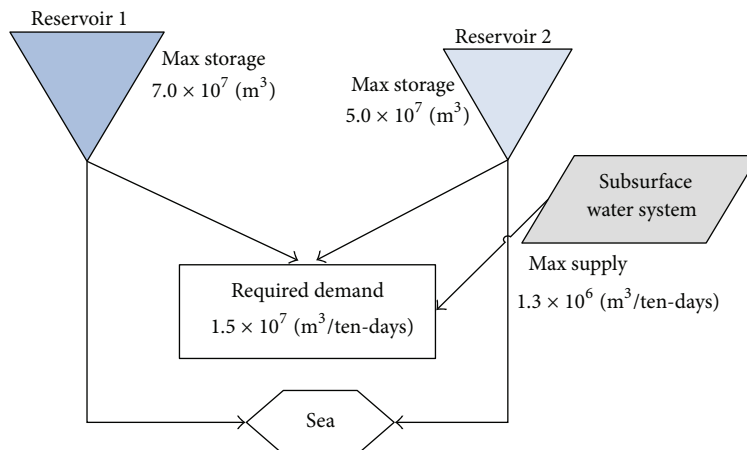

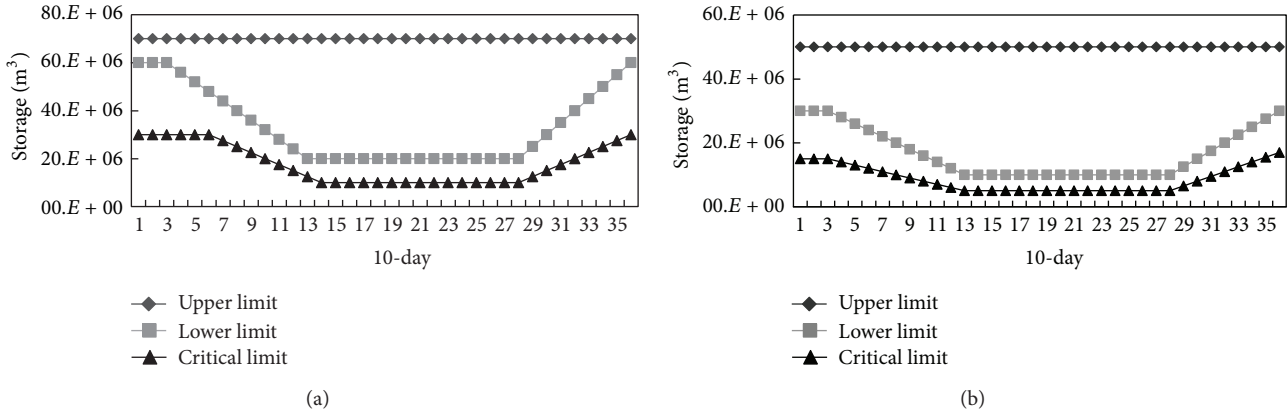FIGURE 4: Schematic diagram of water resources system.

(a)

(b)

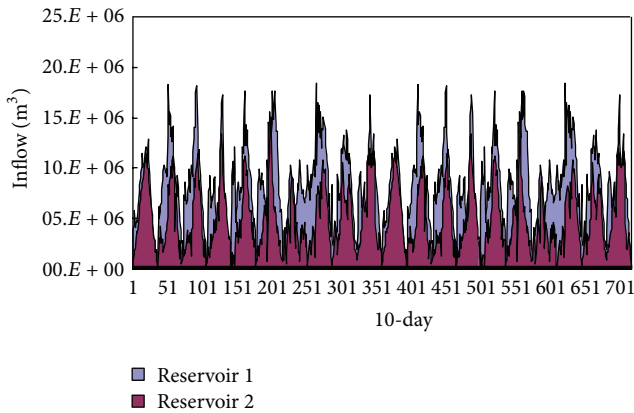FIGURE 5: The operation rule curve of (a) Reservoir 1 and (b) Reservoir 2.

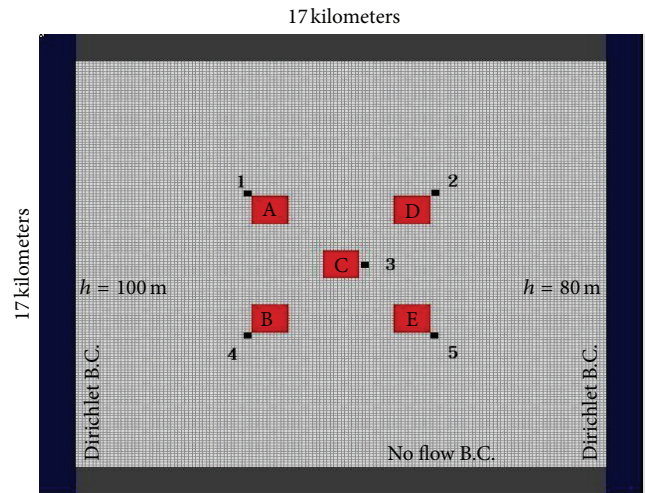
FIGURE 6: Reservoir inflows in surface water system.

(Red blocks mean pumping well clusters and black blocks mean observation wells)

FIGURE 7: Model of subsurface water system, observation, and pumping wells.
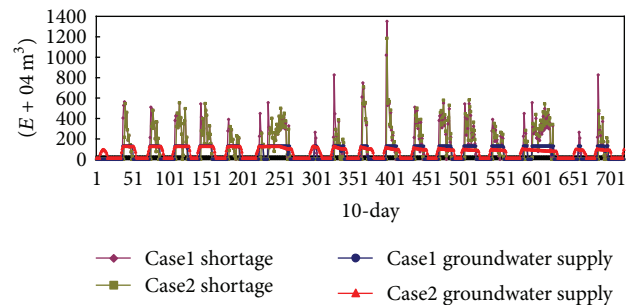
FIGURE 8: Comparison of supply of subsurface water and shortage between Cases 1 and 2.

independent sources. Surface and subsurface water systems contain distinctly different characteristics; for example, surface water is rapid fluctuations and subsurface water varies gradually. Considering the fuzzy rules that abundant water system supplies more water, the FIS is efficiently applicable to the management of surface and subsurface water.

3.2. Comparison of FIS and Simulation-Optimization Model. This study compares the FIS and simulation-optimization models to verify effectiveness of the proposed FIS methodology for conjunctive use of surface and subsurface water. Simulation-optimization approach is used in Case 3 for minimizing the water shortage and balancing the usages between surface and subsurface water (11). In the simulation-optimization model, the surface and subsurface water simulation models including the LP and ANN are embedded in the genetic algorithm (GA) to determine the pumping rate and water allocation in each time step sequentially. For the details of GA refer to McKinney and Lin [35], Chen et al. [36], and Chang et al. [37].

The result reveals that 10-day and annual SI of the FIS and simulation-optimization model (Cases 2 and 3) are similar (Table 4). Both models can decrease the water shortage more than 20% in comparison Case 1. This information allows the

decision makers to control water supply for a long term by the FIS. Similar to the simulation-optimization model, the fuzzy operating rules specify how water is managed throughout the system to achieve system demand requirement. During

TABLE 5: Validation results in subsurface water ANN model.

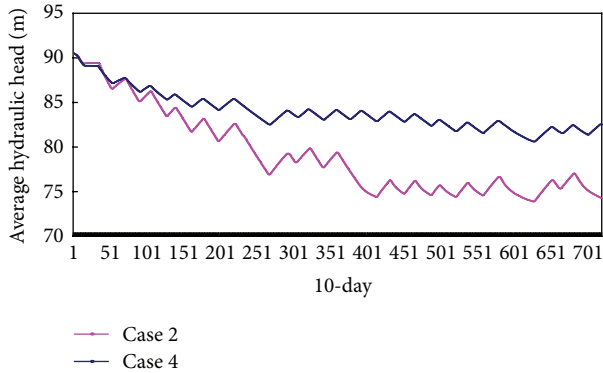|	MSE (m^2)	RMSE (m)	AME (m)
Obs. 1	0.42	0.65	0.51
Obs. 2	0.45	0.67	0.53
Obs. 3	1.04	1.02	0.82
Obs. 4	0.43	0.65	0.52
Obs. 5	0.47	0.69	0.54

FIGURE 9: Comparison of average hydraulic heads in Case 2 and 4.

the drought, subsurface water is used in advance, and surface water is saved. Water supply using the FIS will reduce the impact of shortage. However, problem solving requires hundreds to thousands of numerical simulation runs for searching water supply strategies in the GA approach. For example, the maximum number of generations is twenty, and the population size for each generation is fifty chromosomes. Therefore, 1000 searching possibilities at most are needed in each time step. The computation is more effective using the FIS than the GA. However, the FIS approach obtains near-optimal solutions and saves considerable computational time. The FIS provides an alternative way for conjunctive operations that offer the good chances for water supply management [3–5]. The FIS is easy to apply and extend to a complex water system [3], utilized in controlling humanistic systems in water resources management, and offers an alternative way for conjunctive operation.

3.3. Subsurface Water Table Simulation by ANN and Control by FIS.
The ANN inputs include the hydraulic heads in five observation wells and pumping rates in five pumping wells at current time, and the outputs are hydraulic heads in the observations at next time. The data are generated by the MODFLOW and sets of input-output patterns are generated by a random pumping rate between the minimum and maximum (from 0 to 0.3 cms). The MODFLOW, is a physical finite-difference numerical flow model and a computer program developed by the US Geological Survey [38]. Moreover, a network training function updates weight and bias values according to Levenberg-Marquardt optimization [39]. The transfer functions with a hidden layer and the output layer are hyperbolic tangent. If the training stop criteria (i.e., MSE = 10^{-7}) are not met, the learning algorithm continues.

TABLE 6: Rule table for the operation in conjunctive use operation using FIS within low usage of subsurface water.

	Surface water state				
	Low	Low Med.	Medium	High Med.	High
Subsurface water state					
Low	Low	Low	Low	Low	Low
Low Med.	Medium	Medium	Low	Low	Low
Medium	Medium	Medium	Low	Low	Low
High Med.	Medium	Medium	Low	Low	Low
High	Medium	Medium	Low	Low	Low

The total available data has been divided into two sets, training and validation sets: 2,500 samples were used to train the ANN, and 1,000 samples were used for validation. Table 5 presents the ANN validation results. Accuracy of the ANN model can be quantified when compared with MODFLOW. Comparing relative errors reveals that, among the table, Observation 1 is the lowest error in the estimation. Results demonstrate that relative error with respect to average subsurface water level is 1.3% or less. After the validation, the ANN simulates the subsurface water level with time behind the FIS operating. Accordingly, the ANN obtains better results, and the computing time of the ANN model is about 1/53 of a traditional MODFLOW. This result reveals that the ANN predicts hydraulic heads efficiently at the selected control locations under variable pumping but condensed surrogate for subsurface water flow model in interesting cells [18, 21]. Results show the ANN approach has a great potential to predict subsurface water level because it permits developing complex and nonlinear models.

Figure 9 shows time-varying hydraulic heads in the two FIS cases (Cases 2 and 4) under various pumping strategies. The fuzzy rules for high and low usages in Cases 2 and 4 are represented in Tables 1 and 6. Overall, the average hydraulic heads vary with dry-wet cycles. In Cases 2 and 4, a fuzzy rule-based system determines the pumping rate considering hydraulic head constraint implicitly. Moreover, the FIS will decide to pump a large volume of subsurface water in Case 2 and pump a small volume of subsurface water in Case 4; therefore the hydraulic head in Case 4 is higher than that in Case 2. Appropriate subsurface water usage makes water resources sustainable. Moreover, subsurface water overdraft causes land subsidence problems in many places; therefore preventing the consequences of aquifer exploitation is essential [40, 41]. Results show that the minimum hydraulic head in Case 2 is around 73 m and that in Case 4 is around 81 m (Figure 9), representing that hydraulic head is under control using the FIS. As a result, fuzzy rules consider hydraulic head constraints implicitly for environmental conservation. Accordingly, the FIS is the intelligent control model based on the fuzzy rule and controls humanistic systems in water resources management. In the FIS approach, the rules with the expert experience can satisfy demand and environmental conservation adaptively. The FIS offers the ability for the adaptive management so that the system follows the fuzzy

rule and adapts the supply water based on the states of the system. Thus, the managers can adjust the fuzzy operation strategy to satisfy the water demand and environmental conservation.

4. Conclusions

This study applied a fuzzy inference system (FIS) for the conjunctive use of surface and subsurface water. The FIS determines operating policies between surface and subsurface water based on the current states. The approach with the expert knowledge could obtain efficient and near-optimal solutions when compared to the simulation-optimization approach. After assigning the demand of surface and subsurface water, the ANN and LP simulate the surface and subsurface water states.

Results show that the FIS enhances reliability of water supply and provides a decision for utilizing two water sources. To minimize the impacts of consequential shortages, the FIS follows the operation rules in which abundant water system supplies more, but scarce water system supplies less. The FIS improves shortage performance because the FIS supplies subsurface water early and retains surface water during dry season. The FIS controls the supply between surface and subsurface water and reduces the impact of overpumping of subsurface water. Therefore, the FIS is best utilized in controlling humanistic systems whose behavior is influenced by expert knowledge for water resources management. Direction for future studies could consider an autotuning technology and a neural learning technology or parameter optimization approaches further acquiring the rule from expert knowledge [42].

Acknowledgments

References

[1] L. A. Zadeh, "Fuzzy sets," *Information and Control*, vol. 8, no. 3, pp. 338–353, 1965.

[2] M. Negnevitsky, *Artificial Intelligence: A Guide to Intelligent Systems*, Addison Wesley, Reading, Mass, USA, 2002.

[3] B. P. Shrestha, L. Duckstein, and E. Z. Stakhiv, "Fuzzy rule-based modeling of reservoir operation," *Journal of Water Resources Planning and Management*, vol. 122, no. 4, pp. 262–268, 1996.

[4] S. O. Russell and P. F. Campbell, "Reservoir operating rules with fuzzy programming," *Journal of Water Resources Planning and Management*, vol. 122, no. 3, pp. 165–170, 1996.

[5] D. P. Panigrahi and P. P. Mujumdar, "Reservoir operation modelling with fuzzy logic," *Water Resources Management*, vol. 14, no. 2, pp. 89–109, 2000.

[6] M. Özger, "Comparison of fuzzy inference systems for streamflow prediction," *Hydrological Sciences Journal*, vol. 54, no. 2, pp. 261–273, 2009.

[7] H. Chu and L. Chang, "Application of optimal control and fuzzy theory for dynamic groundwater remediation design," *Water Resources Management*, vol. 23, no. 4, pp. 647–660, 2009.

[8] C. Mahabir, F. E. Hicks, and A. R. Fayek, "Application of fuzzy logic to forecast seasonal runoff," *Hydrological Processes*, vol. 17, no. 18, pp. 3749–3762, 2003.

[9] O. Kisi, M. E. Karahan, and Z. Şen, "River suspended sediment modelling using a fuzzy logic approach," *Hydrological Processes*, vol. 20, no. 20, pp. 4351–4362, 2006.

[10] H. Başağaoğlu and M. A. Mariño, "Joint management of surface and ground water supplies," *Ground Water*, vol. 37, no. 2, pp. 214–222, 1999.

[11] R. C. Peralta, R. R. A. Cantiller, and J. E. Terry, "Optimal large-scale conjuctive water-use planning: case study," *Journal of Water Resources Planning & Management*, vol. 121, no. 6, pp. 471–478, 1995.

[12] C. R. Philbrick and P. K. Kitanidis, "Optimal conjunctive-use operations and plans," *Water Resources Research*, vol. 34, no. 5, pp. 1307–1316, 1998.

[13] S. V. N. Rao, S. M. Bhallamudi, B. S. Thandaveswara, and G. C. Mishra, "Conjunctive use of surface and groundwater for coastal and deltaic systems," *Journal of Water Resources Planning and Management*, vol. 130, no. 3, pp. 255–267, 2004.

[14] D. W. Watkins and D. C. McKinney, "Decomposition methods for water resources optimization models with fixed costs," *Advances in Water Resources*, vol. 21, no. 4, pp. 283–295, 1998.

[15] T. Nishikawa, "Water-resources optimization model for Santa Barbara, California," *Journal of Water Resources Planning and Management*, vol. 124, no. 5, pp. 252–263, 1998.

[16] M. N. Azaiez, "A model for conjunctive use of ground and surface water with opportunity costs," *European Journal of Operational Research*, vol. 143, no. 3, pp. 611–624, 2002.

[17] E. Coppola, *Optimal pumping policy for a public supply wellfield using computational neural network with decision-making methodology [Ph.D. thesis]*, University of Arizona at Tucson, Tucson, Ariz, USA, 2000.

[18] E. Coppola, M. Poulton, E. Charles, J. Dustman, and F. Szidarovszky, "Application of artificial neural networks to complex groundwater management problems," *Natural Resources Research*, vol. 12, no. 4, pp. 303–320, 2003.

[19] E. Coppola, F. Szidarovszky, M. Poulton, and E. Charles, "Artificial neural network approach for predicting transient water levels in a multilayered groundwater system under variable state, pumping, and climate conditions," *Journal of Hydrologic Engineering*, vol. 8, no. 6, pp. 348–359, 2003.

[20] S. Feng, S. Kang, Z. Huo, S. Chen, and X. Mao, "Neural networks to simulate regional ground water levels affected by human activities," *Ground Water*, vol. 46, no. 1, pp. 80–90, 2008.

[21] H. Chu and L. Chang, "Optimal control algorithm and neural network for dynamic groundwater management," *Hydrological Processes*, vol. 23, no. 19, pp. 2765–2773, 2009.

[22] A. W. Minns and M. J. Hall, "Artificial neural networks as rainfall-runoff models," *Hydrological Sciences Journal*, vol. 41, no. 3, pp. 399–417, 1996.

[23] H. R. Maier and G. C. Dandy, "Neural networks for the prediction and forecasting of water resources variables: a review of modelling issues and applications," *Environmental Modelling and Software*, vol. 15, no. 1, pp. 101–124, 2000.

[24] J. Morshed and J. J. Kaluarachchi, "Application of artificial neural network and genetic algorithm in flow and transport simulations," *Advances in Water Resources*, vol. 22, no. 2, pp. 145–158, 1998.

[25] M. Tu, N. Hsu, and W. W.-G. Yeh, "Optimization of reservoir management and operation with hedging rules," *Journal of Water Resources Planning and Management*, vol. 129, no. 2, pp. 86–97, 2003.

[26] J. W. Labadie, "Optimal operation of multireservoir systems: state-of-the-art review," *Journal of Water Resources Planning and Management*, vol. 130, no. 2, pp. 93–111, 2004.

[27] Hydrologic Engineering Center (HEC), *HEC-5 Simulation of Flood Control and Conservation Systems: User's Manual. Version 8*, US Army Corps of Engineers, Davis, Calif, USA, 1998.

[28] C. Wei and N. Hsu, "Multireservoir real-time operations for flood control using balanced water level index method," *Journal of Environmental Management*, vol. 88, no. 4, pp. 1624–1639, 2008.

[29] MATLAB, *Neural Network Tool Box for Use with Matlab: User Guide. Version 4*, vol. 3, The Mathwork, Apple Hill Drive, Mass, USA, 2000.

[30] L. W. Mays and Y. K. Tung, *Hydrosystems Engineering and Management*, McGraw-Hill, New York, NY, USA, 1992.

[31] Hydrologic Engineering Center (HEC), *Reservoir Yield, Generalized Computer Program 23-J2-L245*, US Army Corps of Engineers, Davis, Calif, USA, 1966.

[32] Hydrologic Engineering Center (HEC), *Hydrologic Engineering Methods for Water Resources Development, Volume 8, Reservoir Yield*, US Army Corps of Engineers, Davis, Calif, USA, 1975.

[33] K. Ponnambalam, F. Karray, and S. J. Mousavi, "Minimizing variance of reservoir systems operations benefits using soft computing tools," *Fuzzy Sets and Systems*, vol. 139, no. 2, pp. 451–461, 2003.

[34] J. W. Labadie, "Optimal operation of multireservoir systems: state-of-the-art review," *Journal of Water Resources Planning and Management*, vol. 130, no. 2, pp. 93–111, 2004.

[35] D. C. McKinney and M. -D. Lin, "Genetic algorithm solution of groundwater management models," *Water Resources Research*, vol. 30, no. 6, pp. 1897–1906, 1994.

[36] L. Chen, J. McPhee, and W. W.-G. Yeh, "A diversified multiobjective GA for optimizing reservoir rule curves," *Advances in Water Resources*, vol. 30, no. 5, pp. 1082–1093, 2007.

[37] L. Chang, H. Chu, and C. Hsiao, "Optimal planning of a dynamic pump-treat-inject groundwater remediation system," *Journal of Hydrology*, vol. 342, no. 3-4, pp. 295–304, 2007.

[38] A. W. Harbaugh and M. G. McDonald, "Programmer's documentation for MODFLOW-96, an update to the U.S. Geological Survey modular finite-difference ground-water flow model," Open-File Report 96-486, U.S. Geological Survey, Reston, Va, USA, pp. 220, 1996.

[39] P. E. Gill, W. Murray, and M. H. Wright, *Practical Optimization*, Academic Press, New York, NY, USA, 1981.

[40] O. G. Adrian, D. L. Roudolph, and J. A. Cherry, "Analysis of long-term land subsidence near Mexico City: field investigations and predictive modeling," *Water Resources Research*, vol. 35, no. 11, pp. 3327–3341, 1999.

[41] N. C. Don, N. T. M. Hang, H. Araki, H. Yamanishi, and K. Koga, "Groundwater resources and management for paddy field irrigation and associated environmental problems in an alluvial coastal lowland plain," *Agricultural Water Management*, vol. 84, no. 3, pp. 295–304, 2006.

[42] K. Ying, S. Lin, Z. Lee, and I.-L. Lee, "A novel function approximation based on robust fuzzy regression algorithm model and particle swarm optimization," *Applied Soft Computing Journal*, vol. 11, no. 2, pp. 1820–1826, 2011.

Research Article

Image Matching by Using Fuzzy Transforms

Ferdinando Di Martino and Salvatore Sessa

Dipartimento di Architettura, Università degli Studi di Napoli Federico II, Via Monteoliveto 3, 80134 Napoli, Italy

Correspondence should be addressed to Salvatore Sessa; sessa@unina.it

We apply the concept of Fuzzy Transform (for short, F-transform) for improving the results of the image matching based on the Greatest Eigen Fuzzy Set (for short, GEFS) with respect to max-min composition and the Smallest Eigen Fuzzy Set (for short, SEFS) with respect to min-max composition already studied in the literature. The direct F-transform of an image can be compared with the direct F-transform of a sample image to be matched and we use suitable indexes to measure the grade of similarity between the two images. We make our experiments on the image dataset extracted from the well-known Prima Project View Sphere Database, comparing the results obtained with this method with that one based on the GEFS and SEFS. Other experiments are performed on frames of videos extracted from the Ohio State University dataset.

1. Introduction

Solution methods of fuzzy relational equations have been well studied in the literature (cf., e.g., [1–15]) and applied to image processing problems like image compression [16–19] and image reconstruction [7, 8, 20–22]. In particular, Eigen Fuzzy Sets [23–25] have been applied to image processing and medical diagnosis [2, 6, 7, 16]. If an image I of sizes $N \times N$ (pixels) is interpreted as a fuzzy relation R on the set $\{1, 2, \ldots, N\} \times \{1, 2, \ldots, N\} \rightarrow [0, 1]$, the concepts of the Greatest Eigen Fuzzy Set (for short, GEFS) of I with respect to the max-min composition and of the Smallest Eigen Fuzzy Set (for short, SEFS) of R with respect to the min-max decomposition [2, 24, 25] were studied and used in [26, 27] for an image matching process defined over square images. The GEFS and SEFS of the original image are compared with the GEFS and SEFS of the image to be matched by using a similarity measure based on the Root Mean Square Error (for short, RMSE). The advantage of using GEFS and SEFS is in terms of memory storage is that we can indeed compress an image dataset (in which each image has sizes $N \times N$) in a dataset in which each image is stored by means of its GEFS and SEFS which have total dimension $2N$.

The main disadvantage of using GEFS and SEFS is that we cannot compare images in which the number of rows is different from the number of columns. Our aim is to show

that we can use an F-transform for image matching problems, reducing an image dataset of sizes $N \times M$ (in general, M is not necessarily equal to N) into a dataset of dimensions comparable with that one obtained by using GEFS and SEFS if $M = N$, so having convenience in terms of memory storage.

The F-transform based method [28–30] is used in the literature for image and video compression [29, 31–33], image segmentation [20], and data analysis [22, 34]; indeed, in [31, 32] the quality of the decoded images obtained by using the F-transform compression method is shown to be better than that one obtained with the fuzzy relation equations and fully comparable with the JPEG technique.

The main characteristic of the F-transform method is to maintain an acceptable quality in the reconstructed image even under strong compression rates; indeed in [20] the authors show that the segmentation process can be applied directly over the compressed images. Here we use the direct F-transform in image matching analysis with the aim of reducing the memory used to store the image dataset. In fact, we compress a monochromatic image (or a band of a multiband image) I of sizes $N \times M$ via the direct F-transform to a matrix F of sizes $n \times m$ using a compression rate $\rho = (n \times m)/(N \times M)$.

By using a distance, we compare the F-transform of each image with the F-transform of the sample image. We also
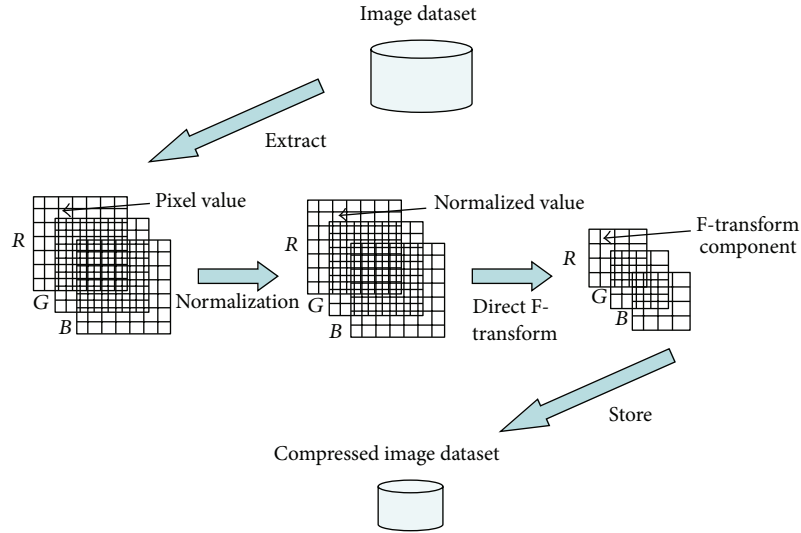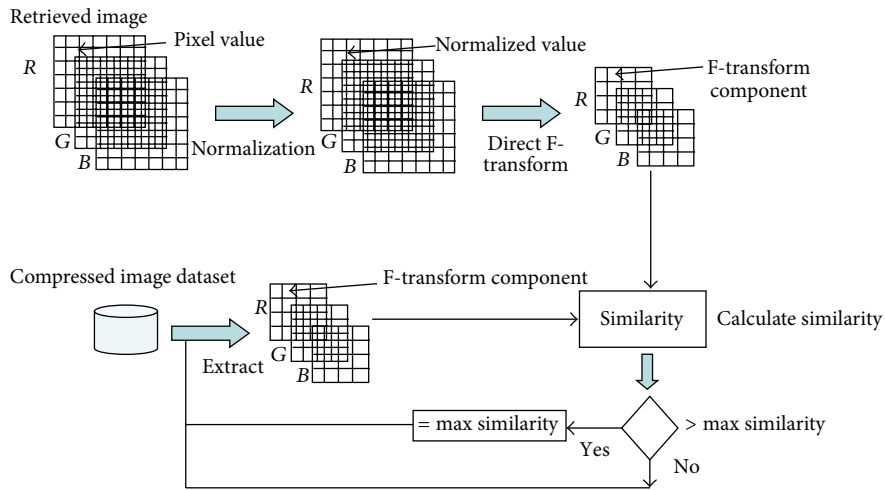
FIGURE 1: The preprocessing phase.

FIGURE 2: F-transform image matching process.

adopt a preprocessing phase for compressing each image with several compression rates. In Figure 1 we show the preprocessing phase on a dataset of color images. We compress each color image in the three monochromatic components corresponding to the three bands R, G, and B.

At the end of the preprocessing phase we can use the compressed image dataset for image matching analysis. Supposing that the original image dataset was composed by s color images of sizes $N \times M$ using a compression rate $\rho = (n \times m)/(N \times M)$, we obtain that the dimension of the compressed image dataset is constituted totally of $3s(n \times m)$ pixels.

In Figure 2 we schematize the image matching process. The sample image is compressed by the F-transform method; then we compare the three compressed bands of each image obtained via F-transform with those ones deduced for the sample image by using the Peak Signal to Noise Ratio (for short, PSNR). At the end of this process, we determine the

image in the dataset with the greatest overall PSNR with respect to the sample image.

Here a monochromatic image or a band of a color image I of sizes $N \times M$ is interpreted as a fuzzy relation R whose entries $R(x, y)$ are obtained by normalizing the intensity $I(x, y)$ of each pixel with respect to the length L of the scale, that is, $R(x, y) = I(x, y)/L$. We show that our F-transform approach can be also applied in image matching processes to images of sizes $M \times N$ (eventually, $M \neq N$), giving analogous results with respect to that one obtained with GEFS and SEFS based method. The comparison tests are made on the 256×256 color image dataset extracted from View Sphere Database, an image dataset consisting in a set of images of objects in which an object is photographed from various directions by using a camera placed on a semisphere whose center is the same considered object. We also use the Ohio State University color video datasets sample for our tests. Each video is composed by frames consisting of color images;
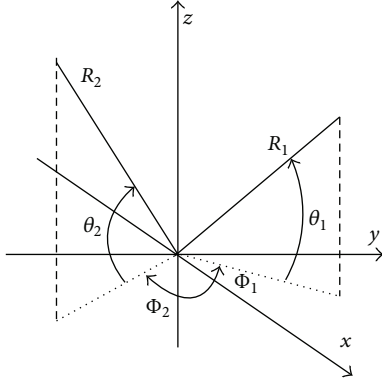
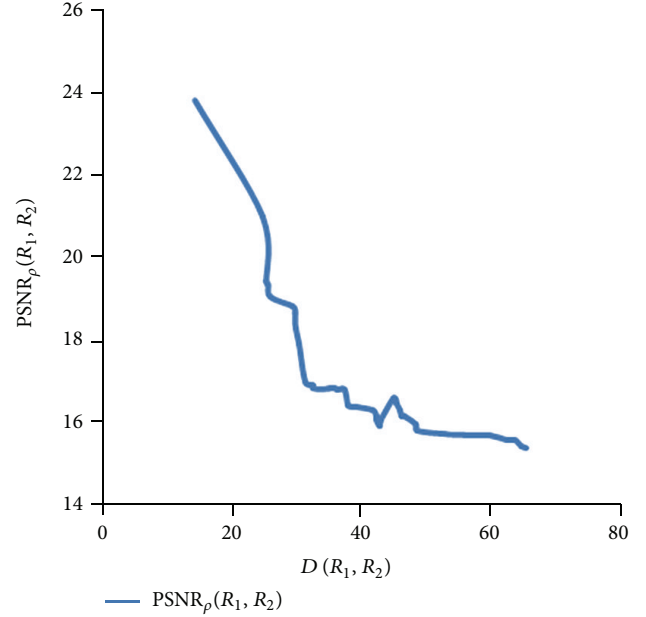FIGURE 3: The angles for two directions R_1 and R_2 (the object is in the origin).

FIGURE 4: Trend of PSNR with respect to D index for the eraser obtained from the comparison with the sample image at $\theta = 11°$ and $\phi = 36°$.

we show the results for the Mom-Daughter and sflowg motions. In Section 2 we recall the concepts of F-transform in two variables. In Section 3 we recall the GEFS and SEFS based method; in Section 4 we propose our image matching method based on the F-transforms. Our experiments are illustrated in Section 5, and Section 6 is conclusive.

2. F-Transforms in Two Variables

Following [29] and limiting ourselves to the discrete case, let $n \geq 2$ and $x_1, x_2, \ldots, x_n$ be a increasing sequence of points (nodes) of $[a, b]$, $x_1 = a < x_2 < \cdots < x_n = b$. We say that the fuzzy sets $A_1, \ldots, A_n : [a, b] \to [0, 1]$ (basic functions) form a fuzzy partition of $[a, b]$ if the following hold:

(1) $A_i(x_i) = 1$ for every $i = 1, 2, \ldots, n$;

(2) $A_i(x) = 0$ if $x \notin (x_{i-1}, x_{i+1})$ for $i = 2, \ldots, n-1$;

(3) $A_i(x)$ is a continuous function on $[a, b]$;

(4) $A_i(x)$ strictly increases on $[x_{i-1}, x_i]$ for $i = 2, \ldots, n$ and strictly decreases on $[x_i, x_{i+1}]$ for $i = 1, \ldots, n-1$;

(5) $\sum_{i=1}^{n} A_i(x) = 1$ for every $x \in [a, b]$.

The fuzzy partition $\{A_1, \ldots, A_n\}$ is said to be uniform if

(6) $n \geq 3$ and $x_i = a + h \cdot (i-1)$, where $h = (b-a)/(n-1)$ and $i = 1, 2, \ldots, n$ (equidistant nodes);

(7) $A_i(x_i - x) = A_i(x_i + x)$ for every $x \in [0, h]$ and $i = 2, \ldots, n-1$;

(8) $A_{i+1}(x) = A_i(x - h)$ for every $x \in [x_i, x_{i+1}]$ and $i = 1, 2, \ldots, n-1$.

Let $m \geq 2$, $y_1, y_2, \ldots, y_m \in [c, d]$ be m nodes such that $y_1 = c < \cdots < y_m = d$. Furthermore, let $B_1, \ldots, B_m : [c, d] \to [0, 1]$ be a fuzzy partition of $[c, d]$, and let $f : P \times Q \to$ reals be an assigned function, $P \times Q \subseteq [a, b] \times [c, d]$, with $P = \{p_1, \ldots, p_N\}$ and $Q = \{q_1, \ldots, q_M\}$ being "sufficiently dense" sets with respect to the chosen partitions; that is for each $i = 1, \ldots, N$ (resp., $j = 1, \ldots, M$) there exists an index $k \in \{1, \ldots, n\}$ (resp., $l \in \{1, \ldots, m\}$) such that $A_k(p_i) > 0$

(resp., $B_l(q_j) > 0$). The matrix $[F_{kl}]$ is said to be the direct F-transform of f with respect to $\{A_1, \ldots, A_n\}$ and $\{B_1, \ldots, B_m\}$ if we have for each $k = 1, \ldots, n$ and $l = 1, \ldots, m$

$$F_{kl} = \frac{\sum_{j=1}^{M} \sum_{i=1}^{N} f\left(p_i, q_j\right) A_k\left(p_i\right) B_l\left(q_j\right)}{\sum_{j=1}^{M} \sum_{i=1}^{N} A_k\left(p_i\right) B_l\left(q_j\right)}. \quad (1)$$

Then the inverse F-transform of f with respect to $\{A_1, A_2, \ldots, A_n\}$ and $\{B_1, \ldots, B_m\}$ is the function $f_{nm}^{F}(p_i, q_j) : P \times Q \to$ reals defined as

$$f_{nm}^{F}\left(p_i, q_j\right) = \sum_{k=1}^{n} \sum_{l=1}^{m} F_{kl} A_k\left(p_i\right) B_l\left(q_j\right). \quad (2)$$

The following existence theorem holds [29].

Theorem 1. *Let* $f : P \times Q \to$ *reals be a given function,* $P \times Q \subseteq [a, b] \times [c, d]$, *with* $P = \{p_1, \ldots, p_N\}$ *and* $Q = \{q_1, \ldots, q_M\}$. *Then for every* $\varepsilon > 0$, *there exist two integers* $n(\varepsilon)$, $m(\varepsilon)$ *and related fuzzy partitions* $\{A_1, A_2, \ldots, A_{n(\varepsilon)}\}$ *of* $[a, b]$ *and* $\{B_1, B_2, \ldots, B_{m(\varepsilon)}\}$ *of* $[c, d]$ *such that the sets* P, Q *are sufficiently dense with respect to such partitions and* $|f(p_i, q_j) - f_{n(\varepsilon)m(\varepsilon)}^{F}(p_i, q_j)| < \varepsilon$ *is satisfied for every* $i \in \{1, \ldots, N\}$ *and* $j \in \{1, \ldots, M\}$.

Let R be a gray image of sizes $N \times M$, seen as $R : (i, j) \in \{1, \ldots, N\} \times \{1, \ldots, M\} \to [0, 1]$, with $R(i, j)$ being the normalized value of the pixel $P(i, j)$ given by $R(i, j) = P(i, j)/Lt$ if Lt is the length of the gray scale. In [27] R is

FIGURE 5: Eraser at $\theta = 11°$ and $\phi = 36°$.

FIGURE 6: Eraser at $\theta = 10°$ and $\phi = 54°$.

FIGURE 7: Trend of PSNR with respect to distance (18) for the pen obtained from the comparison with the sample image at $\theta = 10°$ and $\phi = 54°$.
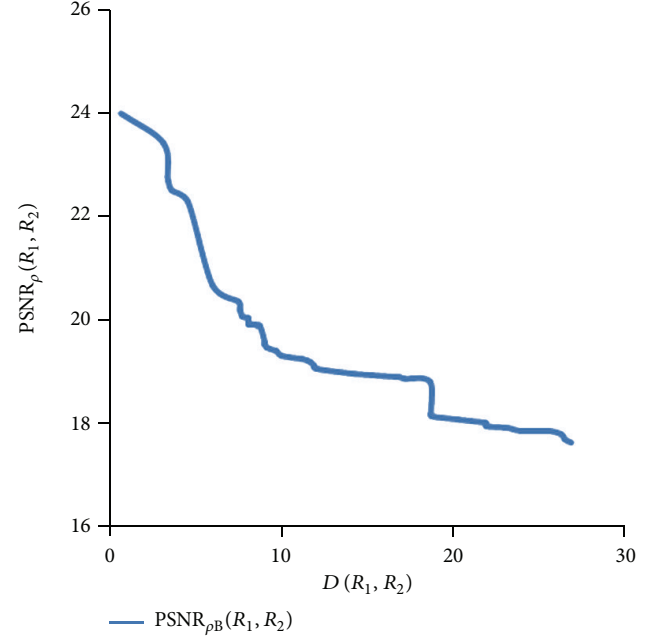

FIGURE 8: Pen at $\theta = 10°$ and $\phi = 54°$.

compressed via the F-transform defined for each $k = 1, \ldots, n$ and $l = 1, \ldots, m$ as

$$F_{kl} = \frac{\sum_{j=1}^{M} \sum_{i=1}^{N} R(i, j) A_k(i) B_l(j)}{\sum_{j=1}^{M} \sum_{i=1}^{N} A_k(i) B_l(j)}, \tag{3}$$

where $p_i = i$, $q_j = j$, $a = c = 1$, $b = N$, $d = M$, and $\{A_1, \ldots, A_n\}$ (resp., $\{B_1, \ldots, B_m\}$), $n \ll N$ (resp., $m \ll M$), is a fuzzy partition of $[1, N]$ (resp., $[1, M]$). The following fuzzy relation is the decoded version of R and it is defined as

$$R_{nm}^F(i, j) = \sum_{k=1}^{n} \sum_{l=1}^{m} F_{kl} A_k(i) B_l(j) \tag{4}$$

for every $(i, j) \in \{1, \ldots, N\} \times \{1, \ldots, M\}$. We have subdivided R in submatrices R_B of sizes $N(B) \times M(B)$, called blocks (cf., e.g., [2, 16]), compressed to blocks F_B of sizes $n(B) \times$

$m(B)(n(B) < N(B), m(B) < M(B))$ via $[F_{kl}^B]$ defined for each $k = 1, \ldots, n(B)$ and $l = 1, \ldots, m(B)$ as

$$F_{kl}^B = \frac{\sum_{j=1}^{M(B)} \sum_{i=1}^{N(B)} R_B(i, j) A_k(i) B_l(j)}{\sum_{j=1}^{M(B)} \sum_{i=1}^{N(B)} A_k(i) B_l(j)}. \tag{5}$$

FIGURE 9: Pen at $\theta = 10°$ and $\phi = 18°$.

FIGURE 10: Frame 1 in Mom-Daughter.

The basic functions $A_1, \ldots, A_{n(B)}$ (resp., $B_1, \ldots, B_{m(B)}$), defined below, constitute a uniform fuzzy partition of $[1, N(B)]$ (resp., $[1, M(B)]$):

$$A_1(x) = \begin{cases} 0.5\left(1 + \cos\dfrac{\pi}{h}(x - x_1)\right), & \text{if } x \in [x_1, x_2], \\ 0, & \text{otherwise,} \end{cases}$$

$$A_k(x) = \begin{cases} 0.5\left(1 + \cos\dfrac{\pi}{h}(x - x_k)\right), & \text{if } x \in [x_{k-1}, x_{k+1}], \\ 0, & \text{otherwise,} \end{cases}$$

$$A_n(x) = \begin{cases} 0.5\left(1 + \cos\dfrac{\pi}{h}(x - x_n)\right), & \text{if } x \in [x_{n-1}, x_n], \\ 0, & \text{otherwise,} \end{cases} \tag{6}$$

where $n = n(B)$, $k = 2, \ldots, n$, $h = (N(B) - 1)/(n - 1)$, $x_k = 1 + h \cdot (k - 1)$, and

$$B_1(y) = \begin{cases} 0.5\left(1 + \cos\dfrac{\pi}{s}(y - y_1)\right), & \text{if } y \in [y_1, y_2], \\ 0, & \text{otherwise,} \end{cases}$$

$$B_t(y) = \begin{cases} 0.5\left(1 + \cos\dfrac{\pi}{s}(y - y_t)\right), & \text{if } y \in [y_{t-1}, y_{t+1}], \\ 0, & \text{otherwise,} \end{cases}$$

$$B_m(y) = \begin{cases} 0.5\left(1 + \cos\dfrac{\pi}{s}(y - y_m)\right), & \text{if } y \in [y_{m-1}, y_m], \\ 0, & \text{otherwise,} \end{cases} \tag{7}$$

where $m = m(B)$, $t = 2, \ldots, m$, $s = (M(B) - 1)/(m - 1)$, $y_t = 1 + s \cdot (t - 1)$. We decompress F_B to $R^F_{n(B)m(B)}$ of sizes $N(B) \times M(B)$ by setting for every $(i, j) \in \{1, \ldots, N_B\} \times \{1, \ldots, M_B\}$

$$R^F_{n(B)m(B)}(i, j) = \sum_{k=1}^{n(B)} \sum_{l=1}^{m(B)} F^B_{kl} A_k(i) B_l(j) \tag{8}$$

which approximates R_B up to an arbitrary quantity ε in the sense of Theorem 1, which, unfortunately, does not give a method for finding two integers $n(B)$ and $m(B)$ such that $|R_B(p_i, q_j) - R^F_{n(\varepsilon)m(\varepsilon)}(p_i, q_j)| < \varepsilon$. Then we prove several values of $n(B)$ and $m(B)$. For every compression rate ρ, we evaluate the quality of the reconstructed image via the PSNR defined as

$$(\text{PSNR})_\rho = 20 \log_{10} \frac{L}{(\text{RMSE})_\rho}, \tag{9}$$

where $(\text{RMSE})_\rho$ is

$$(\text{RMSE})_\rho = \sqrt{\frac{\sum_{i=1}^N \sum_{j=1}^M \left(R(i, j) - R^F_{NM}(i, j)\right)^2}{N \times M}}. \tag{10}$$

Here R^F_{NM} is the reconstructed image obtained by recomposing the blocks $R^F_{n(B)m(B)}{}'$.

3. Max-Min and Min-Max Eigen Fuzzy Sets

Let X be a nonempty finite set, $R : X \times X \to [0, 1]$ and $A : X \to [0, 1]$, such that

$$R \circ A = A, \tag{11}$$

where "$\circ$" is the max-min composition. In terms of membership functions, we have that

$$A(y) = \max_{x \in X}\{\min(A(x), R(x, y)\} \tag{12}$$

for all $x, y \in X$ and A is defined as an Eigen Fuzzy Set of R. Let $A_i : X \to [0, 1]$, $i = 1, 2, \ldots$, be defined iteratively by

$$A_1(z) = \max_{x \in X} R(x, z), \tag{13}$$

$$A_2 = R \circ A_1, \ldots, A_{n+1} = R \circ A_n, \ldots \quad z \in X.$$

It is known [2, 24, 25] that there exists an integer $p \in \{1, \ldots, \text{card } X\}$ such that A_p is the GEFS of R with respect to the max-min composition. We also consider the following:

$$R \,\square\, A = A, \tag{14}$$

where "$\square$" denotes the min-max composition, that is, in terms of membership functions:

$$A(y) = \min_{x \in X} \{\max(A(x), R(x, y))\} \tag{15}$$

for all $x, y \in X$ and A is also defined to be an Eigen Fuzzy Set of R with respect to the min-max composition. It is easily seen that (14) is equivalent to the following:

$$\underline{R} \,\square\, \underline{A} = \underline{A}, \tag{16}$$

where $\underline{R}$ and $\underline{A}$ are pointwise defined as $\underline{R}(x, y) = 1 - R(x, y)$ and $\underline{A}(x) = 1 - A(x)$ for all $x, y \in X$. Since $\underline{A}_p$ for some $p \in \{1, \ldots, \text{card } X\}$ is the GEFS of $\underline{R}$ with respect to the max-min composition, it is immediately proved that the fuzzy set $B : X \rightarrow [0, 1]$ defined as $B(x) = 1 - \underline{A}_p(x)$ for every $x \in [0, 1]$ is the SEFS of R with respect to the min-max composition.

In [27] a distance based on GEFS and SEFS for image matching is used over images of sizes $N \times N$. Indeed, considering two single-band images of sizes $N \times N$, say R_1 and R_2, such distance is given by

$$d(R_1, R_2) = \sum_{x \in X} \left((A_1(x) - A_2(x))^2 + (B_1(x) - B_2(x))^2 \right), \tag{17}$$

where $X = \{1, 2, \ldots, N\}$, A_i, B_i are the GEFS and SEFS of the fuzzy relation R_i, respectively, obtained by normalizing in $[0, 1]$ the pixels of the image I_i, $i = 1, 2$.

In [26, 27] experiments are presented over color images of sizes 256×256 concerning two objects (an eraser and a pen) extracted from View Sphere Database. Each object is put in the center of a semisphere on which a camera is placed in 91 different directions. The camera establishes an image (photography) of the object for each direction which can be identified from two angles θ ($0° < \theta < 90°$) and Φ ($-180° < \Phi < 180°$) as illustrated in Figure 3.

A sample image R_1 (with given $\theta = 11°$, $\Phi = 36°$ for the eraser and $\theta = 10°$, $\Phi = 54°$ for the pen) is to be compared with another image R_2 chosen among the remaining 90 directions. GEFS and SEFS are calculated in the three components of each image in the RGB space, for which it is natural to assume the following extension of (17):

$$D(R_1, R_2) = \frac{1}{3} \left(d_R(R_1, R_2) + d_G(R_1, R_2) + d_B(R_1, R_2) \right), \tag{18}$$

where $d_R(R_1, R_2)$, $d_G(R_1, R_2)$, $d_B(R_1, R_2)$ are the measures (17) calculated in each band R, G, B. For image matching, the GEFS and SEFS components in each band are extracted from each image, thus forming a dataset with reduced storage memory. An image is compared with the images in the dataset using (18). If the dataset contains s color images of sizes $N \times N$

TABLE 1: Best distances from GEFS and SEFS based method with $\rho = 0.007813$ for the eraser image dataset obtained from the comparison with the sample image at $\theta = 11°$ and $\phi = 36°$.

θ	ϕ	$d_R(R_1, R_2)$	$d_G(R_1, R_2)$	$d_B(R_1, R_2)$	$D(R_1, R_2)$
10	54	7.2543	20.4322	15.1914	14.2926
11	−36	18.4459	30.1343	25.7560	24.7787
25	37	16.4410	35.3923	24.2910	25.3748
10	89	18.7165	32.1656	25.8345	25.5722
10	−54	17.3107	34.4895	25.8311	25.8771

FIGURE 11: Frame 2 in Mom-Daughter.

and the dimension of the original dataset is $3sN^2$, then the dimension of the GEFS and SEFS dataset is $6sN$, so we have a compression rate given by

$$\rho = \frac{6sN}{3sN^2} = \frac{2}{N}. \tag{19}$$

So we obtain a compression rate $\rho = 0.007813$ if $N = 256$.

4. The Image Matching Process via F-Transforms

We consider an image dataset formed by color images of sizes $N \times M$. In the preprocessing phase we compress each image of the dataset using the direct F-transform. Each image is divided in blocks of sizes $N(B) \times M(B)$ and each block is compressed in a block of sizes $n(B) \times m(B)$. Thus the images are coded with a compression rate $\rho = (n(B) \times m(B))/(N(B) \times M(B))$. In our experiments we set the sizes of the original and compressed blocks, so that ρ is comparable with (18). For example, for $N = M = 256$, we use $N(B) = M(B) = 24$ and $n(B) = m(B) = 2$, so $\rho = 0.006944$.

In the reduced dataset we store the F-transform components of each image. We use the PSNR between a sample image R_1 and an image R_2 defined for every compression rate ρ (cf. (9)) as

$$\text{PSNR}_\rho(R_1, R_2) = 20 \log_{10} \frac{L}{\text{RMSE}_\rho(R_1, R_2)}, \tag{20}$$

TABLE 2: Best PSNR from the F-transform based method with $L = 255$ and $\rho = 0.006944$ for the eraser image dataset obtained from the comparison with the sample image at $\theta = 11°$ and $\phi = 36°$.

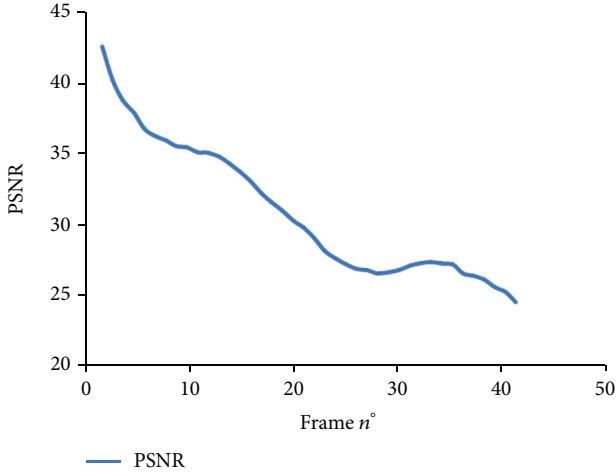| θ	ϕ	$\text{PSNR}_{\rho R}(R_1, R_2)$	$\text{PSNR}_{\rho G}(R_1, R_2)$	$\text{PSNR}_{\rho B}(R_1, R_2)$	$\text{PSNR}_{\rho}(R_1, R_2)$
10	54	25.4702	22.2952	23.7712	23.8455
11	−36	21.8504	20.0625	21.0801	20.9977
25	37	21.4056	17.9865	19.0040	19.4654
10	89	21.3049	17.8858	18.9033	19.3647
10	−54	21.0057	17.5866	18.6041	19.0655

FIGURE 12: Trend of PSNR ($\rho = 0.006944$) with respect to frame number for the video Mom-Daughter.

FIGURE 13: Frame 1 in sflowg.

FIGURE 14: Frame 2 in sflowg.
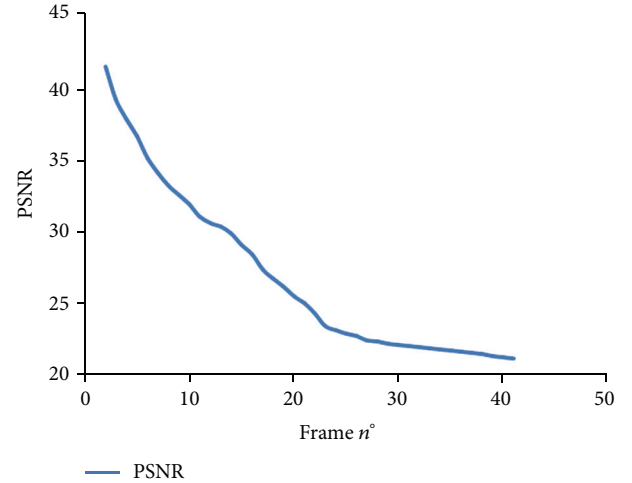

FIGURE 15: Trend of PSNR ($\rho = 0.006944$) with respect to frame number for the video sflowg.

where RMSE (Root Mean Square Error) is given by (cf. (10))

$$\text{RMSE}_{\rho}(R_1, R_2) = \sqrt{\frac{\sum_{i=1}^{N} \sum_{j=1}^{M} (R_1(i, j) - R_2(i, j))^2}{N \times M}}. \quad (21)$$

If we have color images, we define an overall PSNR as

$$\begin{aligned} \text{PSNR}_{\rho}(R_1, R_2) \\ = \frac{1}{3} \Big[\text{PSNR}_{\rho R}(R_1, R_2) + \text{PSNR}_{\rho G}(R_1, R_2) \\ + \text{PSNR}_{\rho B}(R_1, R_2) \Big], \end{aligned} \quad (22)$$

where $\text{PSNR}_{\rho R}(R_1, R_2)$, $\text{PSNR}_{\rho G}(R_1, R_2)$, $\text{PSNR}_{\rho B}(R_1, R_2)$ are the similarity measures (20) calculated in each band R, G, B compression rate ρ. In our experiments we compare the results obtained by using the F-transforms (resp., GEFS and SEFS) based method with the PSNR (20) (resp. (18)). We use the color image datasets of 256 gray levels and of sizes 256×256 pixels, available in the View Sphere Database for each object considered, the best image R_2 of the object itself maximizes the PSNR (22). In other experiments we use our F-transform method over color video datasets in which each frame is formed by images of 256 gray levels and of sizes
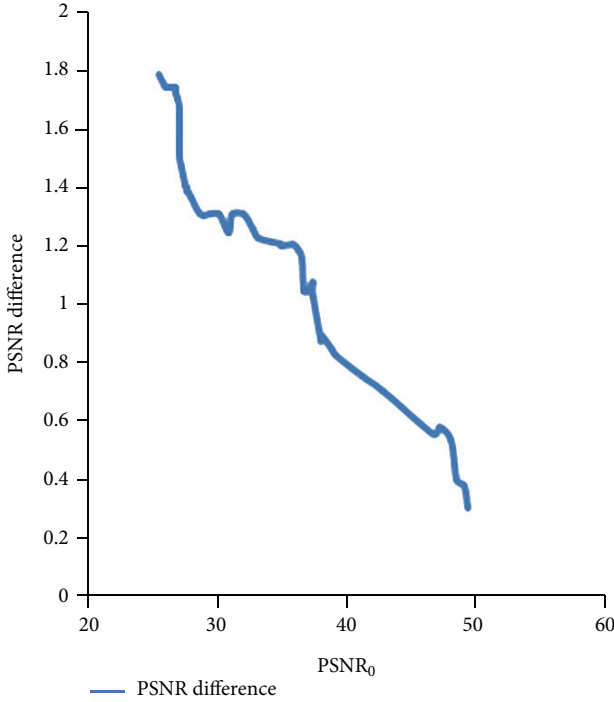
Figure 16: Trend of PSNR difference with respect to $PSNR_0$ ($\rho = 0.006944$).

Table 3: Best distances from GEFS and SEFS based method with $\rho = 0.007813$ for the pen image dataset obtained from the comparison with the sample image at $\theta = 10°$ and $\phi = 54°$.

θ	ϕ	$d_R(R_1, R_2)$	$d_G(R_1, R_2)$	$d_B(R_1, R_2)$	$D(R_1, R_2)$
10	18	0.8064	0.4495	0.9232	0.7264
10	−18	1.2654	1.0980	7.2903	3.2179
68	84	2.7435	1.7468	5.8812	3.4572
11	36	2.1035	5.4634	3.3769	3.6479
10	−54	2.5394	2.0005	9.2138	4.5845

360×24, available in the Ohio University sample digital color video database. A color video is schematically formed by a sequence of frames. If we consider a frame in a video as the sample image, we prove that the image with greatest PSNR with respect to the sample image is an image with frame number close to the frame number of the sample image.

5. Results of Tests

We compare results obtained by using the GEFS and SEFS and F-transform based methods for image matching on all the image datasets, each of sizes 256×256, extracted from the View Sphere Database. In the first image dataset, concerning an eraser, we consider, as sample image R_1, the image obtained from the camera in the direction with angles $\theta = 11°$ and $\phi = 36°$. For brevity, we consider a dataset of 40 test images, and we compare R_1 with the images considered in the remaining 40 other directions. In Table 1 (resp., Table 2) we report the distances (17) and (18) (resp., PSNR (20) and

(22) with $L = 255$) obtained using the GEFS and SEFS (resp., F-transform) based method.

In Figure 4 we show the trend of the index PSNR obtained by the F-Transform method with respect to the distance (18) obtained using the GEFS and SEFS method.

As we can see from Tables 1 and 2, both methods give the same reply: the better image similar with the image eraser in the direction $\theta = 11°$ and $\phi = 36°$ (Figure 5) is given from that one at $\theta = 10°$ and $\phi = 54°$ (Figure 6). The trend in Figure 4 shows that the value of the distance (18) increases as the PSNR decreases.

In order to have a further confirmation of our approach, we have considered a second object, a pen, contained in the View Sphere Database whose sample image R_1 is obtained from the camera in the direction with angles $\theta = 10°$ and $\phi = 54°$. We also limit the problem to a dataset of 40 test images whose best distances (17) and (18) (resp., (20) and (22) with $L = 255$) under the SEFS and GEFS (resp., F-transform) based method, are reported in Table 3 (resp., Table 4).

In Figure 7 we show the trend of the index PSNR obtained by the F-transform method with respect to the distance D obtained by using the GEFS and SEFS method. As we can see from Tables 3 and 4, in both methods the best image similar to the original image in the directions $\theta = 10°$ and $\phi = 54°$ (Figure 8) is given from that one at $\theta = 10°$ and $\phi = 18°$ (Figure 9). Also in this example, the trend in Figure 7 shows that the value of the distance (18) increases as the PSNR decreases.

Now we present the results over a sequence of frames of a video, Mom-Daughter, available in the Ohio University sample digital color video database. Each frame is a color image of sizes 360×240 with 256 gray levels for each band. We use our method with a compression rate $\rho = 0.006944$; that is, in each band every frame is decomposed in 150 blocks, and each block has sizes 24×24 compressed to a block of sizes 2×2. Since $M \neq N$, the GEFS and SEFS based method is not applicable. We set the sample image as the image corresponding to the first frame of the video. We expect that the frame number of the image with higher PSNR with respect to the sample image is the image with frame number close to the frame number of sample image. In Table 5 we report the best results obtained using the F-transform based method in terms of the (20) and (22) with $L = 255$. As expected, albeit with slight variations, all the PSNRs diminish by increasing of the frame number, and the second frame (Figure 11) is the frame with the greatest PSNR w. r. t. the first frame (Figure 10) containing the sample image.

In Figure 12 we show the trend of the PSNR (22) with the frame number. This trend is obtained for all the sample video frames in the video dataset. For reasons of brevity, now we report only the results obtained for another test performed on the sequence of frames of another video in the Ohio sample digital video database, the video sflowg. The PSNR in Figure 15 diminishes by increasing the frame number, and the second frame (Figure 14) is the frame with the greatest PSNR w. r. t. the first frame (Figure 13) containing the sample image.

For supporting the validity of the F-transform method for all the sample frames, we measure, for the frame with the greatest PSNR w.r.t the sample frame, the correspondent

TABLE 4: Best PSNR from the F-transform based method with $L = 255$ and $\rho = 0.006944$ for the pen image dataset obtained from the comparison with the sample image at $\theta = 10°$ and $\phi = 54°$.

θ	ϕ	$\text{PSNR}_{\rho R}(R_1, R_2)$	$\text{PSNR}_{\rho G}(R_1, R_2)$	$\text{PSNR}_{\rho B}(R_1, R_2)$	$\text{PSNR}_{\rho}(R_1, R_2)$
10	18	25.3095	25.2317	23.9915	24.8442
10	−18	24.6794	24.9788	23.4156	24.3579
68	84	24.4219	24.6667	22.6941	23.9276
11	36	24.5678	24.1721	22.5035	23.7478
10	−54	23.7862	23.5642	22.2730	23.2078

TABLE 5: PSNR with $\rho = 0.006944$ for the Mom-Daughter video w.r.t. the first frame.

Frame number	$\text{PSNR}_{\rho R}(R_1, R)$	$\text{PSNR}_{\rho G}(R_1, R)$	$\text{PSNR}_{\rho B}(R_1, R_2)$	$\text{PSNR}_{\rho}(R_1, R_2)$
2	42.2146	42.0278	42.6819	42.3081
3	39.5194	39.6131	40.9278	40.0201
4	37.7658	39.0397	39.0397	38.6151
5	36.9349	37.3071	38.8239	37.6886
6	35.4771	36.5276	37.8853	36.6300

value PSNR_0 obtained by using the original frame instead of the correspondent compressed frame decoded via the inverse F-Transform. In Figure 16 we show the trend of the difference $\text{PSNR}_0 - \text{PSNR}$ with respect to PSNR_0. The trend indicates that this difference is always less than 2. This result shows that if we compress the images in the dataset with rate $\rho = 0.006944$ by using the F-transform method, we can use the compressed image dataset for image matching processes, comparing the decompressed image with respect to a sample image despite the loss of information due to the compression.

6. Conclusions

The results on the images of sizes $N \times M$ ($M = N = 256$) of the View Sphere Image Database show that, using our F-transform based method, we obtain the same results in terms of image matching and in terms of reduced memory storage reached also via the GEFS and SEFS based method, which is applicable only over images with $N = M$, while our method concerns images of any sizes.

Moreover our tests executed on color video frames of sizes $N \times M$ ($M = 360$, $N = 240$ pixels with 256 gray levels) of the Ohio University color videos dataset show that, by choosing the first frame as the sample image, we obtain as image with the highest PSNR that one corresponding to the successive frame, as expected, although a loss of information on the decoded images because of the compression process.

References

[1] I. Bartolini, P. Ciaccia, and M. Patella, "Query processing issues in region-based image databases," *Knowledge and Information Systems*, vol. 25, no. 2, pp. 389–420, 2010.

[2] B. De Baets, "Analytical solution methods for fuzzy relational equations," in *Fundamentals of Fuzzy Sets*, D. Dubois and H. Prade, Eds., vol. 1 of *The Handbooks of Fuzzy Sets Series*, pp. 291–340, Kluwer Academic Publishers, Dordrecht, The Netherlands, 2000.

[3] A. Di Nola, W. Pedrycz, S. Sessa, and E. Sanchez, *Fuzzy Relation Equations and Their Application to Knowledge Engineering*, Kluwer Academic Publishers, Dordrecht, The Netherlands, 1989.

[4] M. Higashi and G. J. Klir, "Resolution of finite fuzzy relation equations," *Fuzzy Sets and Systems*, vol. 13, no. 1, pp. 65–82, 1984.

[5] P. Li and S. C. Fang, "A survey on fuzzy relational equations, part I: classification and solvability," *Fuzzy Optimization and Decision Making*, vol. 8, no. 2, pp. 179–229, 2009.

[6] V. Loia, W. Pedrycz, and S. Sessa, "Fuzzy relation calculus in the compression and decompression of fuzzy relations," *International Journal of Image and Graphics*, vol. 2, no. 4, pp. 617–631, 2002.

[7] A. V. Markovskii, "On the relation between equations with max-product composition and the covering problem," *Fuzzy Sets and Systems*, vol. 153, no. 2, pp. 261–273, 2005.

[8] M. Miyakoshi and M. Shimbo, "Lower solutions of systems of fuzzy equations," *Fuzzy Sets and Systems*, vol. 19, no. 1, pp. 37–46, 1986.

[9] K. Peeva, "Resolution of min-max fuzzy relational equations," in *Fuzzy Partial Differential Equations and Relational Equations*, M. Nikravesh, L. A. Zadeh, and V. Korotkikh, Eds., pp. 153–166, Springer, New York, NY, USA, 2004.

[10] K. Peeva, "Universal algorithm for solving fuzzy relational equations," *Italian Jour-Nal of Pure and Applied Mathematics*, vol. 19, pp. 9–20, 2006.

[11] K. Peeva and Y. Kyosev, "Algorithm for solving max-product fuzzy relational equations," *Soft Computing*, vol. 11, no. 7, pp. 593–605, 2007.

[12] K. Peeva and Y. Kyosev, *Fuzzy Relational Calculus-Theory, Applications and Software*, vol. 22 of *Advances in Fuzzy Systems—Applications and Theory*, World Scientific Publishing, River Edge, NJ, USA, 2004.

[13] E. Sanchez, "Resolution of composite fuzzy relation equations," *Information and Control*, vol. 30, no. 1, pp. 38–48, 1976.

[14] B. S. Shieh, "New resolution of finite fuzzy relation equations with max-min composition," *International Journal of Uncertainty, Fuzziness and Knowledge-Based Systems*, vol. 16, no. 1, pp. 19–33, 2008.

[15] Y. K. Wu and S. M. Guu, "An efficient procedure for solving a fuzzy relational equation with max-Archimedean t-norm composition," *IEEE Transactions on Fuzzy Systems*, vol. 16, no. 1, pp. 73–84, 2008.

[16] F. Di Martino, V. Loia, and S. Sessa, "A method in the compression/decompression of images using fuzzy equations and fuzzy similarities," in *Proceedings of IFSA Conference*, pp. 524–527, 2003.

[17] F. Di Martino, V. Loia, and S. Sessa, "A method for coding/decoding images by using fuzzy relation equations," in *10th International Fuzzy Systems Association World Congress*, T. Bilgic, B. De Baets, and O. Kaynak, Eds., vol. 2715 of *Lecture Notes in Artificial Intelligence*, pp. 436–441, Springer, Berlin, Germany, July 2003.

[18] V. Loia and S. Sessa, "Fuzzy relation equations for coding/decoding processes of images and videos," *Information Sciences*, vol. 171, no. 1-3, pp. 145–172, 2005.

[19] H. Nobuhara, W. Pedrycz, and K. Hirota, "Fast solving method of fuzzy relational equation and its application to lossy image compression/reconstruction," *IEEE Transactions on Fuzzy Systems*, vol. 8, no. 3, pp. 325–334, 2000.

[20] F. Di Martino, V. Loia, and S. Sessa, "A segmentation method for images compressed by fuzzy transforms," *Fuzzy Sets and Systems*, vol. 161, no. 1, pp. 56–74, 2010, Special section: New Trends on Pattern Recognition with Fuzzy Models.

[21] J. Lu, R. Li, Y. Zhang, T. Zhao, and Z. Lu, "Image annotation techniques based on feature selection for class-pairs," *Knowledge and Information Systems*, vol. 24, no. 2, pp. 325–337, 2010.

[22] I. Perfilieva, V. Novák, and A. Dvořák, "Fuzzy transform in the analysis of data," *International Journal of Approximate Reasoning*, vol. 48, no. 1, pp. 36–46, 2008.

[23] L. Chen and P. Wang, "Fuzzy relational equations (I): the general and specialized solving algorithms," *Soft Computing*, vol. 6, pp. 428–435, 2002.

[24] E. Sanchez, "Resolution of Eigen fuzzy sets equations," *Fuzzy Sets and Systems*, vol. 1, no. 1, pp. 69–74, 1978.

[25] E. Sanchez, "Eigen fuzzy sets and fuzzy relations," *Journal of Mathematical Analysis and Applications*, vol. 81, no. 2, pp. 399–421, 1981.

[26] F. Di Martino, S. Sessa, and H. Nobuhara, "Eigen fuzzy sets and image information retrieval," in *Proceedings of IEEE International Conference on Fuzzy Systems*, vol. 3, pp. 1385–1390, IEEE Press, July 2004.

[27] F. Di Martino, H. Nobuhara, and S. Sessa, "Eigen fuzzy sets and image information retrieval," in *Handbook of Granular ComputIng*, W. Pedrycz, A. Skowron, and V. Kreinovich, Eds., pp. 863–872, John Wiley & Sons, Chichester, UK, 2008.

[28] I. Perfilieva, "Fuzzy transforms: application to reef growth problem," in *Fuzzy Logic in Geology*, R. B. Demicco and G. J. Klir, Eds., pp. 275–300, Academic Press, Amsterdam, The Netherlands, 2003.

[29] I. Perfilieva, "Fuzzy transforms: theory and applications," *Fuzzy Sets and Systems*, vol. 157, no. 8, pp. 993–1023, 2006.

[30] I. Perfilieva and E. Chaldeeva, "Fuzzy transformation," in *Proceedings of 9th IFSA World Congress and 20th NAFIPS International Conference*, pp. 1946–1948, 2001.

[31] F. Di Martino, V. Loia, I. Perfilieva, and S. Sessa, "An image coding/decoding method based on direct and inverse fuzzy transforms," *International Journal of Approximate Reasoning*, vol. 48, no. 1, pp. 110–131, 2008.

[32] F. Di Martino and S. Sessa, "Compression and decompression of images with discrete fuzzy transforms," *Information Sciences*, vol. 177, no. 11, pp. 2349–2362, 2007.

[33] I. Perfilieva and B. De Baets, "Fuzzy transforms of monotone functions with application to image compression," *Information Sciences*, vol. 180, no. 17, pp. 3304–3315, 2010.

[34] F. Di Martino, V. Loia, and S. Sessa, "Fuzzy transforms method and attribute dependency in data analysis," *Information Sciences*, vol. 180, no. 4, pp. 493–505, 2010.